

UNCLASSIFIED

AD NUMBER

AD401911

LIMITATION CHANGES

TO:

Approved for public release; distribution is unlimited.

FROM:

Distribution authorized to U.S. Gov't. agencies and their contractors;
Administrative/Operational Use; APR 1963. Other requests shall be referred to Arnold Engineering Development Center, Arnold AFB, TN 37389.

AUTHORITY

AEDC ltr, 30 May 1972

THIS PAGE IS UNCLASSIFIED

FOR ERRATA

AD 401911

THE FOLLOWING PAGES ARE CHANGES

TO BASIC DOCUMENT

AD 401911

Errata AEDC-TDR-63-22,
April 1963*

Please note the following corrections:

1. Page xii Re_X Reynolds number, $in.^{-1}$ should be changed to Re_X Reynolds number based on the length X
2. Page 5 paragraph 4, line 4 should be changed to: with a greater variety of sonic jet nozzle configurations (single and multiple)
3. Page 61 The schlierens (not the labeling or the plotted data) should be interchanged.

401911

*W. T. Strike, C. J. Schueler, and J. S. Deitering. "Interactions Produced by Sonic Lateral Jets Located on Surfaces in a Supersonic Stream." Arnold Engineering Development Center, Arnold Air Force Station, Tennessee. AEDC-TDR-63-22, April 1963. (Unclassified Report)

C. 1

DOC_NUM	SER	CN
UNC28885-PDC	A	1



INTERACTIONS PRODUCED BY SONIC LATERAL JETS LOCATED ON SURFACES IN A SUPERSONIC STREAM

By

W. T. Strike, C. J. Schueler,

and J. S. Deitering

von Kármán Gas Dynamics Facility
ARO, Inc.

TECHNICAL DOCUMENTARY REPORT NO. AEDC-TDR-63-22

April 1963

AFSC Program Area 750A, Project 8953, Task 895305

(Prepared under Contract No. AF 40(600)-1000 by ARO, Inc.,
contract operator of AEDC, Arnold Air Force Station, Tenn.)

ARNOLD ENGINEERING DEVELOPMENT CENTER
AIR FORCE SYSTEMS COMMAND
UNITED STATES AIR FORCE

This document has been approved for public release
and sale; its distribution is unlimited.

UNCLASSIFIED

pl. AF 3011 May 72
Signed William C. Cline (KON)

NOTICES

Qualified requesters may obtain copies of this report from ASTIA. Orders will be expedited if placed through the librarian or other staff member designated to request and receive documents from ASTIA.

When Government drawings, specifications or other data are used for any purpose other than in connection with a definitely related Government procurement operation, the United States Government thereby incurs no responsibility nor any obligation whatsoever; and the fact that the Government may have formulated, furnished, or in any way supplied the said drawings, specifications, or other data, is not to be regarded by implication or otherwise as in any manner licensing the holder or any other person or corporation, or conveying any rights or permission to manufacture, use, or sell any patented invention that may in any way be related thereto.

ASTIA release in OTS not authorized and foreign announcement and dissemination by ASTIA is limited.

INTERACTIONS PRODUCED BY SONIC LATERAL JETS
LOCATED ON SURFACES IN A SUPERSONIC STREAM

By

W. T. Strike, C. J. Schueler, and J. S. Deitering
von Kármán Gas Dynamics Facility

ARO, Inc.

a subsidiary of Sverdrup and Parcel, Inc.

April 1963

ARO Project No. VT2027

ABSTRACT

A flat plate, a hollow cylinder, and a nine-caliber ogive containing lateral sonic jets were tested at Mach numbers 2.99, 3.98, and 5.01 in the 12-Inch Supersonic Tunnel (E-1) of the von Kármán Gas Dynamics Facility. The interaction forces generated on these bodies were investigated for various sonic nozzle configurations including single circular nozzles, multiple circular nozzles, and slots of various width and span sizes. The nozzles were operated at jet stagnation to free-stream static pressure ratios from 10 to 2000.


The force produced on a surface by the interaction of the lateral jet with the supersonic free stream was evaluated from model pressure distributions and compared with various theoretical estimates. Good agreement was obtained between the present experimental data and the theoretical estimates based on a linear combination of the viscous and inviscid estimates of the jet interaction force. Also, good agreement was obtained between the integrated pressure data and some force measurements.

These theoretical and experimental results indicated that significant jet interaction forces are produced. In general, circular sonic jets produced the maximum interaction force when located about 30 jet nozzle diameters forward of the trailing edge of a planar surface or at the base edge of a body of revolution. Rectangular nozzles (slots) generated the largest force when located at the model trailing edge.

PUBLICATION REVIEW

This report has been reviewed and publication is approved.


Donald R. Eastman, Jr.
DCS/Research


Jean A. Jack
Colonel, USAF
DCS/Test

CONTENTS

	<u>Page</u>
ABSTRACT	iii
NOMENCLATURE	xi
1.0 INTRODUCTION	1
2.0 EXPERIMENTAL APPARATUS AND TECHNIQUES	
2.1 Wind Tunnels	5
2.2 Models	6
2.3 Instrumentation and Precision	7
3.0 TEST PROCEDURES AND CONDITIONS	7
4.0 RESULTS AND DISCUSSION	
4.1 Sonic Nozzle Characteristics	9
4.2 Flat Plate Flow Characteristics.	9
4.3 The Lateral Jet Flow Field.	10
4.4 Pressure Distributions and Moment Loading	13
4.5 Two-Dimensional Theoretical Analysis	16
4.6 Three-Dimensional Theoretical Analysis.	21
4.7 Experimental Flat Plate Results	23
4.8 Lateral Jet from a Body of Revolution	27
5.0 CONCLUDING REMARKS.	30
REFERENCES.	32
APPENDIX	37

ILLUSTRATIONS

Figure

1. Flight Corridor	43
2. The 12-Inch Supersonic Tunnel (E-1)	44
3. Flat Plate and Nozzle Block Configurations.	45
4. Flat Plate Installation	46
5. Hollow Cylinder and Nine-Caliber Ogive Configurations	46
6. Discharge Coefficient of Sharp Edge Nozzles	47
7. Flat Plate Boundary-Layer Characteristics	48
8. Two-Dimensional Lateral Jet Flow Field.	49
9. General Direction of the Oil Flow Lines	49

<u>Figure</u>	<u>Page</u>
10. Flow Patterns with Isobars at $M_\infty = 3.98$, $Re_X = 0.6 \times 10^6$	
a. 0.125-in. -diam Circular Nozzle	50
b. 0.125-in. -diam Multiple Circular Nozzles, $e/d_j = 12.3$	50
c. 0.125-in. -diam Multiple Circular Nozzles, $e/d_j = 3.1$	51
d. 0.131- by 3-in. Rectangular Nozzle	51
11. Comparison of the Flow Field and Pressure Distribution Generated by an Air Jet and a Vertical Spoiler at $M_\infty = 3.98$, $Re_X = 2.0 \times 10^6$	
a. Air Jet Spoiler, 0.131- by 3.0-in. Slot, $p_j/p_\infty = 31$	52
b. Vertical Spoiler, Height = 0.5 in. and Width = 3 in.	53
12. Typical Pressure Distribution Generated by the Interaction of a Lateral Jet from 0.028- by 3-in. Slot into a Supersonic Stream, $M_\infty = 3.98$	
a. $Re_X = 1.7 \times 10^6$, $p_j/p_\infty = 480$, $FN_O/q_\infty = 3.5 \text{ in.}^2$	54
b. $Re_X = 3.5 \times 10^6$, $p_j/p_\infty = 480$, $FN_O/q_\infty = 3.8 \text{ in.}^2$	55
c. $Re_X = 3.5 \times 10^6$, $p_j/p_\infty = 231$, $FN_O/q_\infty = 2.7 \text{ in.}^2$	56
d. $Re_X = 1.8 \times 10^6$, $p_j/p_\infty = 934$, $FN_O/q_\infty = 5.9 \text{ in.}^2$	57
13. Influence of Jet Nozzle Configuration and Pressure Ratio on Boundary-Layer Separation Location, $M = 3.98$	
a. Circular Nozzle	58
b. Rectangular Nozzle	58
14. Influence of Multiple Circular Nozzle Configurations on Boundary-Layer Separation Location, $Re_X = 1.8 \times 10^6$, $M_\infty = 3.98$	59
15. Pitot Pressure Distribution Downstream of a Jet from a 0.131- by 3-in. Rectangular Slot	
a. $M_\infty = 2.99$, $p_j/p_\infty = 9$	60
b. $M_\infty = 2.99$, $Re_X = 1.9 \times 10^6$, $p_j/p_\infty = 29, 119$. .	61
c. $M_\infty = 3.98$, $Re_X = 1.9 \times 10^6$, $p_j/p_\infty = 31, 101$. .	62
d. $M_\infty = 3.98$, $Re_X = 1.9 \times 10^6$, $p_j/p_\infty = 207$	63
e. $M_\infty = 5.01$, $Re_X = 2.2 \times 10^6$, $p_j/p_\infty = 45, 62$. .	64
f. $M_\infty = 5.01$, $Re_X = 2.2 \times 10^6$, $p_j/p_\infty = 470$. . .	65

<u>Figure</u>	<u>Page</u>
16. Pitot Pressure Distribution Downstream of a Jet from a Circular Nozzle, $d_j = 0.25$ in.	
a. $M_\infty = 2.99$, $Re_X = 1.7 \times 10^6$	66
b. $M_\infty = 5.01$, $Re_X = 2.1 \times 10^6$	67
17. Influence of Nozzle Configuration on the Radial Load and Pressure Distribution, $M_\infty = 3.98$, $Re_X = 3.6 \times 10^6$	68
18. Influence of Slot Span on the Radial Load and Axial Pressure Distribution of a 0.057- by 3-in. Slot, $M_\infty = 3.98$, $Re_X = 1.8 \times 10^6$	69
19. Influence of Reynolds Number on the Radial Load and Pressure Distribution of a 0.125-in. -diam Circular Nozzle, $M_\infty = 3.98$	70
20. Influence of Reynolds Number on the Radial Load and Pressure Distribution of a 0.131- by 3-in. Slot, $M_\infty = 3.98$	71
21. Influence of Reynolds Number on the Radial Load and Axial Pressure Distribution of a 0.028- by 3-in. Slot, $M_\infty = 3.98$	72
22. Influence of Jet Pressure on the Radial Load and Axial Pressure Distribution of a 0.028- by 3-in. Slot, $Re_X = 1.8 \times 10^6$, $M_\infty = 3.98$	73
23. Influence of Jet Pressure on the Radial Load and Axial Pressure Distribution of a 0.125-in. -diam Nozzle, $Re_X = 1.8 \times 10^6$, $M_\infty = 3.98$	74
24. Influence of Mach Number on the Radial Load and Axial Pressure Distributions of a 0.028- by 3-in. Slot, $Re_X = 1.5$ to 2.2×10^6	75
25. Influence of Mach Number on the Radial Load and Axial Pressure Distribution of a 0.125-in. -diam Circular Nozzle, $Re_X = 1.5$ to 2.2×10^6	76
26. The Effective Spoiler Height Generated by Rectangular Sonic Nozzle Jets	
a. $M_\infty = 2.99$	77
b. $M_\infty = 3.98$	78
c. $M_\infty = 5.01$	79
27. Plateau Pressure Produced by a Separated Boundary Layer at Various Mach Numbers	80

<u>Figure</u>	<u>Page</u>
28. Theoretical and Experimental Correlation of the Pressure Loading Factor Generated by Separated Boundary Layers	
a. Laminar Boundary-Layer Separation	81
b. Turbulent Boundary-Layer Separation	81
29. Estimated Ratio of Interaction Force to Jet Reaction Force of a Sonic, Two-Dimensional Lateral Jet	82
30. The Effective Spoiler Height Generated by Circular Sonic Nozzle Jets	83
31. Estimated Ratio of Interaction Force to Jet Reaction Force of a Circular Sonic Lateral Jet	
a. $p_j/p_\infty = 100$	84
b. $p_j/p_\infty = 1000$	84
32. Comparison of the Theoretical Interaction Force Ratio, f_{n_i}/k_j with the Experimental Values of Rectangular Nozzles	85
33. The Two- and Three-Dimensional Effects of Circular Nozzle Configurations at $M_\infty = 3.98$, $Re_x = 0.6$ to 3.6×10^6	86
34. The Two- and Three-Dimensional Effects of 0.057-in. -width Slots of Various Aspect Ratios, $M_\infty = 3.98$, $Re_x = 0.6$ to 3.6×10^6	87
35. Variation of Interaction Force, F_{n_o}/q_∞ , Generated Upstream of the Jet versus $(p_j/p_\infty)A_e$	
a. Circular and Rectangular Nozzles, $M_\infty = 2.99$	88
b. Circular Nozzles, $M_\infty = 3.98$	88
c. Rectangular Nozzles, $M_\infty = 3.98$	89
d. Circular and Rectangular Nozzles, $M_\infty = 5.01$	89
36. Influence of the Pressure Field Aft of the Jet Nozzle on the Resultant Interaction Force, $M_\infty = 3.98$, $Re_x = 1.8$ to 3.6	90
37. The Effect of Mach Number on the Sonic Nozzle Jet Interaction Force	
a. Rectangular Nozzles	91
b. Circular Nozzles	92
38. Center of Pressure on the Interaction Load Ahead of the Nozzle Jet	93

<u>Figure</u>		<u>Page</u>
39.	Influence of the Jet Pressure Ratio on the Ratio of the Interaction to Jet Reaction Force for Various Nozzle Configurations	
	a. $M_\infty = 2.99$, Circular Nozzles	94
	b. $M_\infty = 2.99$, Rectangular Nozzles	94
	c. $M_\infty = 3.98$, Circular Nozzles	95
	d. $M_\infty = 3.98$, Rectangular Nozzles	95
	e. $M_\infty = 5.01$, Circular Nozzles	96
	f. $M_\infty = 5.01$, Rectangular Nozzles	96
40.	Comparison of Resultant Force Produced by a Lateral Jet from a Circular Sonic Nozzle and a Slot at Various Altitudes.	97
41.	Comparison of AEDC Results with Amick and Hays (Ref. 13) Empirical Relationship	97
42.	Typical Flow Patterns Generated about the Hollow Cylinder by Lateral Jets from Rectangular and Circular Nozzles, $Re_X = 3.9 \times 10^6$, $M_\infty = 3.98$	98
43.	Typical Flow Pattern about a Nine-Caliber Ogive Generated by a Lateral Jet from a 0.25-in.-diam Circular Nozzle, $M_\infty = 3.98$	
	a. $Re_X = 6.0 \times 10^6$	99
	b. $Re_X = 3.2 \times 10^6$, with a Boundary-Layer Trip Mounted on the Model Nose.	100
	c. $Re_X = 3.2 \times 10^6$	101
44.	Typical Flow Patterns about a Nine-Caliber Ogive Generated by a Lateral Jet from a 0.05- by 3-in. (Circumferential Distance) Rectangular Slot, $M_\infty = 3.98$	
	a. $Re_X = 3.2 \times 10^6$, $p_j/p_\infty = 193$	102
	b. $Re_X = 3.2 \times 10^6$, $p_j/p_\infty = 380$	103
	c. $Re_X = 6.0 \times 10^6$, $p_j/p_\infty = 32$	104
	d. $Re_X = 5.8 \times 10^6$, $p_j/p_\infty = 237$	105
45.	Influence of the Boundary-Layer Jet Interaction on the Pressure Distribution at $M_\infty = 3.98$ on a Nine-Caliber Ogive	
	a. 0.25-in.-diam Circular Nozzle	106
	b. 0.05- by 3-in. Rectangular Nozzle	107
46.	Comparisons of the Interaction Loads Generated by a Jet from a 0.25-in.-diam Circular Nozzle on the Hollow Cylinder, Ogive, and Flat Plate at $M_\infty = 3.98$. .	108

<u>Figure</u>	<u>Page</u>
47. Comparisons of the Interaction Loads Generated by a Jet from a 0.05-in. Rectangular Nozzle on the Hollow Cylinder, Ogive, and Flat Plate at $M_\infty = 3.98$	109
48. Comparison of Theoretical and Experimental Interaction Forces Generated on a Nine-Caliber Ogive of Nominal Mach Number 4 by a Lateral Jet	110
49. Influence of the Relative Location of the Jet Nozzle on the Interaction Coefficient, Nine-Caliber Ogive, Nominal Mach Number of 4	111

NOMENCLATURE

A/A^*	Stream tube area ratio relationship for isentropic flow (see Fig. 26)
A_b	Model base area, in. ²
A_e	Effective jet nozzle cross-sectional throat area, $A_e = CA_j$, in. ²
A_j	Jet nozzle cross-sectional throat area, in. ²
C	Nozzle discharge coefficient, ratio of actual mass flow/ideal mass flow
C_{N_i}	Interaction force coefficient, $F_{N_i}/q_\infty A_b$
C_{pp}	Boundary-layer separation plateau pressure coefficient, $(p_p - p_\infty)/q_\infty$
C_{ps}	Pressure coefficient at point of boundary-layer separation, $(p_s - p_\infty)/q_\infty$
D	Maximum model diameter, in.
d_e	Effective jet nozzle diameter or effective slot width in the streamwise direction, in.
d_j	Jet nozzle diameter or slot width in the streamwise direction, in.
e	Multiple circular nozzle spacing from center to center, in.
F_j	Three-dimensional jet reaction force of a sonic nozzle, $CA_j p_\infty [1.268(p_j/p_\infty) - 1]$, lb
F_{N_i}	Interaction load, the force generated by the interaction of a lateral jet with the approaching boundary layer and supersonic free stream, positive in the direction of F_j , lb
F_{N_x}	Interaction force over an area extending over the full model span from the model leading edge to model station x , positive in the direction of F_j , $2p_\infty \int_0^\pi \int_{d_j/2}^{R\phi} \frac{\Delta p}{p_\infty} r dr d\phi$, lb
F_{NT}	Total lateral jet control force, $F_{N_i} + F_j$, lb
f_j	Two-dimensional jet reaction force per unit span for a sonic nozzle, $Cd_j p_\infty [1.268(p_j/p_\infty) - 1]$, lb/in.
f_{n_i}	Local interaction load along $\phi = 0$ ray on a flat plate positive in the direction of f_j , $p_\infty \int_{d_j/2}^{z,s} \frac{\Delta p}{p_\infty} dx, \text{ lb/in.}$

h	Spoiler height, in.
K	Parameter defined in Ref. 31 where $K = k_2/k_1$ and k is "ratio of the mean velocity in the dissipative region to the external velocity." Subscript 1 represents the parameter before separation and 2, after boundary-layer separation.
L	Model length, total axial model length of integrated pressure distribution or axial distance from model leading edge to boundary-layer rake location, in.
ℓ	Rectangular jet nozzle span, in.
M_∞	Free-stream Mach number
\dot{m}	Mass flow, lb/sec
N	Boundary-layer velocity-profile parameter, $u/u_\infty = (y/\delta)^{1/N}$
n	Local moment loading along an angular ray ϕ , $p_\infty \int_{d_{j/2}}^{R\phi} \frac{\Delta p}{p_\infty} r dr, \text{ lb}$
p	Model static pressure, psia
p_j	Jet stagnation pressure, psia
p_o	Free-stream stagnation pressure, psia
p_p	Plateau pressure resulting from separated boundary layer, psia
p_s	Pressure at the point of boundary-layer separation, psia
p'	Model static pressure when $p_j = 0$, psia
p_o'	Pitot pressure in jet stream, psia
p_∞	Free-stream ambient pressure, psia
Δp	Model differential pressure, $p - p'$, psia
q_∞	Free-stream dynamic pressure, psia
Re_L	Reynolds number based on the length, L
Re_s	Reynolds number based on the length from the model leading edge to the point of boundary-layer separation, $Re_s \times 10^{-6} = \tilde{Re}_s$
Re_x	Reynolds number, in.^{-1}
$R\phi$	Radial distance from the centroid of the area of the jet nozzle configuration to the flat plate edge, sides, or downstream limit of integration, x , in.

r	Radial distance from jet nozzle configuration cross-sectional area centroid, in.
u	Velocity in the boundary layer, in. /sec
u_{∞}	Free-stream velocity, in. /sec
X	Axial position of the jet nozzle area centroid relative to the model nose or leading edge, in.
x	Model axial position relative to the jet nozzle area centroid, in. (see Figs. 3 and 5)
x_{cp}	Center of pressure of the local interaction load upstream of the nozzle along $\phi = 0$, in.
x_{sep}	Boundary-layer separation length from the jet nozzle area centroid, in. (see Fig. 8)
y	Displacement from the model surface, in.
α	Separated boundary-layer flow deflection angle, deg
γ	Ratio of specific heats, $\gamma = 1.4$
δ	Boundary-layer thickness, in.
δ^*	Boundary-layer displacement thickness, in.
θ	Boundary-layer momentum thickness, in.
ϕ	Angular location of the pressure orifice rays, deg (see Fig. 3)
ψ	Angular displacement about the body of revolution, deg (see Fig. 5)
Δ^*	Jet free-stream interaction shock displacement relative to the upstream nozzle edge, in.
ρ/ρ_0	Ratio of the ambient to stagnation density downstream of a normal shock

1.0 INTRODUCTION

As manned vehicles and unmanned missiles traverse the upper regions (high altitudes) of the corridor of continuous flight (see Fig. 1), the need for control systems with broader aerodynamic operational characteristics increases. The high altitude, high Mach number environment requires that the control systems be as operational and reliable at a finite dynamic pressure as in a near vacuum. Also as a result of high speeds, the response of these control systems must be rapid and predictable. As auxiliary controls, reaction jets have provided a means of controlling the attitude and trajectory of high altitude, high Mach number, manned vehicles such as the X-15 research airplane and the Mercury capsule. Similar controls will be used by the Apollo and Dyna Soar manned vehicles at the high altitudes above the flight corridor.

At the lower altitudes, reaction jets may provide a means of augmenting conventional aerodynamic control surfaces or may even replace these control surfaces, provided the reaction jet fuel requirements can be made economically feasible. The present experimental and theoretical program will demonstrate some of the useful control forces generated by lateral jets operating in an environment similar to the conditions experienced by the vehicles flying in the upper and lower regime of the corridor of continuous supersonic flight. These results deal more directly with the basic flow phenomena of interaction loading produced by a jet on a flat plate, a hollow cylinder, and an ogive in a supersonic free stream.

The following is a review of investigations on the discharge of flow into a moving stream. At subsonic speeds, the effects of a lateral airstream exhausting into a moving free stream have been investigated as part of the development of air jet flaps, auxiliary air outlets, vertical-take-off vehicles using an air jet stream for lift, heating or cooling an airstream, and many other air jet applications. One theoretical approach to the basic problem of the interaction of a lateral jet with a moving stream was developed by Ehrick (Ref. 1). Aside from a number of experimental investigations into various applications utilizing air jets,

Manuscript received January 1963.

some basic information on jet penetration into a subsonic stream may be found in Refs. 2 and 3. A test program to determine the influence of a transonic stream on the discharge coefficient of a lateral jet was experimentally evaluated at the NACA, and some results are presented in Ref. 4. Also the effectiveness of air jet controls on a particular type of missile configuration was obtained in the Mach number range of 0.6 to 1.8 (Ref. 5). A fairly complete summary of the use of air jets as boundary-layer control systems, air jet flaps, lateral jets from unswept and swept wings, and ground effects of air jet flap systems at subsonic, transonic, and supersonic speeds (Mach numbers up to 2.5) is presented by Lachman (Ref. 6).

The discharge of low energy air or hot exhaust gases from a high speed (transonic, supersonic, or hypersonic) vehicle has also generated problems pertaining to lateral jets. In the past, extensive experimentation was conducted to analyze the axial-thrust penalties without evaluating the inherent normal and side forces resulting from jet momentum and flow interaction. Another area of practical interest, associated with air disposal, is the degree of penetration and influence of the exhaust jets as the discharged gases wash over the surfaces of the body. This might become increasingly important if one assumes that the exhaust gases are hot and corrosive, and they would therefore have an effect on the vehicle's structure.

During the launch and boost phases of flight, a means of controlling vehicle trajectory has been obtained by regulating the thrust direction of the propulsion system. The operation of a thrust vector control system can be achieved by engine gimbaling, jet vane deflectors, or by directing secondary flow into the mainstream from outlets in the wall downstream of the nozzle throat in order to create a region of separated and deflected flow. The injection of secondary flow into the mainstream to control the thrust vector of a propulsion system has been investigated by various aircraft companies and research organizations; for example, see Refs. 7, 8, and 9.

As pointed out by H. Arnzen (Ref. 10) a lateral jet could be used in combination with conventional aerodynamic controls to provide an "all altitude" control system for non-orbital and re-entry vehicles. Since conventional control systems become inadequate at the higher altitudes above the flight corridor due to lower dynamic pressures (see Fig. 1), a control system which is not dependent on the existence of some finite dynamic pressure is required. One solution to this problem has been found by using lateral reaction jets to control the attitude of the "all altitude" vehicle. As a result of past investigations, it appears that reaction controls similar to those on the X-15, which function adequately in near

vacuum space, will generate larger control forces for a given jet momentum at lower altitudes because of lateral jet interactions with the boundary layer and local flow field.

Depending on the jet strength, the location of the jets on the vehicle, the state of the boundary layer, and the free-stream Mach number, experimental evidence and theoretical solutions of the forces produced by the interference of jet flow with the boundary layer and enveloping supersonic free stream have shown that the net resulting forces are many times larger than the reaction force of the isolated jet in a vacuum environment. A few test programs have included some basic information about the forces generated by lateral jets. Tests were conducted in the S5 wind tunnel of O.N.E.R.A. at Mach number 1.94 to evaluate the loads generated by air at near sonic velocity issuing from single and multiple circular nozzles and single slots mounted in the tunnel floor. Part of this program included a comparison of jet spoiler with a plain vertical spoiler, and these results are presented in Ref. 6 (pp. 63-65). As pointed out by Ph. Poisson-Quinton and L. Lepage in Ref. 6, a comparison of the power required to overcome the drag of a plain spoiler with the power required to supply compressed air to the jet spoiler indicated that the air jet spoiler was more effective.

The influence of high pressure air issuing in the spanwise direction below a wing and normal to a Mach number 2 free stream was investigated by Falanga and Janos (Ref. 11). Additional tests were conducted by Janos (Ref. 12) at Mach number 2 to measure the pressure loading and forces produced by a lateral jet from an unswept flat plate. As in the case of the other investigations, these results indicated that the ratio of the interaction force to jet reaction force increased with decreasing jet pressure ratio (p_j/p_∞). The evaluation of the pressure distributions indicated that the sonic nozzles with jet exit Mach number up to 1.7 generated larger loads than the jet from partially contoured supersonic nozzles (nozzle exit angle > 0). The effect of a lateral jet from sonic, conical, and sharp edge orifices mounted in a flat plate were studied at Mach numbers 3.69 and 3.85 by Amick and Hays (Ref. 13). Included in the analysis of Ref. 13 is an empirical relationship between the ratio of the interaction force to the jet reaction force as a function of the model geometry and jet pressure ratio. An investigation was made by Cubbison, Anderson, and Ward (Ref. 14) to determine the loads generated by a sonic lateral jet from the flat surface of an arrow-shaped model (Mach numbers 2.92, 3.92, 4.84, and 6.4).

The influence of the character of the boundary layer on the loading generated by a lateral two-dimensional sonic jet from a flat plate at Mach number 6 was evaluated from pressure results obtained by Romeo

and Sterrett (Ref. 15). As in the case of the results presented in Ref. 6, these results indicate that two-dimensional sonic air jet behaved like a plain spoiler or forward facing step.

Several tests have been conducted with lateral air jets from bodies of revolution. Pressure measurements were made at Mach number 1.9 with a lateral jet from a circular (sonic) nozzle and a conical supersonic nozzle mounted in the cylindrical section of a 10-deg cone-cylinder by Morkovin, Pierce, and Craven (Ref. 16). As a result of the flow field generated by the lateral jet located 1.8 body diameters from the model base, the net side force was less than the isolated jet reaction force. It was also noted in Ref. 16 that the change in angle of attack from 0 to 14 deg with the nozzle jet on the lee side of the model did not alter the basic jet interaction flow results.

Additional tests have been conducted at supersonic speeds on nine-caliber tangent ogives having various base diameters, model lengths, nozzle configurations, and jet nozzle axial locations on the model. Vinson, Amick, and Liepman (Ref. 17) conducted tests at Mach numbers 2.8 and 3.9 on a three-caliber ogive. The model base diameter was 2 in., and the lateral jet nozzle was a straight-walled, circular nozzle located at various distances from the model base. The influence of angle of attack and character of the boundary layer approaching the jet on the force produced by the interaction of the jet with the approaching free stream and boundary layer was evaluated from internal strain-gage balance measurements. These results indicated that the state of the boundary layer had a negligible effect on the jet interaction force. Similar force measurements were made at Mach number 3.99 by Amick and Hays (Ref. 13) with a 1.5-in. base diam, nine-caliber ogive containing similar sonic nozzles located 0.5 and 2.5 body diameters from the model base. In general, these results indicated that the ratio of interaction force to jet reaction force increased as the jet nozzle was moved toward the model base and as the jet momentum was decreased.

The addition of fins to a 2-in. base diam, nine-caliber ogive having a lateral jet was investigated by Carvalho and Hays (Ref. 18) at Mach number 3.97. In this investigation, sonic and supersonic conical air jet nozzles of various throat diameters were located at several model stations ahead of the model base. With the same jet mass flow issuing from the sonic and supersonic nozzles the ratio of the interaction force to jet reaction force was equal to, or in some cases, larger for the sonic nozzle configurations. The addition of fins to the body in the area containing the lateral jet increased the net side force produced by the jet. In general, these results indicated that the nozzle configuration of the jet, the axial location of the jet, the surroundings of the jet, and the character of the boundary layer on the body of revolution play an

important role in determining the magnitude of the interaction force produced by the jet.

A theoretical estimate of the interaction force generated by a two-dimensional jet was proposed by Vinson, Amick, and Leipman (Ref. 17). The jet was assumed to act like a plain spoiler in the presence of a boundary layer with a height equal to the product of the jet width per unit span and the area ratio (A/A^*) based on the jet stagnation to free-stream static pressure. Thus the interaction force represented the loading which resulted from the separated boundary layer produced by the lateral jet disturbance.

A viscous type of weak jet interaction theory was presented in Ref. 13 by Amick and Hays. In this case, the jet was assumed to be too weak to separate the boundary layer, but an oblique shock equal in strength to the ratio of p_j/p_∞ would be generated.

The theoretical inviscid loading generated by the interaction of a lateral jet from a circular nozzle into a supersonic stream was developed by C. Ferrari (Ref. 19) utilizing Newtonian approximations. As in the previous case, the assumption was made that the jet stream did not mix with the enveloping supersonic stream, and it was assumed that the lateral jet generated a detached shock which partially enclosed the jet stream tube. The pressure loading associated with the boundary-layer separation (viscous effects) generated by a lateral jet was neglected in the theoretical analysis. Another inviscid analysis using the blast wave theory has been recently developed by J. E. Broadwall (Ref. 9).

In general, the purpose of the present program is to present results similar to those described over a wider Mach number range ($M_\infty = 2.99, 3.98, \text{ and } 5.01$), Reynolds number range ($Re_x = 0.6 \text{ to } 6.0 \times 10^6$), and with a greater variety of sonic jet nozzle configurations (single and circular orifices and slots). The tests on a flat plate, a hollow cylinder, and a nine-caliber ogive containing lateral sonic jets were tested in the 12-Inch Supersonic Tunnel (E-1), von Kármán Gas Dynamics Facility (VKF), Arnold Engineering Development Center (AEDC), Air Force Systems Command (AFSC). These results are compared with various theoretical and other experimental results.

2.0 EXPERIMENTAL APPARATUS AND TECHNIQUES

2.1 WIND TUNNELS

The 12-Inch Supersonic Tunnel (E-1) (Fig. 2) is an intermittent, variable density wind tunnel with a manually adjusted, flexible-plate-type nozzle. The tunnel operates at Mach numbers from 1.5 to 5 at

stagnation pressures from 5 to 60 psia and at stagnation temperatures up to about 100°F. A description of the tunnel and its calibration is given in Refs. 20 and 21.

2.2 MODELS

Three basic stainless steel models, consisting of an 8- by 15.50-in. flat plate, a 3.50-in. -diam hollow cylinder, and a nine-caliber, 3.50-in. -diam tangent ogive, were used in the experimental program. All models were strut mounted off the tunnel floor and instrumented with 0.05 outside diameter pressure taps. All model surfaces containing pressure taps were finished to 20 micro-inches (rms).

2.2.1 Flat Plate

The flat plate model shown in Fig. 3 was instrumented with 101 static pressure taps. Interchangeable nozzle blocks containing various sonic nozzle configurations (single and multiple circular nozzles and rectangular nozzles with variable spans) were tested and are also listed in Fig. 3. The "O"-ring seals were fitted around the nozzle block to prevent high pressure air leakage. The orientation of the nozzle blocks with respect to the free-stream flow is shown in Figs. 3 and 4.

To measure the net interaction loads generated by the lateral jets on the flat plate, two moment strain-gage sections were cut into the exterior surface of the high-pressure air jet line (see Fig. 3) which was also part of the support structure for the flat plate. The gage sections consisted of diametrically opposite flat surfaces at two axial positions.

Two total head rakes were used in conjunction with the flat plate test. The first rake was a conventional boundary-layer rake which could be moved to any model station from $x = -3.20$ to 4.50 in. A second rake, which was over four inches high, was used to monitor the pitot pressure variations in the lateral air jet stream at model station 5.25 in. (see Fig. 4).

2.2.2 Hollow Cylinder

An illustration of the hollow cylinder model is shown in Fig. 5. A 0.50-in. outside diameter tube attached along the inner surface of the hollow cylinder supplied high pressure air to circular interchangeable nozzle blocks. The air jet nozzle opening was located on the ring opposite the split ring tabs, and a rubber "O-ring" seal was used to prevent air leakage around the split ring nozzle blocks. The nozzle configurations

consisted of a single 0.25-in. -diam circular nozzle and a rectangular nozzle aligned radially with curvature lengths of one and three inches and width of 0.050 in. The hollow cylinder was instrumented with 40 static pressure taps.

2.2.3 Ogive

The front section of the hollow cylinder was detachable and could be replaced with a nine-caliber tangent ogive nose (see Fig. 5). In the ogive-cylinder configuration a total of 41 pressure taps were used, and the air jet nozzle configurations were similar to the ones used in the hollow cylinder tests.

2.3 INSTRUMENTATION AND PRECISION

A rotary valve pressure scanning system utilizing 1-psid and 15-psid transducers was used to measure the model surface pressures. Additional 5-psid and 50-psid transducers were used to measure total head rake pressures. All transducer systems were referenced to essentially a vacuum (less than 50 microns of mercury in most cases) and were calibrated to provide three ranges for each transducer. The uncertainty of the pressure measurements was not more than ± 0.005 psia for the 1-psid transducer to ± 0.250 psia for the 50-psid transducer.

The model support system for the flat plate was gaged as a two-component moment type of balance. At the upstream gage, the maximum allowable moment was 1400 in. -lb and at the downstream gage, 2,000 in. -lb, with an overall force repeatability of ± 0.6 lb in the absence of any zero shifts. As a result of some gage output zero reading shifts, the test results were evaluated on the basis of the faired curves through the gage readings.

Some shadowgraph pictures were made of the flat plate, but for the most part flow patterns were recorded with schlieren and fluorescent oil flow pictures.

3.0 TEST PROCEDURES AND CONDITIONS

Preliminary pressure tests were made to evaluate the properties of the flow field over the flat plate. The static pressure distribution and boundary-layer thickness over the flat plate were measured at Mach numbers 2.99 and 3.98 in the Reynolds number range of 10^6 to 10^7 based on the length from the model leading edge to the boundary-layer rake.

The following tables contain the range of jet pressure ratios (p_j/p_∞) covered for each model nozzle configuration at each Mach number:

JET PRESSURE RATIOS

Flat Plate

Nozzle Configuration			p_j/p_∞ Range		
	Circular	Rectangular	At Free-Stream Mach Number		
d_j , in.	e/d_j	l/d_j	2.99	3.98	5.01
0.250	-	-	10→730	30→1590	30→2000
0.125	-	-	60→900	30→1740	470→2000
↓	12	-	470	30→900	480
	6	-		30→900	
	3	-	220→380	70→500	100
0.131	-	24	10→120	30→300	45→470
0.057	-	17.5	20 , 240	25→470	
↓		35		30→470	
		53		30→1570	
0.028	-	107	10→360	5→880	30→980
Re_x Range $\times 10^{-6}$			0.5 1.8	0.6 1.8 3.6	2.2

Hollow Cylinder

$$M_\infty = 3.98$$

Nozzle Configuration	p_j/p_∞ Range
single circular nozzle $d_j = 0.25$ in.	34→950
rectangular nozzle $d_j = 0.05$ in., $l/d_j = 20$ $d_j = 0.05$ in., $l/d_j = 60$	34→200 100→200
$Re_x \times 10^{-6}$	2.1 and 3.9

Nine-Caliber Ogive

$$M_\infty = 3.98$$

Nozzle Configuration	p_j/p_∞ Range
single circular nozzle $d_j = 0.25$ in.	200→900
$d_j = 0.25$ in. with a boundary-layer trip on the ogive nose	200→900
rectangular nozzle $d_j = 0.05$ in., $l/d_j = 60$	30→380
$Re_x \times 10^{-6}$	3.2 and 6.1

4.0 RESULTS AND DISCUSSION

4.1 SONIC NOZZLE CHARACTERISTICS

As part of the test program, the relationship of the jet stagnation (plenum chamber) pressure with the nozzle jet reaction force and with the jet mass flow were experimentally evaluated. Two procedures were utilized; the first was an evaluation of the nozzle mass flow discharge coefficient. At a given nozzle stagnation pressure and temperature, the rate of mass decrease in a nitrogen container was compared to the ideal mass flow rate passing through a sonic nozzle of a given cross-sectional area. The second procedure was based on the ratio of the reaction force as measured by a moment balance to the ideal reaction force of a sonic nozzle.

These calibration procedures are based on the assumption that the exit Mach numbers (M_j) of the sharp edge nozzles are sonic, but the results of Ref. 22 demonstrated that the exit Mach number of sharp edge nozzles (circular or rectangular) was a function of the nozzle geometry and was supersonic ($M_j > 1$). Neglecting the fact that the nozzle exit Mach number was actually supersonic, the jet mass flows, momentum parameters, and reaction force values were evaluated as if the exit Mach number were sonic. Within the precision of the calibration procedures, the discharge coefficient accounted for the effective area in the mass flow computation and the exit Mach number in the reaction force computation. Figure 6 includes Figs. 9 and 10 of Ref. 22 and illustrates the favorable agreement of the present calibration results with those obtained by Weir, York, and Morrison (Ref. 22).

4.2 FLAT PLATE FLOW CHARACTERISTICS

Except for the pressure distribution produced by the viscous interaction associated with the leading edge of a flat plate in supersonic or hypersonic flow, and in the absence of any jet disturbance, the maximum deviation in the model surface static pressure from the calibrated free-stream static pressure was approximately 10 percent. The mean value of the model static pressure was within 5 percent of the free-stream static pressure. The analysis of the distribution of the incremental pressure change generated by a lateral jet over the plate was referenced to the actual pressure variation measured on the plate in the absence of the jet.

At Mach numbers 2.99 and 3.98, the boundary-layer characteristics were evaluated in the region occupied by the flat plate air jet nozzle

blocks. Examples of the velocity profiles obtained at Mach numbers 2.99 and 3.98 and various Reynolds numbers, 0.8 in. upstream and 3.20 in. downstream of the nozzle block, are shown in Fig. 7a. The variation of the form factor δ^*/θ with the Reynolds number based on the boundary-layer rake location relative to the flat plate leading edge is shown in Fig. 7b. Based on the results in Fig. 7 and the balance of the boundary-layer rake results, the boundary layer was turbulent at an $Re_L > 4 \times 10^6$ at Mach number 2.99 and possibly at an Re_L of 5×10^6 at Mach number 3.98. As shown in Fig. 7, a good correlation existed between Tucker's turbulent boundary-layer form factors of Ref. 23 and the present Mach number 2.99 results in the Reynolds number range above 4×10^6 . At a Reynolds number less than 10^6 at both Mach numbers, the form factors approach the theoretical laminar values predicted by Mack (Ref. 24). Based on the observation during the progress of the experimental investigation, the boundary layer at Mach number 5.01 was primarily laminar.

4.3 THE LATERAL JET FLOW FIELD

4.3.1 Influence on the Model Surface

A general description of the flow field generated by a two-dimensional lateral jet is illustrated in Fig. 8. In many ways, a jet acts like a vertical spoiler or step, insofar as being another mechanism which causes boundary-layer separation. The separation produces a local change in the flow direction, which generates an oblique shock and a rise in the pressure in the region of separation. As in the case of spoilers, the length of separation and the plateau pressure level are influenced by the state of the boundary layer and its separation; that is, whether it was a laminar, transitional, or a turbulent boundary-layer separation (see Fig. a).

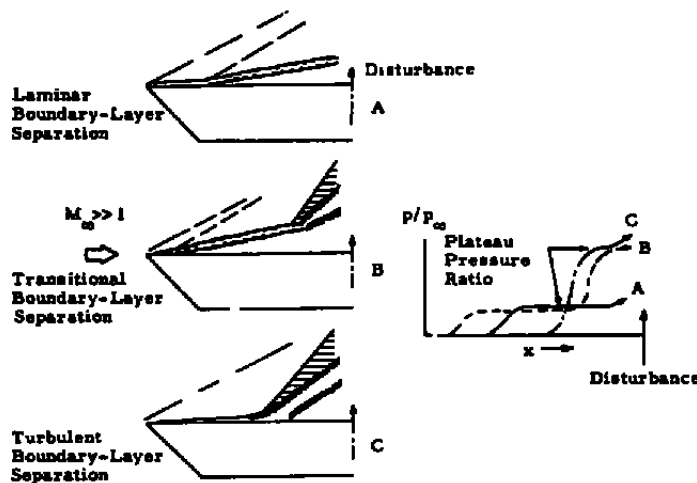


Fig. a Boundary-Layer Separation

Depending on the ratio of the jet stagnation pressure to the quiescent air pressure, a sonic jet produced a slightly curved shock, normal to the under-expanded jet stream at a given distance from the nozzle exit. In the case of a circular nozzle, this curved shock is usually referred to as a Mach disc. Lateral motion of a planar surface containing a jet or, in the present case, a lateral jet on a flat plate in a supersonic stream, produced a similarly displaced curved "jet" shock but shifted slightly downstream from its position in quiescent air. Of course, an additional shock was generated by the interference between the jet stream and the supersonic free stream, and this is herein referred to as the "jet free-stream interaction" shock.

The local flow inclosed by the separated boundary layer, the jet, and the model surface contained two experimentally observed regions of circulation (see Figs. 8 and 9). Boundary-layer separation produced the larger region of circulation, but at least one additional region of circulation existed immediately ahead of the jet. Flow in this region appeared to rotate in the opposite direction to the boundary-layer separation circulation. These circulation directions were based on the combined evaluations of oil flow, shadowgraph, and schlieren pictures.

Directly downstream of the jet (rectangular or circular) nozzle, a field of low pressures ($p \ll p_\infty$) was generated in another region of circulation which was maintained by the downstream portion of the air jet stream. Based on the oil flow pictorial evidence, the circulation immediately upstream of the nozzle was stronger than the downstream circulation; that is, the oil did not flow as rapidly or did not move at all in the region immediately aft of the nozzle. The relationship between the oil flow field over the plate and the primary pressure ridges and valleys is summarized schematically in Fig. 9.

Samples of the oil flow pictorial results with the corresponding schlieren photographs of the typical flow field generated by various nozzle jet configurations are presented in Fig. 10. Superimposed on the oil flow photographs are the corresponding isobars in the form of a pressure ratio, p/p_∞ . The boundary-layer separation locations obtained from the oil flow and schlieren pictures agreed.

A successive comparison of Figs. 10a through d will illustrate the influence of nozzle configuration on the flow field as a change was made from a single-circular to multiple-circular nozzle and finally a rectangular nozzle (slot). Also the flow field and pressure distribution produced by a jet from a slot was compared to a 1/2-in. high spoiler in Fig. 11. Except for the absence of a compression wave (jet shock) produced by an under-expanded sonic nozzle, the flow field (as shown in Fig. 11) of the

solid spoiler was similar to the air jet disturbance. The isobars ($p/p_\infty = \text{constant}$) upstream of the spoiler were shaped similarly to those resulting from the air jet. Although the disturbance generated by the lateral jet was weaker or produced a smaller flow deflection, the integrated local load and location of the center pressure of the loading produced by the air jet and plain spoiler are in reasonable agreement. This comparison, which was similar to the one described in Ref. 6, suggests that a correlation between spoilers or steps and air jets exists. One basic difference between a jet and spoiler is that an air jet does not produce any pressure drag which would be transmitted to the plate.

An example of the Reynolds number and jet pressure ratio, p_j/p_∞ , effects on the flow field and on the flat plate pressure distribution produced by a sonic jet from a slot (0.028 by 3 in.) in a Mach number 3.98 free stream is shown in Fig. 12. For a given jet pressure ratio, doubling the Reynolds number altered the local flow properties (see Figs. 12a and b), but the net interaction load ahead of the air jet nozzle (F_{N_0}/q_∞) was only slightly affected (approximately a 9 percent change). Herein, the "interaction load" refers to that force produced by the interaction of the jet with approaching boundary-layer and free-stream flow and does not include the reaction force of the jet.

At two free-stream Reynolds numbers, the influence of the jet pressure ratio on the flow properties over a flat plate is illustrated in Figs. 12b and c and a and d. As the jet pressure ratio increased, the location of the peak in the pressure distribution and the root of the jet free-stream interaction shock moved together upstream away from the jet. Doubling the jet pressure and, in this case, the jet momentum did not double the interaction force. Thus, the ratio of the interaction force ahead of the nozzle (F_{N_0}) to the jet reaction force (F_j) decreased with increasing jet pressure ratio with these particular flow conditions and model geometry. With respect to these test results, the characteristic low pressure field aft of the rectangular sonic nozzle had a span about equal to the nozzle span.

A summary of the visual evidence of the flow field generated by a lateral jet is presented in Figs. 13 and 14. These figures represent the variation of the point of boundary-layer separation with the Reynolds number at Mach number 3.98 for various nozzle configurations. Increasing the Reynolds number resulted in shifting the point of separation toward the jet nozzle (see Fig. 13). At a given Reynolds number and for a given jet momentum (a function of the product of the cross-sectional area of the jet nozzle and the jet pressure ratio), the length of separation relative to the nozzle was greater for the smaller circular nozzle than the larger one, but less than the separation length generated by a rectangular nozzle.

Figure 14 illustrates the interdependence of the jet pressure ratio and the "hole density" of a lateral jet on the length of the separated boundary layer. Increasing the circular nozzle density produced a consistent increase in the length of separation.

4.3.2 Lateral Jet Wake Flow Field

Typical schlieren pictures and pitot pressure measurements downstream of and in the lateral jet are presented in Figs. 15 and 16. The total head rake was located 5.2 in. aft of the jet nozzle. In some pictures (15a for example) a disturbance created by roughness in the model side plates has been labeled and was subsequently removed. These side disturbances had no measurable effect on the pressure results.

The influence of Reynolds number on the jet wake did not appear to be significant (see Fig. 15a), but increasing the Mach number and jet pressure ratio tended to increase the pitot pressure gradient in the jet stream (compare Fig. 15b with c). As expected, the jet penetration increased with the jet momentum and decreasing Mach number.

In some cases, strong jets were generated which distorted the entire flat plate leading edge shock (see Fig. 15d and f). Under these conditions and based on the results obtained with weaker jets, the interaction force was usually higher than the anticipated value. Of course the plate span (8 in.) would also have an effect on the correlation of the interaction force, but the span size did not have as strong an influence on the interaction load correlation as the length of the plate ahead of the jet nozzle.

A comparison of the schlieren pictures taken at free-stream Reynolds number (Re_x) of 0.5×10^6 with one at 1.7×10^6 in Fig. 15a illustrates a comparison of a laminar with a transitionally separated boundary layer. The best example of the pictures presented herein of a turbulent-separated boundary layer is shown in Fig. 15b for $p_j/p_\infty = 29$. This example is a marginal case because the boundary layer at the origin of separation was still laminar, but the balance of the region of separation was turbulent. The separations shown in Figs. 11, 15c, d, and f are indicative of transitional boundary-layer separations, whereas Figs. 10a, b, 15e, and 16b are representative of laminar separations.

4.4 PRESSURE DISTRIBUTIONS AND MOMENT LOADING

The influence of jet nozzle configuration, Reynolds number, jet pressure ratio (p_j/p_∞), and Mach number on the pressure distribution and

radial moment loading about the area centroid of the cross section of the jet nozzle are presented in Figs. 17 through 25. The pressure distributions represent the variation in the surface static pressure along the central axis of the flat plate with respect to center of the jet nozzle block. The resultant interaction load generated by the lateral jet was evaluated in the following manner:

$$F_{N_I} = F_{N_x} = 2 \int_0^\pi n \, d\phi$$

where

$$n = p_\infty \int_{d_j/2}^{R\phi} (\Delta p/p_\infty) r \, dr$$

The factor n actually represents the local moment about the air jet cross-sectional area centroid along a particular radial line, ϕ (see Fig. 3 for a definition of ϕ). The local force along a radial ϕ would be evaluated as follows:

$$f_{n_I} = p_\infty \int_{d_j/2}^{R\phi} (\Delta p/p_\infty) \, dr$$

and the local center of pressure would be evaluated as

$$x_{cp} = n/f_{n_I}$$

The subscript, x , of F_{N_x} represents the axial limit of integration over the flat plate. Therefore the limits $d_j/2$ to $R\phi$ represent the integral value along one angular ray ($\phi = \text{constant}$) from the lip of the jet nozzle to either the limit defined by the geometry of the model (the flat plate leading edge or sides) or the axial limit of integration aft of the nozzle, $x = 0, 2$, or 4.5 in. downstream of the nozzle. For example, F_{N_0} represents all the load generated over the entire flat plate upstream of the lateral jet. Hereafter the term n will be referred to as the local "load distribution" although actually it is the local moment loading about the air jet nozzle area centroid.

The influence of multiple circular nozzle density on the pressure and load distribution generated over a flat plate at Mach number 3.98 by a lateral jet is presented in Fig. 17. For a constant jet pressure ratio, the separation length increased with an increase in the number of 0.125-in. circular sonic nozzles. In the case of the 0.131- by 3-in. slot and the nine hole multiple nozzle configurations, the jet mass flows (momentums) were nearly equal and produced similar axial pressure and radial load (n) distributions.

A basic difference in the interaction loading produced by a single circular nozzle and a slot is illustrated in the load distribution shown

in Fig. 17. In general, a major portion of the force generated by a single circular nozzle was located aft of the nozzles ($\phi > 90$ deg) along radial lines between $\phi = 120$ and 150 deg. The lateral jet from a circular nozzle and the detached shock wave which partially envelopes the jet stream generated boundary-layer separation upstream and on each side of the circular nozzle. This boundary-layer separation and the pressure rise associated with the enveloping detached shock wave generate a pressure field similar to the one shown in Fig. 10a and schematically illustrated in Fig. 9b. Of course, the magnitude of this high pressure ridge shown in Fig. 9b decreased as it extended downstream of the circular nozzle.

In contrast, a rectangular nozzle or closely spaced multiple hole nozzle generated a load distribution which was primarily located ahead of the jet. Rectangular jets produced this type of load distribution at all jet pressure ratios, Mach numbers, and Reynolds numbers investigated in this program.

The influence of the span of a rectangular sonic nozzle ($d_j = 0.057$ in.) on the pressure and load distributions produced by the jet is summarized in Fig. 18. In this case, the Reynolds number was 1.8×10^6 and the pressure distributions and schlieren pictures indicated that the boundary-layer separation was transitional. As in the case of a single circular nozzle with turbulent boundary-layer separation, a large percentage of the load occurred downstream of the rectangular nozzle with a one-inch span. For the two- and three-inch span slots, the typical concentration of the load ahead of a rectangular nozzle was obtained. Reducing the rectangular nozzle span reduced the flow field to one similar to that obtained with a single circular nozzle.

In Fig. 19 the pressure distribution and the schlieren pictures obtained at Reynolds number 0.6×10^6 indicated that the separation was laminar, and at 3.5×10^6 it appeared to be turbulent. Also presented in this figure is the pressure distribution along the central axis of the plate in the absence of a lateral jet at a Re_x of 0.6×10^6 . This illustrates the influence of the viscous leading edge effects which were accounted for in the analysis of the lateral jet pressure data. Most of the loading produced by the interaction of a jet from a single circular nozzle with the supersonic stream was located downstream of the nozzle when the separated boundary layer was turbulent or transitional, and upstream when it was laminar. In this case, the larger interaction force was obtained in the presence of laminar separation.

The influence of Reynolds number on 0.131- and 0.028-in. width slots is shown in Figs. 20 and 21. The pressure distributions for these slots at the minimum Reynolds number (0.6×10^6) were in this case

indicative of laminar boundary-layer separation. At the Reynolds number of 1.5×10^6 , the pressure distributions indicate that the separated boundary layer was transitional. These estimates of the character of the separated boundary layer were confirmed by schlieren pictures of the flow field. Most of the interaction loading promoted by a lateral jet from a rectangular nozzle occurred upstream of the nozzle and was essentially independent of the character of the separated boundary layer.

An example of the pressure and load distributions generated at Mach number 3.98 over a flat plate by a sonic lateral jet of various strengths (p_j/p_∞ ratios) from rectangular and circular nozzles are shown in Figs. 22 and 23. These distributions were obtained at a Reynolds number of 1.8×10^6 . As expected, an increase in jet pressure increased the interaction load distribution.

The Mach number effect on the local distribution produced by a 0.028-in. width rectangular and a 0.125-in. -diam circular jet is shown in Figs. 24 and 25. The pressure distributions and schlieren observations of the slot (Fig. 24) indicate that the separation was laminar at Mach number 5.01, whereas at Mach numbers 2.99 and 3.98 the state of separation was transitional. Although not clearly indicated in the pressure distributions of the circular jet in Fig. 25, the Mach number 5.01 schlierens indicated that the separated boundary layer was laminar, and at Mach numbers 2.99 and 3.98 the schlierens indicated that the boundary-layer separation was transitional.

4.5 TWO-DIMENSIONAL THEORETICAL ANALYSIS

4.5.1 Viscous Jet Interaction Load

Based on the analogy described in Ref. 6 which compared the flow phenomenon of a plain spoiler (or step) with a two-dimensional lateral (spoiler) jet, the following analysis is proposed for the case of a lateral jet on a surface in a supersonic stream. It has been shown experimentally that a jet disturbs a turbulent boundary layer in the same manner as a plain spoiler (see Ref. 6, pp. 65 and Ref. 15, Fig. 7). Also, in the presence of transitional boundary-layer separation, similar loading was generated by a plain spoiler and a jet spoiler (see Fig. 11). The step causes the boundary layer to separate at some given distance ahead of the step with a resulting increase in the pressure in the region of separated flow.

In an attempt to provide a theoretical basis for the interaction effects observed in experiments of a lateral jet from a body of revolution

at supersonic speeds, an analysis was made by Vinson, et. al. (Ref. 17). The assumption was made that the jet expanded isentropically without mixing with the surrounding airstream, separated the boundary-layer flow, and caused the free-stream flow to turn through an angle, α , as shown in Fig. b.

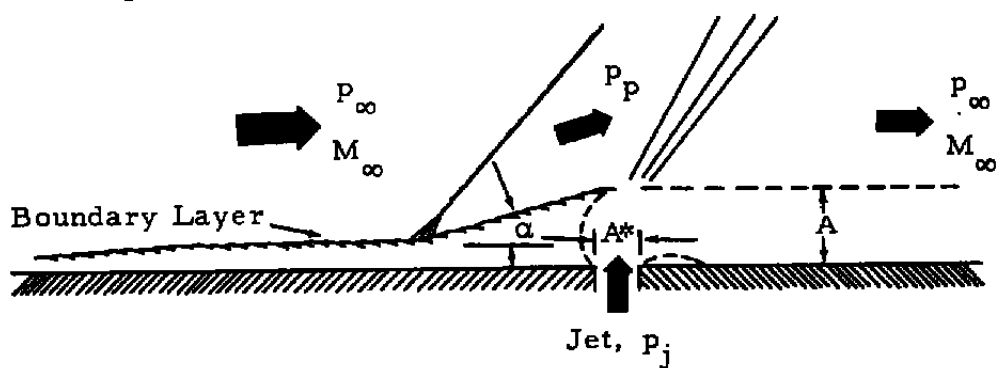


Fig. b Theoretical Model

The area ratio A/A^* , which is only a function of the pressure ratio, p_j/p_∞ , becomes the ratio of the effective jet spoiler height to the effective jet width for a unit span. At various free-stream conditions, rectangular nozzle widths, and jet pressure ratios (p_j/p_∞), measurements of the effective two-dimensional jet spoiler height as defined in Fig. 26 were compared to the area ratio term (A/A^*). These measurements were obtained from schlierens similar to the ones shown in Figs. 10d, 11a, and 12. The effective jet spoiler height based on the flow direction associated with the separated boundary layer coincided with the peak in the curvature of the jet shock (see Fig. 26).

At various free-stream Mach numbers and two-dimensional jet nozzle widths, a comparison of the measured effective jet spoiler height with the area ratio based on the jet pressure ratio is shown in Fig. 26. The smaller nozzle width for a given jet pressure ratio produced a higher ratio of effective spoiler height to nozzle width. With an increase in Mach number for a given jet pressure ratio, the effective spoiler height based on the experimental, faired curves tends to decrease slightly.

Since a lateral jet promotes boundary-layer separation, the factors which influence regions of separated flow should also apply in part to the problem of jet-separated boundary-layer interaction. Some of these factors are (1) Reynolds number, (2) the type of flow separation (laminar or turbulent), (3) Mach number, (4) location of transition within the separated flow region, and (5) the strength or effective spoiler height of the jet. For the present analysis, these factors are important because

of their influence on the pressure distribution within the region of separated flow preceding the jet.

The pressure rise produced by a separated boundary layer ahead of a vertical spoiler has been theoretically and empirically defined for laminar and turbulent boundary-layer separation as a function of free-stream Mach number and the Reynolds number of separation. A graphical presentation of the theoretical and experimental results from Refs. 27 through 33 of the relationship of the pressure rise (the plateau pressure) produced by a separated boundary layer as a function of the free-stream conditions, Mach number and Reynolds number, is shown in Fig. 27. In the present analysis, the plateau pressures resulting from laminar and turbulent boundary-layer separation were evaluated on the basis of Ref. 27 by Gadd and Ref. 28 by Erdos, respectively.

Since the separated boundary layer acted as a flow deflector, the flow deflection angle was selected from the oblique shock table of Ref. 25, which would produce a pressure rise equal to the separated boundary-layer plateau pressure. This assumption provided a relationship between the ratio of the pressure rise to the flow deflection angle and the free-stream Mach number for various separation Reynolds numbers and is shown in Figs. 28a and b for laminar and turbulent boundary-layer separation. Included in Fig. 28 are experimental data from Refs. 29, 30, and 33. Thus the estimate of the flow deflection angle, α , the effective jet spoiler height, h , and the pressure rise produced by the boundary layer provided the information required to evaluate the viscous portion of the lateral jet interaction force acting upstream of the jet.

$$F_{N_i} = \left(\frac{\Delta p}{p_\infty} / \alpha \right) p_\infty a \frac{h}{\tan \alpha} \text{ per unit width}$$

When nondimensionalized by F_j the expression becomes

$$\frac{F_{N_i}}{F_j} = \frac{\left(\frac{\Delta p}{p_\infty} / \alpha \right) \left(\frac{h}{d_e} \right)}{\left[1.268 \left(\frac{p_j}{p_\infty} \right) - 1 \right]}$$

where the expression for h/d_e is defined in Fig. 26 by the A/A^* ratio, and it was assumed that $\alpha/\tan \alpha \approx 1$.

The influence of the separation Reynolds number, jet pressure ratio, and free-stream Mach number on the two-dimensional jet viscous interaction to jet reaction force ratio is shown in Fig. 29. For a two-dimensional lateral jet, the following conditions will theoretically increase the ratio of the viscous portion of the interaction loading to the jet reaction force: (1) a decrease in the jet pressure ratio, (2) an increase in the free-stream Mach number, (3) a decrease in the separation Reynolds

number, and (4) a change in the character of the boundary-layer separation from laminar to turbulent. If an allowance was made for the actual influence of the jet width on the effective spoiler height as shown in Fig. 26, then a decrease in the nozzle width in some cases would also theoretically generate a higher interaction force ratio (FN_i/F_j).

4.5.2 Inviscid Jet Interaction Load

The previous analysis does not include the pressure loading or interaction force resulting from the inviscid interaction of the jet stream with the free-stream flow. In the absence of boundary-layer viscous effects, the shock produced by the jet would locally promote additional loading on the model surface in the immediate vicinity of the air jet nozzle. The assumption is made that the jet acts as a two-dimensional flat-nosed blunt body having a height, h , in a supersonic stream.

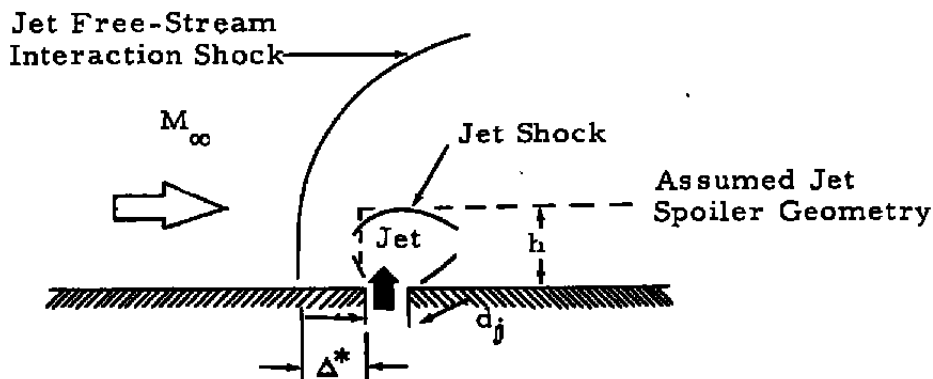


Fig. c Inviscid Theoretical Flow Field

The maximum pressure loading on the plate between the jet nozzle and the detached shock (jet free-stream shock) was assumed to be equal to the product of the static pressure obtained downstream of a normal shock and the shock detachment distance, Δ^* .

An estimate of the shock detachment distance was obtained from Ref. 34 (pp. 253, 254) and in terms of the present nomenclature, is as follows:

$$\frac{\Delta^*}{h} = \left(\frac{\rho}{\rho_0} \right) 1.578 \sqrt{\frac{5 + M_\infty^2}{6 M_\infty^2}} \quad \text{when} \quad \gamma = 1.4$$

The incremental increase in pressure generated by the normal shock would be defined as

$$\frac{\Delta p}{p_\infty} = \frac{7}{6} (M_\infty^2 - 1)$$

Therefore the ratio of the two-dimensional interaction force to the sonic jet reaction force can be estimated from the following relationship:

$$\frac{F_{Ni}}{F_j} = \frac{\left(\frac{\Delta p}{p_\infty}\right) \left(\frac{\Delta^*}{h}\right) \left(\frac{h}{d_s}\right)}{\left[1.268 \left(\frac{p_j}{p_\infty}\right) - 1\right]}$$

This relation is assumed to represent the maximum inviscid interaction load that could be generated on a planar surface by the interaction of a two-dimensional lateral jet with the supersonic free stream.

4.5.3 Net Interaction Load

Observations of the experimental pressure distributions produced by a lateral jet in a supersonic stream revealed that the initial pressure rise can be attributed to boundary-layer separation, but the additional pressure rise located between the nozzle and the jet free-stream interaction shock was assumed to be created by the interaction of the jet stream with the supersonic free stream (see Figs. d and 17).

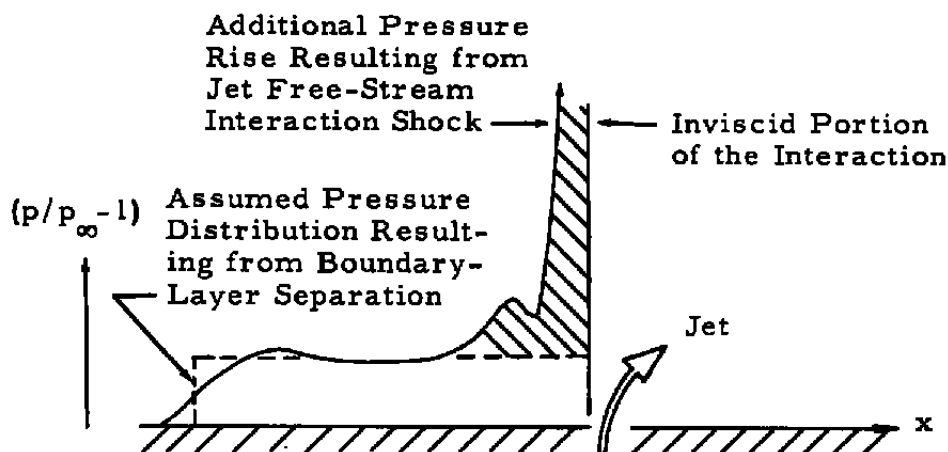


Fig. d Typical Two-Dimensional Pressure Distribution

As a first approximation, it has been assumed that the net interaction load may be obtained by simply adding the viscous and inviscid theoretical estimates.

Thus

$$\frac{F_{Ni}}{F_j} (\text{net}) = \frac{F_{Ni}}{F_j} (\text{inviscid}) + \frac{F_{Ni}}{F_j} (\text{viscous})$$

for a given jet spoiler height or in this case jet pressure ratio, p_j/p_∞ . The results are summarized in Fig. 29.

4.6 THREE-DIMENSIONAL THEORETICAL ANALYSIS

4.6.1 Viscous Jet Interaction Force

To utilize the results obtained in the two-dimensional analysis in evaluating the interaction load generated by a circular jet, a change in the assumed pressure distribution ahead of the jet must be made. The isobars of the pressure distribution generated by the interaction of a circular jet with a supersonic stream were observed to lie in concentric elliptical or nearly circular lines about the jet in the two upstream quadrants. Therefore the interaction load on a planar surface was also assumed to be distributed in the form of a concentric circle about the circular nozzle. The area over which the separated boundary-layer plateau pressure acts was defined as being equal to

$$\frac{1}{2} \left(\frac{h}{\tan \alpha} \right)^2 \pi$$

where "h" is the effective circular nozzle spoiler height for a particular nozzle jet pressure ratio (p_j/p_∞), and α is the flow deflection angle of the separated boundary layer. Therefore the interaction force acting upstream of the jet becomes

$$F_{N_1} = \left(\frac{\Delta p}{p_\infty} / \alpha \right) p_\infty a \frac{\pi}{2} \left(\frac{h}{\tan \alpha} \right)^2$$

Since the ratio ($\alpha/\tan \alpha$) may be assumed to be equal to unity, the ratio of the viscous interaction force to jet reaction force was evaluated in the following manner:

$$\frac{F_{N_1}}{F_j} = \frac{2 \left(\frac{\Delta p}{p_\infty} / \alpha \right) \left(\frac{h}{d_j} \right)^2 \cot \alpha}{\left[1.268 \left(\frac{p_j}{p_\infty} \right) - 1 \right]}$$

Utilizing theoretical oblique shock results, the flow deflection angle, α , can be related to the plateau pressure of the separated boundary layer. The other factors in the above expression are known except the ratio of the effective jet spoiler height to jet diameter. The relationship between the effective spoiler height of a circular jet operating at various jet pressure ratios was determined experimentally and is shown in Fig. 30. As in the case of the two-dimensional (rectangular) jet, schlierens were used as illustrated to evaluate the jet spoiler height. The jet spoiler height to jet nozzle diameter was primarily a function of the jet pressure ratio and independent of the free-stream Mach number in the range from 4 to 5, Reynolds number, and nozzle diameter in the range $0.062 \leq d_j \leq 0.25$ in.

An estimate of the viscous effects on the interaction forces generated by a circular lateral jet in a supersonic stream are shown in Fig. 31.

Because of the influence of the flow separation angle in the interaction force expression, an increase in the ratio of the interaction force to the jet reaction force occurred with an increase in the Reynolds number (Re_S) or when the boundary-layer separation changed from a turbulent to laminar state. Unlike the two-dimensional theoretical results, an increase in the jet pressure ratio for the circular nozzle increased the viscous portion of the resultant interaction force.

4.6.2 Inviscid Jet Interaction Force

Assuming that the jet is strong or that the boundary-layer thickness is insignificantly small relative to the jet exhaust nozzle diameter, the mechanism involves a jet which expands from an outlet and causes a strong compression wave in the supersonic free stream to envelope the upstream portion of the lateral circular jet. The problem was analyzed by Ferrari in Ref. 19 for a circular jet located on a flat plate and a cylindrical body. The general model for this analysis is illustrated below (Fig. e):

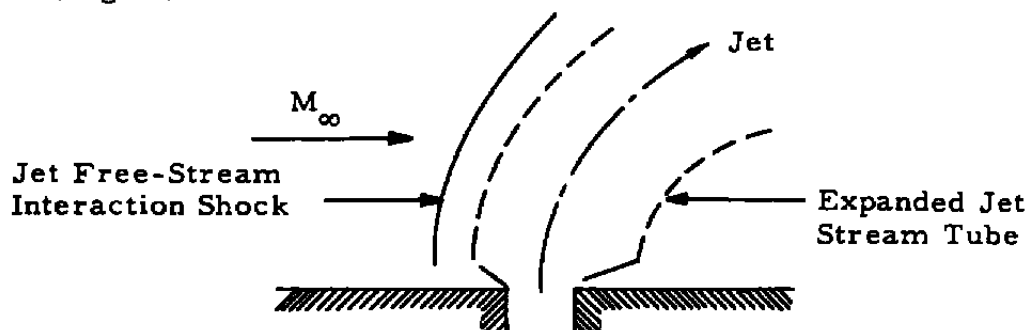


Fig. e Theoretical Model

In developing this theory it was assumed that no boundary-layer flow is present, that no mixing between jet and free stream occurs, and that a detached shock wave is generated by the jet. Using hypersonic approximations, the shape of the detached shock and the affected surface area containing the circular jet are determined on the basis of an assumed contour for the expanded jet stream. This theoretical approach predicts an increase in the inviscid interaction force ratio (F_{N1}/F_j) with Mach number and decreasing jet pressure ratio.

Since the pressure distribution resulting from the separated boundary layer (viscous effect) was assumed to be in the form of a step function, an additional rise above the plateau pressure was attributed to the inviscid interaction phenomenon (see Figs. f and 17).

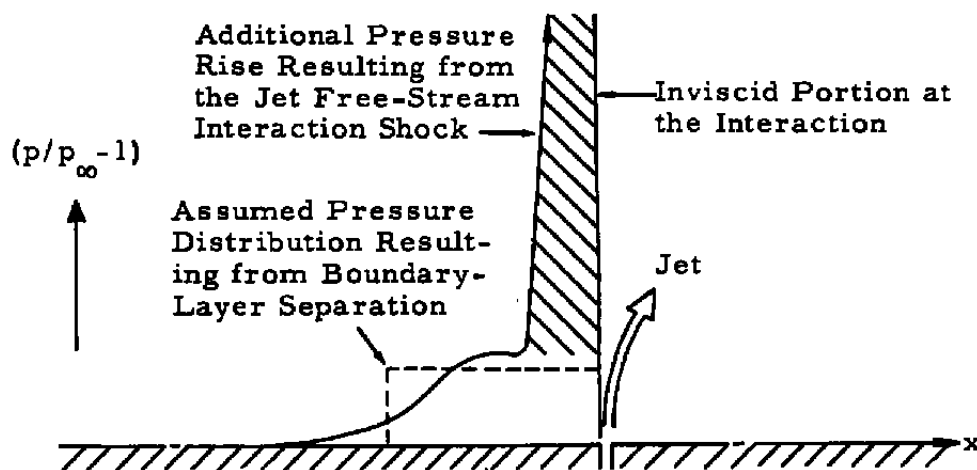


Fig. f Assumed Pressure Distributions

A description of the procedure for computing this inviscid jet interaction force described in Ref. 19 is presented in the appendix. An estimate of the combined effects of the viscous and inviscid interaction generated by a circular lateral jet was obtained by adding the theoretical inviscid interaction forces for a given jet pressure ratio and Mach number obtained in Ref. 19 to the viscous estimates presented herein. The results of this combination of interaction forces are presented in Fig. 31.

4.7 EXPERIMENTAL FLAT PLATE RESULTS

4.7.1 Two-Dimensional Analysis

Since the theoretical results were based on a two-dimensional analysis, a comparison was made with the experimentally evaluated local interaction force (f_{n1}) upstream of the jet along the central ray ($\phi = 0$) of the plate. As shown in Fig. 32, the theoretical and experimental results indicated that an increase in the two-dimensional force ratio (f_{n1}/f_j) was obtained with an increase in free-stream Mach number and decrease in jet pressure ratio (p_j/p_∞). Also the experimental results indicated that a decrease in the jet width or increase in the rectangular nozzle aspect ratio (l/d_j) increased the two-dimensional interaction force ratio and the agreement between the experimental and theoretical results improved. These results indicated that the high aspect ratio rectangular nozzles produced an interaction force more nearly equal to the two-dimensional theoretical analysis which assumes that the aspect ratio is infinite.

The two-dimensional interaction to jet reaction force ratios were nearly equal when produced by 3-in. span rectangular nozzles of different

widths but with the same jet mass flow or in this case jet momentum. For example, compare the force ratio (f_{nj}/f_j) produced by the 0.028- by 3-in. slot at a jet pressure ratio of 500 with the force ratios associated with the 0.131- by 3-in. slot at p_j/p_∞ of 100. Therefore this two-dimensional analysis and the subsequent results presented herein, pertaining to the net experimental interaction force produced by lateral sonic jets, indicated that the interaction force appeared to correlate best as a function of the jet mass flow (or momentum). Although the present theoretical approach was based on the relationship of the interaction force ratio and the jet pressure ratio instead of the jet momentum, the theory as shown in these and subsequent figures did provide a satisfactory estimate of the interaction force and indicated the influence of the Mach number, the jet strength (p_j/p_∞), and character of the boundary layer on the interaction force ratio.

An indication of the three-dimensional character of the interaction produced by a jet from a single circular nozzle as compared to a multiple nozzle or slot is presented in Fig. 33 for $\phi = 0$. As the density of the multiple circular nozzle increased ($e/d_j \rightarrow 0$) and approached the cross-sectional area of the slot, A_j (holes) $\rightarrow A_j$ (slot), the interaction force ratio approached the value produced by the jet from the slot.

For a given nozzle width ($d_j = 0.057$ in.) the effect of the slot span on the local interaction force ratio generated along the central ray ($\phi = 0$) ahead of the jet is shown in Fig. 34. Increasing the nozzle span resulted in an increase in the ratio of the local interaction force to jet reaction force. As in the case of the 0.131-in. slot, an increase in jet momentum (an increase in p_j/p_∞) of the 0.057-in. slot decreased the interaction force ratio.

4.7.2 Net Interaction Force

The net interaction load (FN_O) ahead of the nozzle for various free-stream Mach numbers, Reynolds numbers, and nozzle configurations versus the jet momentum (mass flow) parameter, $(p_j/p_\infty) A_e$, is presented in Fig. 35. For an equivalent jet momentum and Reynolds number, the rectangular nozzles generated larger interaction forces than the circular nozzles. In general, an increase in the hole density of the nozzle configuration increased the interaction force for a given jet momentum at $(p_j/p_\infty) A_e > 5$ and Reynolds numbers $\geq 1.9 \times 10^6$ (see Fig. 35b). Not only the local interaction (f_{nj}) but also the resultant interaction force (FN_O) tend to indicate that a reduction in the slot span reduced the interaction force value for a given jet momentum (see Fig. 35c).

Within the accuracy of the integrated test results, the influence of the state of the boundary layer (or free-stream Reynolds number) was

not significant at Mach numbers 3.98 and 5.01. In the case of the Mach number 2.99 results (Fig. 35a), the higher ratio of the interaction force to the free-stream dynamic pressure was obtained at the lowest Reynolds number.

Except for the Mach number 2.99 data with laminar separation ahead of the lateral jet, the best fairing of the results of Fig. 35 was of the following form:

$$\frac{F_{Ni}}{q_{\infty}} = \text{constant} \left(\frac{p_j}{p_{\infty}} A_e \right)^{3/4}$$

The jet pressure ratio (p_j/p_{∞}) was taken as an upper limit in the theoretical relationships of Refs. 17 and 19, expressing the interaction force as a function of the jet pressure ratio, and the following result was obtained:

$$\frac{F_{Ni}}{q_{\infty}} = \text{constant} \left(\frac{p_j}{p_{\infty}} \right)^{3/4} A_e, \quad \frac{p_j}{p_{\infty}} > 100$$

Although these theoretical and experimental relationships are not exactly identical, for a given jet nozzle cross-sectional area, the rate of change of the interaction force with the jet pressure ratio was similar.

Since a large share of the load generated by the interference of a jet from a single circular nozzle occurred aft of the nozzle station, the inclusion of this load increased the net interaction load as shown in Fig. 36a. In this figure, the resultant interaction force from the model leading edge to model stations x are plotted against the aft limit of integration, x/d_j . The value at $x/d_j = 64$ represents an estimate of the interaction load obtained from the internal strain-gage force measurements. These results suggested that an increase in the aft length of the plate would increase the net interaction force for a circular nozzle up to a maximum value at $x/d_j = 36$ ($x/L = 1.6$) for $p_j/p_{\infty} = 100$.

An increase in the aft limit of integration for the rectangular nozzle produced a slight decrease in the resultant interaction force (see Fig. 36b). As in the case of the circular nozzle, a high pressure field partially enclosed and extended downstream of the rectangular nozzle as illustrated in Fig. 9, but the influence of this high pressure field on the plate was apparently not large enough to outweigh the negative loading located immediately aft of the rectangular air jet.

The Mach number influence on the interaction loading is summarized in Fig. 37 for rectangular and circular nozzles. In general, the interaction loading decreases with increasing Mach number for a constant jet momentum which is proportional to $(p_j/p_{\infty}) A_e$. For a constant jet

momentum, in general, the rectangular nozzles generated a larger interaction force than the circular nozzles as the free-stream Mach number was increased (compare Figs. 37a with b). At Mach number 2.99 and $Re_x = 1.9$ to 3.7×10^6 , the maximum interaction force ($FN_{4.5}$) produced by the circular nozzle was about equal to the force produced by the rectangular nozzle.

4.7.3 Interaction Force Center of Pressure

The center of pressure (cp) location of the interaction load ahead of the lateral jet at Mach numbers 2.99, 3.98, and 5.01 is shown in Fig. 38. Increasing the jet momentum moved the center of pressure (cp) upstream. At Mach numbers 2.99 and 3.98, the cp location was displaced further upstream from a rectangular nozzle jet, but at Mach number 5.01 it was displaced further upstream from the circular jet. The effect of Reynolds number on the cp location was not significant.

4.7.4 Theoretical and Experimental Comparisons

The jet interaction results of Fig. 35 are presented again in Fig. 39 in the form of the ratio of the interaction force to the jet reaction force (FN_O/F_j) versus the jet pressure ratio (p_j/p_∞) and compared with various theoretical estimates. The correlation of the theoretical and experimental results improved with increasing Mach number. Included on each figure is the theoretical estimate of the inviscid interaction force and the theoretical net interaction force which includes the viscous and inviscid effects.

In general, the experimentally evaluated ratio of interaction force to jet reaction force produced by a circular nozzle fell within the theoretical estimates (see Figs. 39a, c, and e). These results indicated that the interaction force ratio (FN_O/F_j) increased with decreasing jet pressure ratio.

Although the theoretical results show that the interaction produced by laminar separation was larger, the scatter in the experimental results concealed the influence of the character of the separated boundary layer on the interaction force produced by a circular jet. Similarly, the theoretical results indicate that the interaction force ratio increased with the free-stream Mach number, but the experimental results do not clearly substantiate this trend.

The rates of change in the interaction force ratio produced by the rectangular nozzle jets with the jet pressure ratio agree with the theoretical trends (see Figs. 39b, d, and f). The theoretical results bracket

most of the experimental results at Mach numbers 3.98 and 5.01. In general, the experimental interaction force ratios exceeded the Mach number 2.99 theoretical estimates. As in the case of the circular nozzles, the experimentally determined rectangular nozzle jet interactions do not clearly define the influence of the character of the boundary layer on the jet interaction force ratio.

Based on the present experimental results obtained at Mach number 5, the variation of the resultant control force produced by a lateral sonic jet located on a flat surface is shown in Fig. 40 at various altitudes within the flight corridor. In this particular case the force produced by a 0.028- by 3-in. slot was compared with the force produced by a single 0.25-in. -diam circular nozzle operating at the same jet momentum, and the comparison indicates that the slot was more effective at all altitudes. Since the variation in Mach number had only a 10 percent effect on the interaction force produced by the lateral jet, these particular curves of jet control force versus altitude are applicable in the Mach number range from 2.99 to 5.01. The effect of operating a lateral jet at the lower altitudes ($\approx 10^3$ ft) theoretically increased the resultant jet control force by a factor of at least four times the value present at altitudes above the flight corridor (altitudes $\approx 10^5$ ft).

An empirically determined correlation factor was proposed in Ref. 13, which would include the effects of the surface geometry of the flat plate, the relative location of the circular nozzle jet, and the sonic nozzle diameter on the interaction force ratio. This correlation technique was applied to the present integrated pressure results and is presented in Fig. 41. Although the jet nozzle diameter appeared to be correlated, the plate geometry yields three distinct curves for three ratios of plate length containing the interaction load to the length from the model leading edge to the jet location (L/X). For a given jet pressure ratio and nozzle diameter, this disagreement indicated that the rate of change of the resultant interaction load increased more rapidly than indicated by the correlation factor as the nozzle location was moved forward of the flat plate trailing edge.

4.8 LATERAL JET FROM A BODY OF REVOLUTION

In many respects the flow generated by a lateral jet from a sonic nozzle on a hollow cylinder or a nine-caliber ogive was similar to a jet from a sonic nozzle on a flat plate. In Figs. 42 through 44, examples of the pictorial representation of the flow generated about a hollow cylinder and an ogive by a lateral jet are presented in the form of oil flow and schlieren pictures. As in the case of the flat plate results, the oil flow picture (Fig. 42a) and the pressure distributions revealed the same

typical high pressure ridges associated with circular nozzles. Also the low pressure field just downstream of the nozzle between these high pressure ridges was observed. As in the case of the flat plate, this low pressure field downstream of the nozzle promoted little oil flow. A similar correlation pertaining to a rectangular nozzle jet flow field on a hollow cylinder and a flat plate was observed by noting the similarities of the oil flow patterns and the high and low pressure fields.

The difference in the boundary-layer separation distances generated by the same circular jet nozzle with a similar jet momentum on the hollow cylinder and the ogive is compared in Figs. 42a and 43a. Although the jet momentum from the nozzle on the ogive was slightly smaller, the separation distance was 25 percent larger than the separation distance on the hollow cylinder. In both cases, the separation appeared to be turbulent. The rectangular nozzle jet generated a separation which, in the presence of a turbulent boundary layer on the ogive, was only slightly larger than the separation length on the cylinder (compare Figs. 42b and 44d).

In Fig. 43, the influence of Reynolds number and the state of the boundary layer on the separation generated by the same circular nozzle with nearly the same jet momentum were compared. The separation length in Figs. 43a and b are identical; in both cases the separation appeared to be fully turbulent. The Reynolds number of the first figure (43a) was twice that of the second (Fig. 43b), but a boundary-layer trip was added to the model nose when the lower Reynolds number results were recorded. Removing the trip resulted in the flow field shown in Fig. 43c, where the separation distance was larger and partially laminar or transitional in character.

4.8.1 Local Interaction Pressure Loading

Typical pressure distributions obtained in the presence of a lateral jet on an ogive at Mach number 3.98 are shown in Fig. 45. This represents the axial pressure distribution at two body coordinates, $\psi = 0$ and 59 deg (see Fig. 5). The influence of Reynolds number, the state of the boundary layer, and the jet pressure ratio (p_j/p_∞) on the pressure distribution is compared with the basic distribution obtained in the absence of any jet. Again the longer length of interaction region was obtained at the lower Reynolds number. In comparison with the flat plate results, the pressure aft of the jet nozzle on the bodies of revolution appeared to be much lower and extended over a larger surface area.

4.8.2 Net Interaction Force

As a result of the disturbance generated by the nozzle block attachment tab (see Figs. 42 through 44), the pressure data was only integrated

up to the model station occupied by the nozzle block ($x = 0$). These results for the hollow cylinder and ogive are shown in Figs. 46 and 47. In general, the interaction forces generated on the hollow cylinder agreed quite well with the results obtained on the flat plate. A change in the Reynolds number from 2.0 to 3.9×10^6 had no significant effect on the interaction force produced on the hollow cylinder by the lateral jet.

The interaction loads generated by the lateral jet on the ogive were slightly less than those obtained on the hollow cylinder. Doubling the Reynolds number or a change in the character of the boundary layer from laminar to turbulent increased the interaction force generated by the circular sonic jet on the ogive. The magnitude of the incremental increase in the interaction force resulting from the turbulent boundary-layer separation relative to the force obtained in the presence of laminar separation increased with the jet momentum (see Fig. 46).

4.8.3 Theoretical Estimates and Experimental Comparisons

The similarity in the pressure and flow field results of the flat plate and hollow cylinder should not yield the same interaction forces because of the differences in the geometry of the bodies involved. For example, if a given flat plate load distribution could be directly superimposed on a hollow cylinder, the particular size or curvature of the cylinder would have a direct influence on the magnitude of the interaction force. Thus the relative size of the jet nozzle to the local curvature of the surface containing the nozzle and jet momentum would have a direct influence on the interaction force.

On a flat plate, the maximum interaction force of a circular sonic jet was theoretically obtained in the presence of laminar separation. At jet pressure ratios (p_j/p_∞) above 100, the jet interaction force in the presence of turbulent separation on the ogive was larger than the value obtained in the presence of laminar boundary layer separation (see Fig. 48). This influence of the character of the boundary-layer separation and the free-stream Reynolds number on the jet interaction force on a body of revolution can be estimated theoretically. Utilizing the assumed theoretical viscous pressure loading described for a circular jet located on a flat plate in section 4.6, the additional assumption was made that this flat plate loading about a circular jet is simply wrapped around the body of revolution. This technique provided a rough theoretical estimate of the jet interaction force produced by the separated boundary layer ahead of the jet free-stream interaction shock and when added to the inviscid results provided in Ref. 19 by C. Ferrari yielded the result shown in Fig. 48. Included in Fig. 48 are the theoretical inviscid results of Ref. 19.

The theoretical and experimental variation of the jet interaction force generated in the presence of turbulent boundary-layer separation relative to the force obtained with laminar separation agreed fairly well. These theoretical results were evaluated for a sonic nozzle to body diameter ratio (d_j/D) of 0.070 and a separation Reynolds number of 106. The inviscid interaction generated by the lateral circular jet (as derived in Ref. 19) was primarily a function of the jet pressure ratio and free-stream Mach number; the viscous portion of the jet interaction derived herein depended on the jet nozzle diameter to body diameter ratio, jet pressure ratio (which determines the effective jet spoiler height), the separation Reynolds number, the character of the separated boundary layer, and the free-stream Mach number. Therefore the theoretical curve (dashed lines) presented in Fig. 48 for the net interaction load generated by a lateral circular jet on an ogive represent one particular set of conditions.

As shown by a comparison of the theoretical results with the present experimental data and the data of Refs. 17 and 18 in Fig. 48, the present theoretical analysis not only predicts the influence of the character of the boundary layer ahead of the jet on the interaction loading but also the influence of the sonic nozzle to body diameter ratio, d_j/D , on the interaction loading. A comparison of the present experimental results with those of Ref. 18 which were obtained for two larger d_j/D ratios indicated that the interaction force ratio decreased as the d_j/D ratio increased, and this result was theoretically substantiated but not shown in Fig. 48.

The present experimental results are compared with other results in Fig. 49 on the same general basis as the flat plate results, namely, the interaction force versus the jet momentum parameter, $(p_j/p_\infty)A_e$. Included in this figure are the experimentally determined interaction coefficients generated on a hollow cylinder. The results in this form indicated that with increasing jet momentum, the interaction force coefficient increased if the state of the boundary-layer separation was turbulent and decreased or remained the same if the separation was laminar. Also moving the jet forward of the model base reduced the interaction force coefficient. Unlike the flat plate or hollow cylinder results, the jet interaction force for a given jet momentum on the nine-caliber ogive was quite sensitive to the state of the boundary layer, the model size to jet nozzle diameter ratio, the relative axial location of jet nozzle, and free-stream Reynolds number.

5.0 CONCLUDING REMARKS

The following significant results were obtained with the present test models at Mach numbers 2.99, 3.98, and 5.01 in the overall Reynolds number range from 0.5 to 6.0×10^6 and are briefly summarized.

1. In many respects a lateral sonic jet produced the same type of flow field as a vertical spoiler (step) in a supersonic stream.
2. The interaction force produced by lateral jets increased if any one of the following parameters were increased: the jet momentum, the density of the multiple circular nozzle configuration, the span (or aspect ratio) of a rectangular nozzle; or if a single circular sonic nozzle was replaced by a rectangular sonic nozzle with the same effective throat area; or if the single circular nozzle was located forward of the trailing edge of a planar surface. In the case of the ogive, the interaction force also increased if the separated boundary layer ahead of the lateral jet was turbulent and the jet parameter $(p_j/p_\infty)A_e \geq 10$, if the nozzle was located at the most aft model station near the model base, or if the free-stream Reynolds number was increased.
3. A linear combination of the theoretical estimates of the jet interaction force ratio (F_{N_i}/F_j) produced by the viscous and inviscid interaction of a lateral jet with a supersonic stream were in reasonably good agreement with the experimental results.
4. As shown theoretically and experimentally, the ratio of the interaction force to the jet reaction force generally increased with decreasing jet pressure ratio and increasing free-stream Mach number.

For a given Re_δ value, a plane surface containing a rectangular lateral sonic jet theoretically produced the largest interaction force in the presence of turbulent separation, but a circular jet produced the maximum interaction in the presence of laminar separation. On a body of revolution for jet pressure ratios > 200 , a circular jet experimentally and theoretically produced the largest interaction in the presence of turbulent separation when the ratio of $d_j/D = 0.07$. For weaker jets ($p_j/p_\infty < 200$), laminar separation produced the higher circular jet interaction force.

5. In the case of the flat plate data, the correlation between the theoretical and experimental results tended to improve at the higher Mach numbers. In most cases, the theoretical estimates of the interaction force generated by a lateral circular jet located at the aft station of a body of revolution fell within the experimental values based on laminar and turbulent boundary-layer separation.

6. These experimental results indicated that a single circular jet should be placed about 30 nozzle diameters forward of the trailing edge of planar surfaces and at the base edge of bodies of revolution to achieve the maximum interaction force. In general, the best nozzle configuration for most applications appeared to be a rectangular nozzle (slot) or multiple circular nozzle configuration located at the model trailing edge.

REFERENCES

1. Ehrich, Fredric F. "Penetration and Deflection of Jets Oblique to a General Stream." Journal of Aeronautical Sciences, Vol. 20, No. 2, February 1953. p. 99-104.
2. Ruggeri, Robert S., Edmund, Callaghan E. and Bowden, Dean T. "Penetration of Air Jets Issuing From Circular, Square, and Elliptical Orifices Directed Perpendicularly to an Air Stream." NACA TN 2019, February 1950.
3. Jordinson, R. "Flow in a Jet Directed Normal to the Wind." ARC TR-18 783, RM 3074, October 1956.
4. Dewey, Paul E. and Vick, Allen R. "An Investigation of the Discharge and Drag Characteristics of Auxiliary-Air Outlets Discharging into a Transonic Stream." NACA TN 3466, July 1955.
5. Schult, Eugene D. "Free-Flight Roll Performance of a Steady-Flow Jet-Spoiler Control on an 80° Delta-Wing Missile between Mach Numbers of 0.6 and 1.8." NACA RM L57J28, January 1958.
6. Lachmann, G. V. (editor). Boundary Layer and Flow Control - Its Principles and Applications. Vol. I. Pergamon Press, New York, 1961.
7. Hickey, D. P. "Correlation of Certain Thrust Vectoring Control Systems." Douglas Report, SM-27957, October 1961.
8. Hunter, Paul A. "An Investigation of the Performance of Various Reaction Control Devices." NASA Memo 2-11-59L, March 1959.
9. Broadwall, James E. "An Analysis of the Fluid Mechanics of Secondary Injection for Thrust Vector Control (Revised). STL Report No. 6120-7744-Mu-000, March 1962.
10. Arnzen, H. E. "Flight Controls: A Look Into the Future." Space/Aeronautics, Vol. 33, No. 2, February 1960. p. 46-9

11. Falanga, Ralph A. and Janos, Joseph J. "Pressure Loads Produced on a Flat-Plate Wing by Rocket Jets Exhausting in a Spanwise Direction below the Wing and Perpendicular to a Free-Stream Flow of Mach Number 2.0." NACA RM L58D09, June 1958.
12. Janos, Joseph J. "Loads Induced on a Flat-Plate Wing by an Air Jet Exhausting Perpendicularly Through the Wing and Normal to a Free-Stream Flow of Mach Number 2.0." NASA TN D-649, March 1961.
13. Amick, James L. and Hays, Paul B. "Interaction Effects of Side Jets Issuing from Flat Plates and Cylinders Aligned with a Supersonic Stream." University of Michigan WADD-TR-60-329, June 1960.
14. Cubbison, Robert W., Anderson, Bernhard H. and Ward, James J. "Surface Pressure Distributions with a Sonic Jet Normal to Adjacent Flat Surfaces at Mach 2.92 to 6.4." NASA TN D-580, February 1961.
15. Romeo, David J. and Sterrett, James R. "Aerodynamic Interaction Effects Ahead of a Sonic Jet Exhausting Perpendicularly from a Plate into a Mach Number 6 Free Stream." NASA TN D-743, April 1961.
16. Morkovin, M. V., Pierce, C. A., Jr. and Craven, C. E. "Interaction of a Side Jet with a Supersonic Main Stream." Univ. of Michigan, Engineering Research Bulletin No. 35, September 1952.
17. Vinson, P. W., Amick, J. L. and Liepman, H. P. "Interaction Effects Produced by Jet Exhausting Laterally near Base of Ogive-Cylinder Model in Supersonic Main Stream." NASA Memo 12-5-58W, February 1959.
18. Carvalho, Gerard F. and Hays, D. B. "Jet Interference Experiments Employing Body-Alone and Body-Fin Configurations at Supersonic Speeds." University of Michigan Technical Report, CM - 979, December 1960.
19. Ferrari, Carlo. "Interference between a Jet Issuing Laterally from a Body and the Enveloping Supersonic Stream." Johns Hopkins University, Bumblebee Series Rpt No. 286, AD-226-477, April 1959.
20. Test Facilities Handbook, Vol. 4. "von Kármán Gas Dynamics Facility." Arnold Engineering Development Center, July 1962.

21. Anderson, A. "Summary Report on Calibration of Tunnel E-1, A 12-Inch Mach 5 Supersonic Wind Tunnel." AEDC-TN-58-8, March 1958.
22. Weir, Alexander, Jr., York, J. L. and Morrison, R. B. "Two- and Three-Dimensional Flow of Air Through Square-Edged Sonic Orifices." Transactions of the ASME, Vol. 78, No. 3, April 1956, p. 481-8.
23. Tucker, Maurice. "Approximate Calculation of Turbulent Boundary-Layer Development in Compressible Flow." NACA TN 2337, April 1951.
24. Mack, Leslie M. "Calculation of the Laminar Boundary Layer on an Insulated Flat Plate by the Klunker-McLean Method." JPL, California Institute of Technology, Progress Report No. 20-352, July 1958.
25. Ames Research Staff. "Equations, Tables and Charts for Compressible Flow." NACA Report 1135, 1953.
26. Hakkinen, R. J., Greber, I., Trilling, L., and Abarbanel, S. S. "The Interaction of an Oblique Shock Wave with Laminar Boundary Layer." NASA Memo 2-18-59W, March 1959.
27. Gadd, G. E. "Interactions between Wholly Laminar or Wholly Turbulent Boundary Layers and Shock Waves Strong Enough to Cause Separation." Journal of Aeronautical Sciences, Vol. 20, No. 11, November 1953, p. 729-39.
28. Erdos, John, and Pallone, Adrian. "Shock-Boundary Layer Interaction and Flow Separation." Research and Advanced Development Division, AVCO Corporation, RAD-TR-61-23, August 1961.
29. Chapman, Dean R., Kuehn, Donald M., and Larson, Howard K. "Investigations of Separated Flows in Supersonic and Subsonic Streams with Emphasis on the Effect of Transition." NACA TN 3869, March 1957.
30. Sterrett, James R. and Emery, James C. "Extension of Boundary-Layer-Separation Criteria to a Mach Number of 6.5 by Utilizing Flat Plates with Forward-Facing Steps." NASA TN D-618, December 1960.
31. Crocco, Luigi and Probstein, Ronald F. "The Peak Pressure Rise across an Oblique Shock Emerging from a Turbulent Boundary Layer over a Plane Surface." AD 45651, Princeton University Rpt 254, AD 45651, March 1954.

32. Love, Eugene S. "Pressure Rise Associated with Shock-Induced Boundary-Layer Separation." NACA TN 3601, December 1955.
33. Bogdonoff, Seymour M. "Some Experimental Studies of the Separation of Supersonic Turbulent Boundary Layers." Presented at the Heat Transfer and Fluid Mechanics Institute Meeting, June 1955, OSR-TN-56-64, AD 81056.
34. Truitt, Robert W. Hypersonic Aerodynamics. The Ronald Press Company, New York, 1959.

APPENDIX

The computational procedure for evaluating the inviscid interaction force produced by a lateral jet from a circular sonic nozzle on a surface in a supersonic stream was obtained from the theoretical analysis of C. Ferrari (Ref. 19). A synopsis of the theory and the equations used in the computation of the theoretical interaction force is summarized in this appendix. In the theory, the jet stream was assumed to remain unmixed with the external stream, and the internal characteristics of the jet are examined by balancing the external stream pressure force on the periphery of the jet stream tube with the internal forces of the jet. Once the external cross-sectional shape of the jet was defined, an estimate of the shape of the centerline path of the jet was determined. With an approximate evaluation of the jet stream tube contour, an estimate was made of the shape and position of the detached shock wave relative to the expanded lateral jet stream. The flow field between the detached shock and the jet stream in the vicinity of the surface containing the sonic jet nozzle was then approximated on the basis of Lighthill's treatment of the hypersonic blunt-body problem.

The following computing procedure was used to evaluate Ferrari's equation which defines the magnitude of the ratio of the inviscid interaction force (FN_i) produced on a planar surface in a supersonic stream by a lateral circular sonic jet to the jet reaction force (F_j). In general, the terms of the nomenclature used in Ref. 19 will also be used in the following equations required to evaluate FN_i/F_j .

$$\frac{FN_i}{F_j} = \frac{\gamma + 3}{2(\gamma + 1)} \frac{\epsilon}{2} \left(\frac{\gamma M_\infty^2}{2} \right) \left\{ \left[1 + \frac{\gamma}{8} \left(\frac{\gamma + 3}{\gamma + 1} \right) M_\infty^2 \right]^{\frac{\gamma' + 1}{4\gamma'}} \left(\frac{\gamma' + 1}{\gamma' - 1} \right)^{\frac{1}{4}} \times \right. \\ \left. \left(\frac{p_j}{p_\infty} \right)^{\frac{\gamma' - 1}{2\gamma'}} \left[\left(\frac{p_j}{p_\infty} \right)^{\frac{\gamma' - 1}{\gamma'}} - 1 \right]^{\frac{1}{4}} \left[1 - \frac{p_\infty}{2p_j} \left(\frac{\gamma' + 1}{2} \right)^{\frac{1}{\gamma' - 1}} \right] \times \right. \\ \left. \left[\left(\frac{\frac{p_j}{p_\infty}}{1 + \frac{\gamma}{8} \frac{\gamma + 3}{\gamma + 1} M_\infty^2} \right)^{\frac{\gamma - 1}{\gamma'}} - 1 \right]^{\frac{1}{4}} \right\}^{-1} \quad (1)$$

In this and the following relationships, γ' refers to the ratio of specific heats of the lateral jet and γ , of the free-stream flow. All the other terms in Eq. 1 are defined in the present nomenclature except " ϵ ", which represents a factor based on the geometry of the flow field interaction

produced by the lateral jet and the supersonic free stream, and ϵ is evaluated in the following manner.

The general shape of the cross section of the jet stream lying in a plane perpendicular to the jet stream (Fig. g) centerline was assumed to be elliptical. The semi-minor axis, l_0 , of the ellipse extends upstream, and the semi-major axis, R , lies in the plane of the ellipses perpendicular to the free-stream direction. The jet stream was assumed to expand to the free-stream static pressure along the semi-major axis and therefore

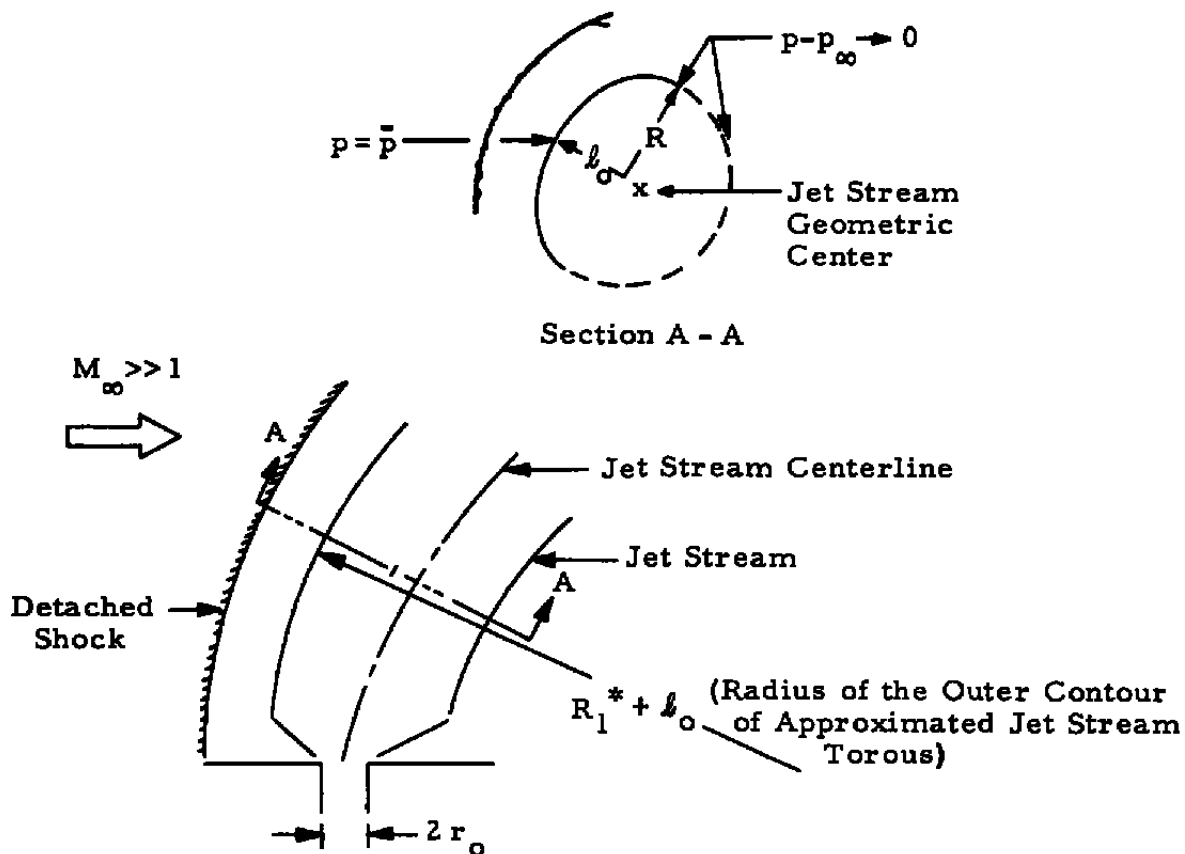


Fig. g Nomenclature and Flow Field Used in Ref. 19, Fig. 9

$$\left(\frac{R}{r_0}\right)^2 = \left(\frac{2}{\gamma' + 1}\right)^{\frac{\gamma' + 1}{2(\gamma' - 1)}} \frac{\left(\frac{p_j}{p_\infty}\right)^{\frac{\gamma' + 1}{2\gamma'}}}{\sqrt{\left(\frac{2}{\gamma' - 1}\right) \left[\left(\frac{p_j}{p_\infty}\right)^{\frac{\gamma' - 1}{\gamma'}} - 1\right]}} \quad (2)$$

where r_0 is the radius of the circular sonic nozzle.

Along the semi-minor axis an estimate was made of the static pressure \bar{p} applied on the upstream portion of the jet stream tube by the free-stream flow. From hypersonic approximations pressure \bar{p} was defined as follows:

$$\frac{\bar{p}}{P_{\infty}} = 1 + \frac{\gamma}{8} \frac{\gamma+3}{\gamma+1} M_{\infty}^2 \quad \text{and} \quad (3)$$

therefore

$$\left(\frac{\ell_o}{r_o}\right)^2 = \left(\frac{2}{\gamma'+1}\right)^{\frac{\gamma'+1}{2(\gamma'-1)}} \frac{\left(\frac{p_j}{\bar{p}}\right)^{\frac{\gamma'+1}{2\gamma'}}}{\sqrt{\left(\frac{2}{\gamma'-1}\right) \left[\left(\frac{p_j}{\bar{p}}\right)^{\frac{\gamma'-1}{\gamma'-1}} - 1\right]}} \quad (4)$$

These terms for R/r_o and ℓ_o/r_o are tabulated in Ref. 25 for various pressure ratios.

An estimate of the radius of curvature of the jet stream centerline with elliptical cross section was also made, and it was computed with the following equations:

$$\frac{R_1^*}{\ell_o} = \frac{2b \left(\frac{\gamma'}{\gamma'-1}\right) \left(\frac{\gamma+1}{\gamma+3}\right) \frac{P_o}{\gamma M_{\infty}^2} + C_{f''}}{C_{f'}} \quad (5)$$

where R_1^* was the radius of curvature of jet stream centerline.

$$C_{f'} = \frac{(R/\ell_o)^3}{(R/\ell_o)^2 - 1} \left\{ 1 - \frac{\ell_o/R}{2 \sqrt{(R/\ell_o)^2 - 1}} \log \frac{R/\ell_o + \sqrt{(R/\ell_o)^2 - 1}}{R/\ell_o - \sqrt{(R/\ell_o)^2 - 1}} \right\} \quad (6)$$

$$C_{f''} = - \left(\frac{R}{\ell_o}\right)^2 \frac{\pi}{4} \frac{1}{1 + \frac{R}{\ell_o}} \left(1 + \frac{1}{1 + \frac{R}{\ell_o}}\right) \quad (7)$$

$$b = \pi (R/\ell_o) \quad \text{and}$$

$$P_o = \left(1 + \pi \frac{\gamma+3}{2(\gamma+1)} \gamma M_{\infty}^2\right)^{\frac{1}{\gamma'}} \left(\frac{p_j}{P_{\infty}}\right)^{\frac{\gamma'-1}{\gamma'}} \\ - \frac{\gamma'+1}{2\gamma'} \left(1 + \gamma \frac{\gamma+3}{2(\gamma+1)} \pi M_{\infty}^2\right)$$

where

$$\pi = \frac{\ell - \left(\frac{\ell_o}{R}\right)^2 K}{\ell + \pi \left[1 - \left(\frac{\ell_o}{R}\right)^2\right]}$$

The values E and K are the complete elliptical integrals of the first and second kinds, respectively, based on the common modulus of $\sqrt{1 - \left(\frac{l_0}{R}\right)^2}$.

With the expanded jet stream cross sections approximated as being circular instead of elliptical, the radius of curvature of these circular sections were defined as R_C and $R_C/l_0 = (R/l_0)^2$. Therefore the jet stream may be replaced with a torus with an external radius of $R_1^* + l_0$ and for an initial approximation with circular cross sections of radius R_C . When this torus has a hole (1) $R_1^* + l_0 > 2R_C$ and if the hole was missing, then (2) $R_1^* + l_0 < 2R_C$. Therefore two procedures must be taken, depending on the particular geometry of the torus, which was a function of the free-stream conditions and the jet strength.

For the case where $R_1^* + l_0 > 2R_C$, a jet stream parameter α_1 was evaluated in the following manner:

$$\alpha_1 = \cosh^{-1} \frac{(R_1^*/l_0) + 1 - (R_C/l_0)}{R_C/l_0}$$

The corresponding parameter of α on the detached shock was defined as α_s and

$$\alpha_1 - \alpha_s = \left(\frac{\gamma - 1}{2} \right) \frac{\sinh \alpha_s}{2 + \cosh \alpha_s}$$

The ratio of the approximating radius of the circular cross section of detached shock wave, namely R_s , to the radius of curvature of the expanded jet stream, R_C , is defined as

$$R_C/R_s = \sinh \alpha_s / \sinh \alpha_1$$

If $R_1^* + l_0 < 2R_C$, then the value of the parameter corresponding to α_1 was redefined as β_1 and evaluated as follows:

$$\beta_1 = \cos^{-1} \frac{(R_1^*/l_0) + 1 - R_C/l_0}{R_C/l_0}$$

The corresponding detached shock parameter, namely β_s , was related to β_1 as follows:

$$\beta_1 - \beta_s = \left(\frac{\gamma - 1}{2} \right) \frac{\sin \beta_s}{2 + \cos \beta_s}$$

and

$$R_C/R_s = \sin \beta_s / \sin \beta_1$$

And the elliptical transformed coordinate (ρ_s) of the shock was then related to that of the jet stream, namely (ρ_1), by the following relationship:

$$\rho_1/\rho_s = \frac{3-\gamma}{2}$$

where

$$\rho_1 = \frac{\left(\frac{R_c}{R_s}\right)\left(\frac{2}{3-\gamma}\right)}{\sqrt{\left[\left(\frac{R_c}{R_s}\right)\left(\frac{2}{3-\gamma}\right)\right]^2 - 1}}$$

and

$$c = \frac{2}{3-\gamma} \frac{\rho_s}{\sqrt{\rho_1^2 - 1}} \left(\frac{\rho_s}{\sqrt{\rho_s^2 - 1}} + 1 \right)^{-1}$$

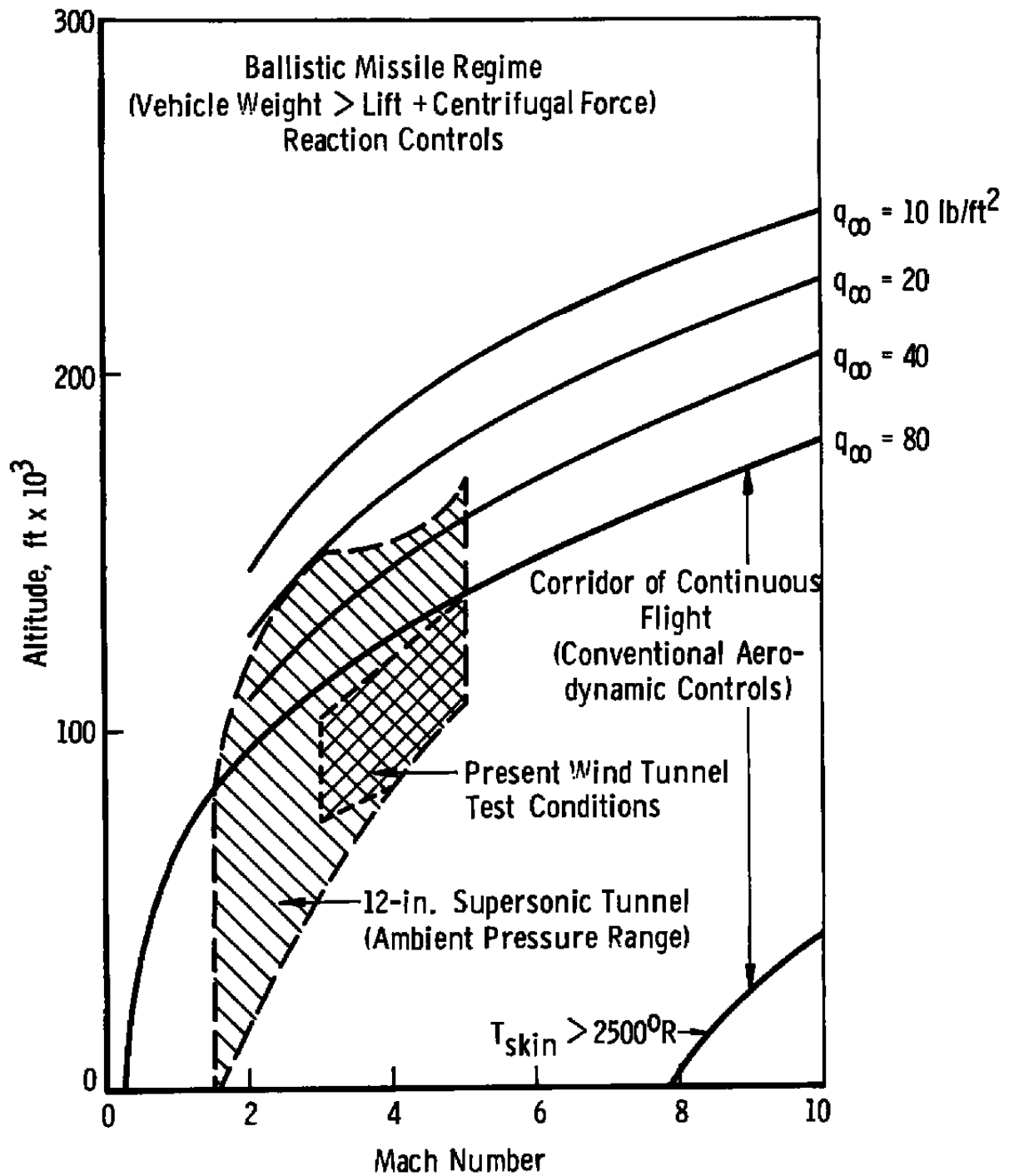
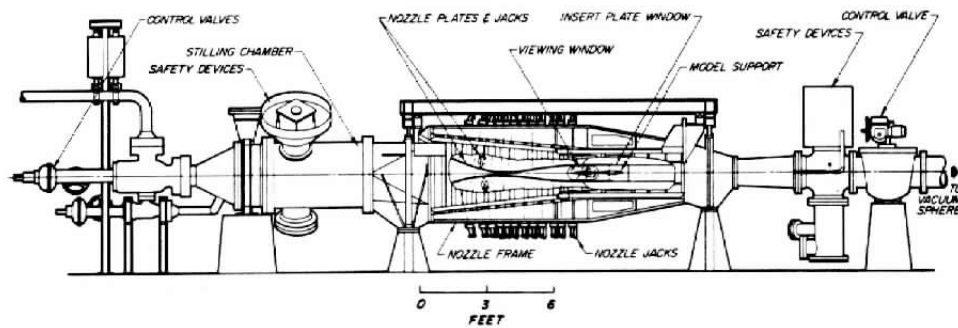


Fig. 1 Flight Corridor



Assembly

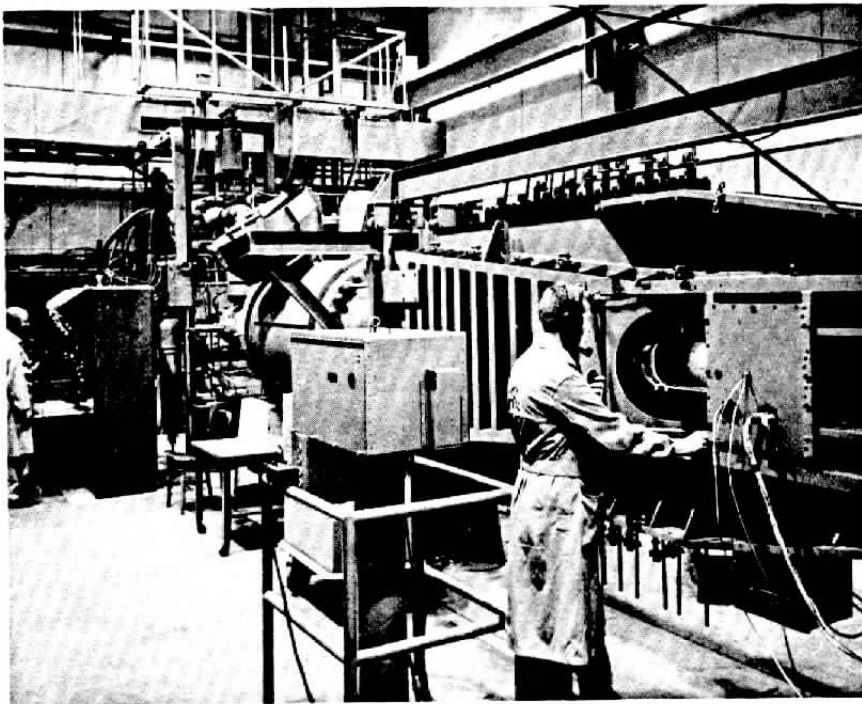


Fig. 2 The 12-Inch Supersonic Tunnel (E-1)

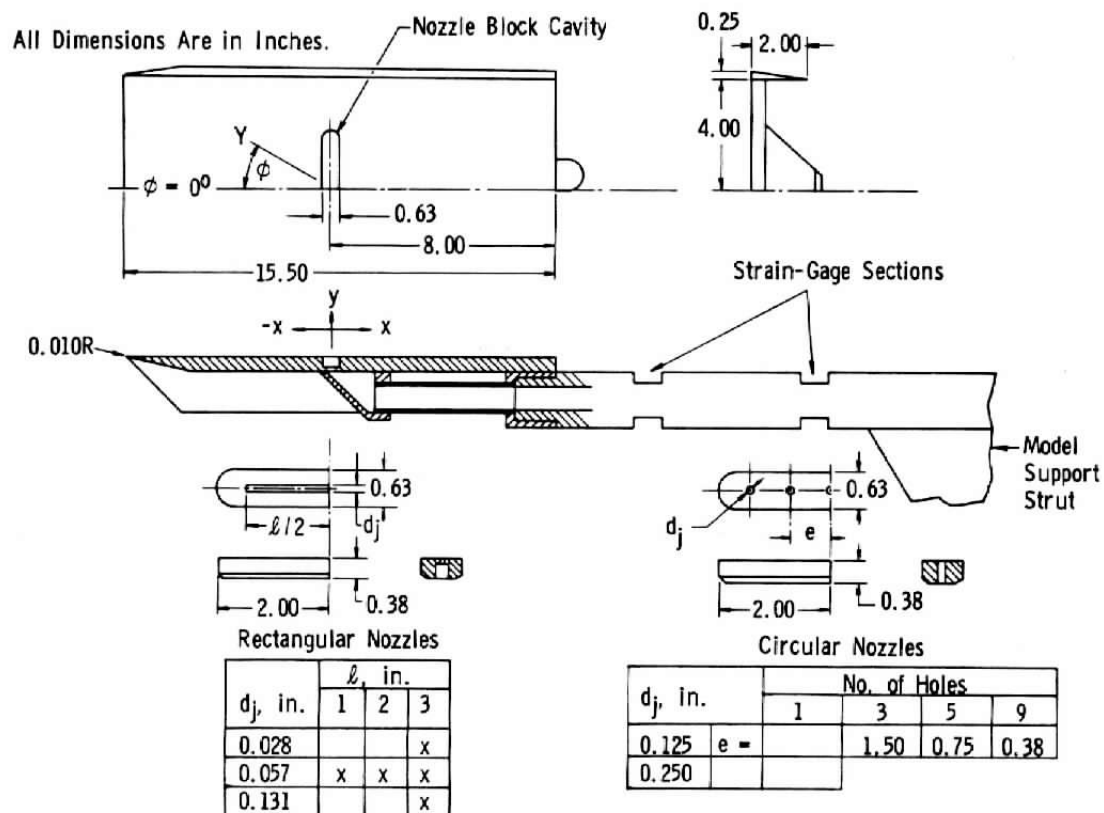


Fig. 3 Flat Plate and Nozzle Block Configurations



Fig. 4 Flat Plate Installation

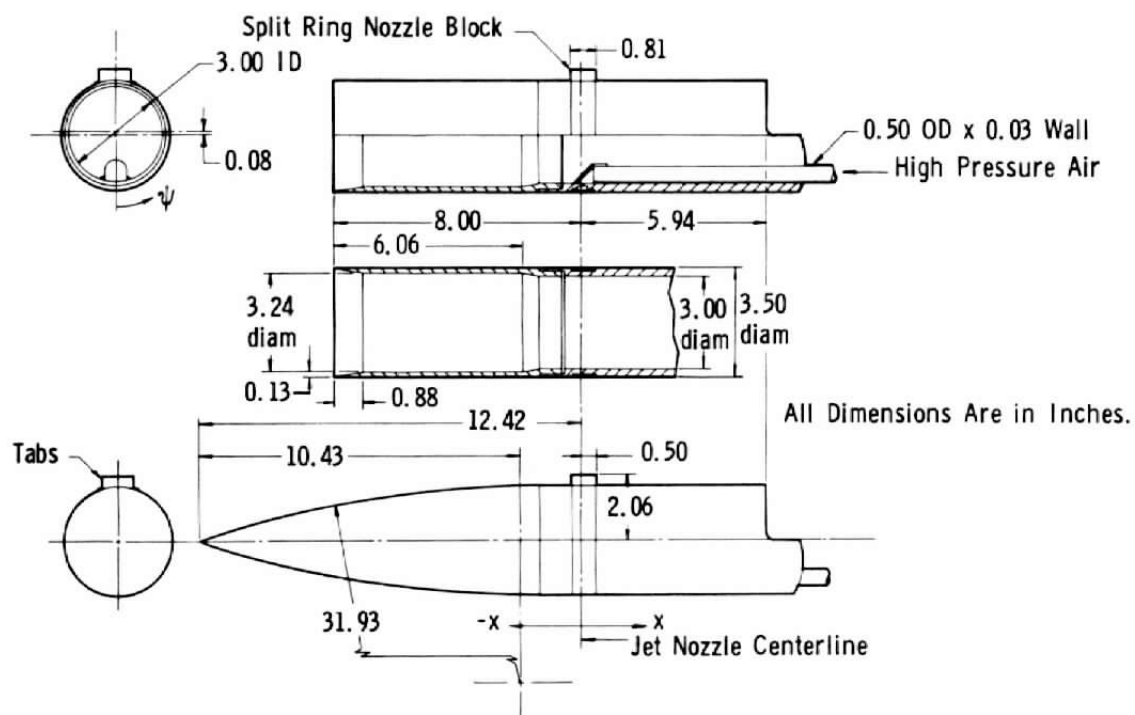


Fig. 5 Hollow Cylinder and Nine-Caliber Ogive Configurations

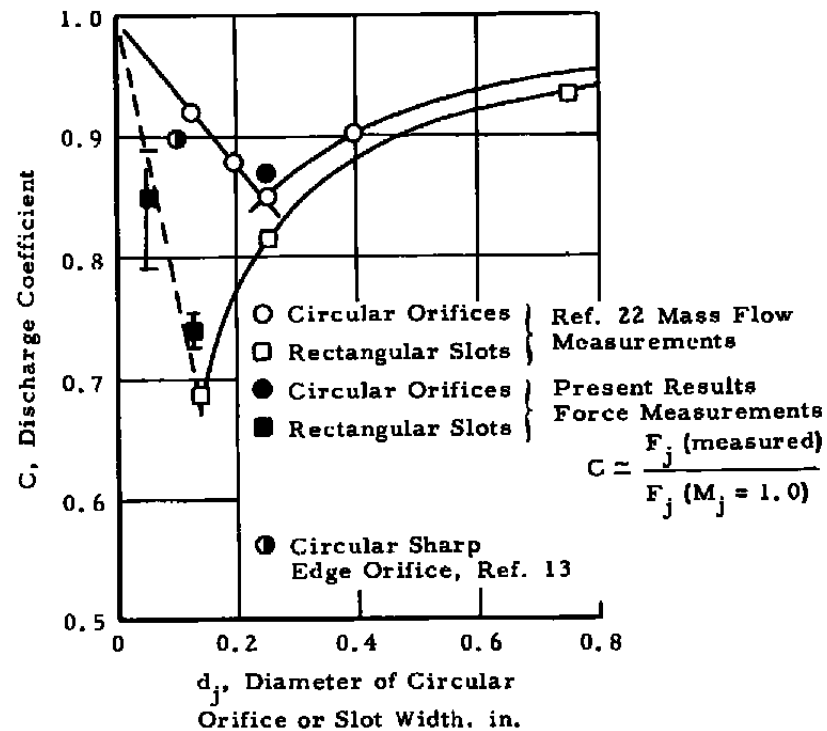
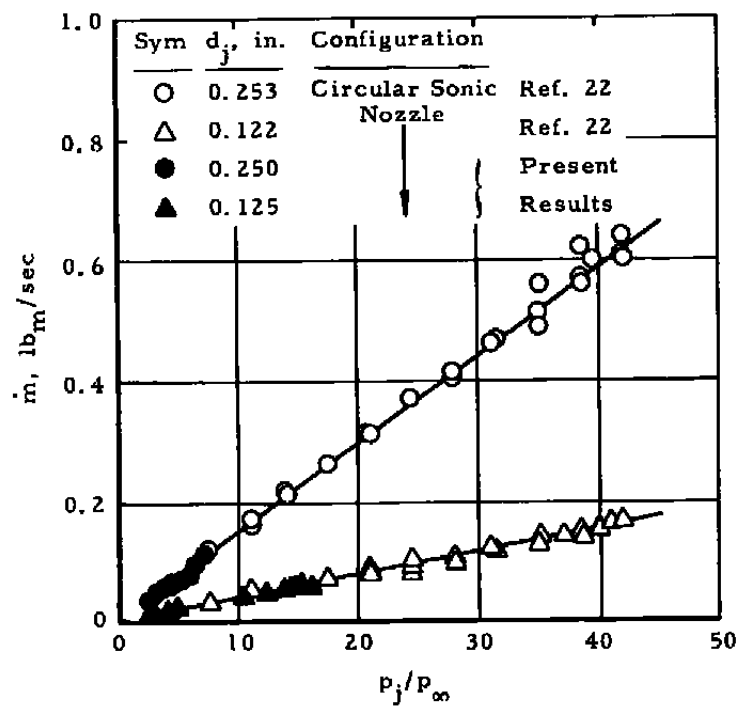
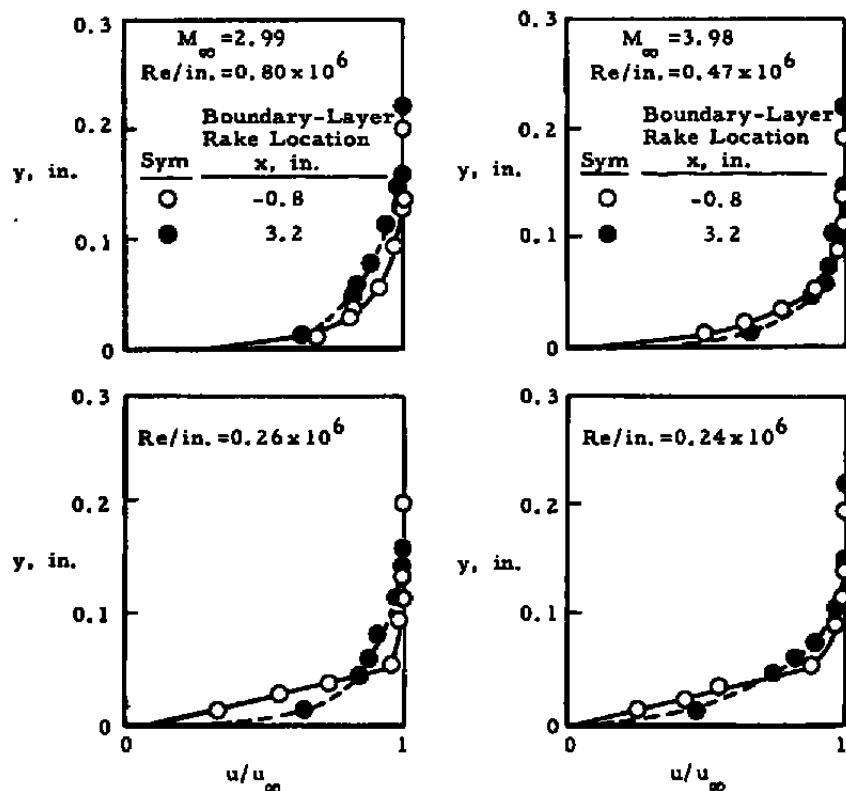


Fig. 6 Discharge Coefficient of Sharp Edge Nozzles



a. Typical Boundary-Layer Profiles

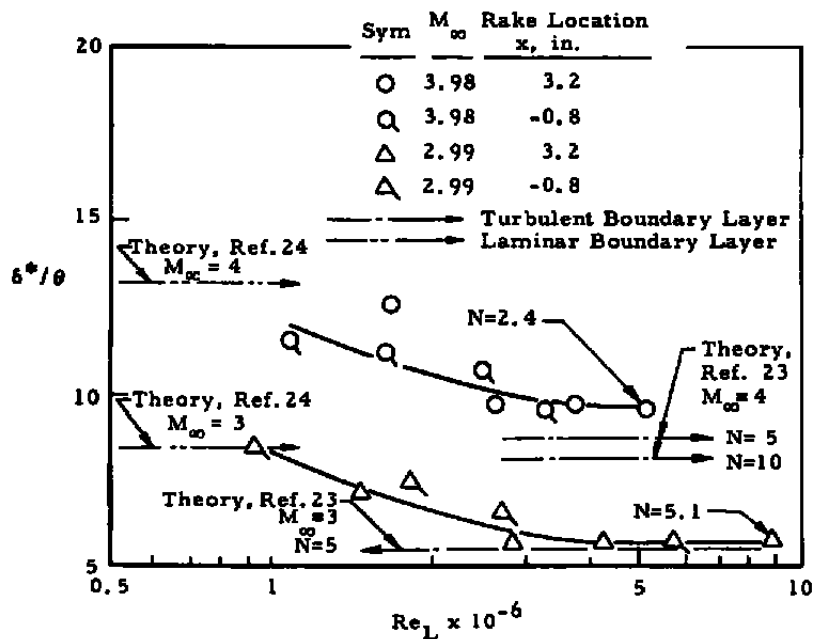
b. δ^*/θ versus Re_L

Fig. 7 Flat Plate Boundary-Layer Characteristics

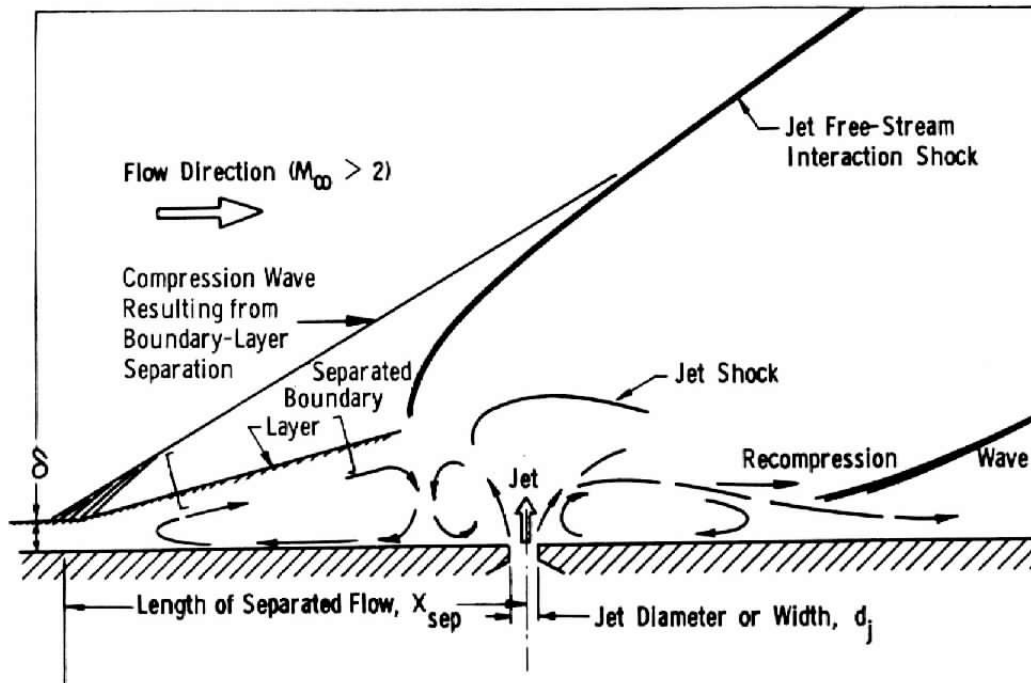


Fig. 8 Two-Dimensional Lateral Jet Flow Field

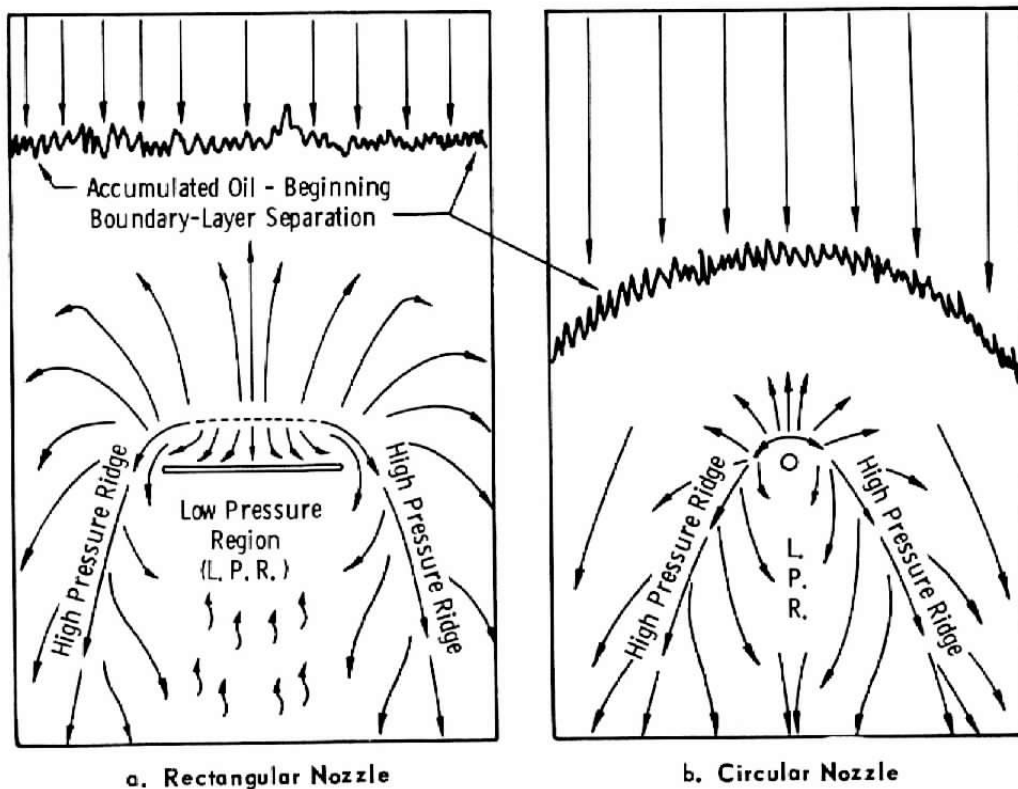
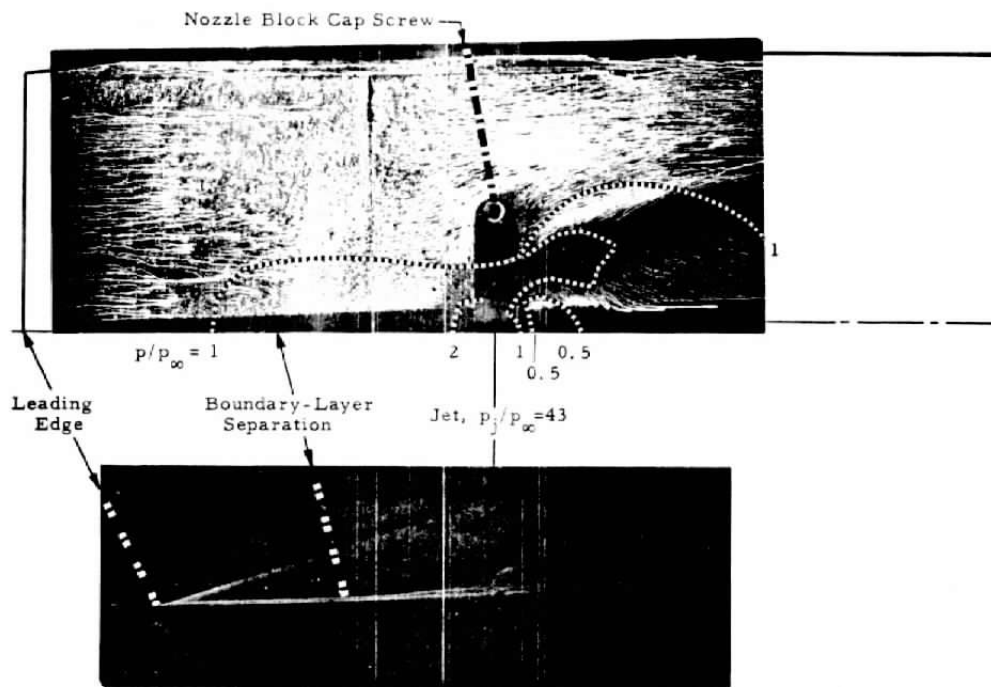


Fig. 9 General Direction of the Oil Flow Lines



a. 0.125-in.-diam Circular Nozzle

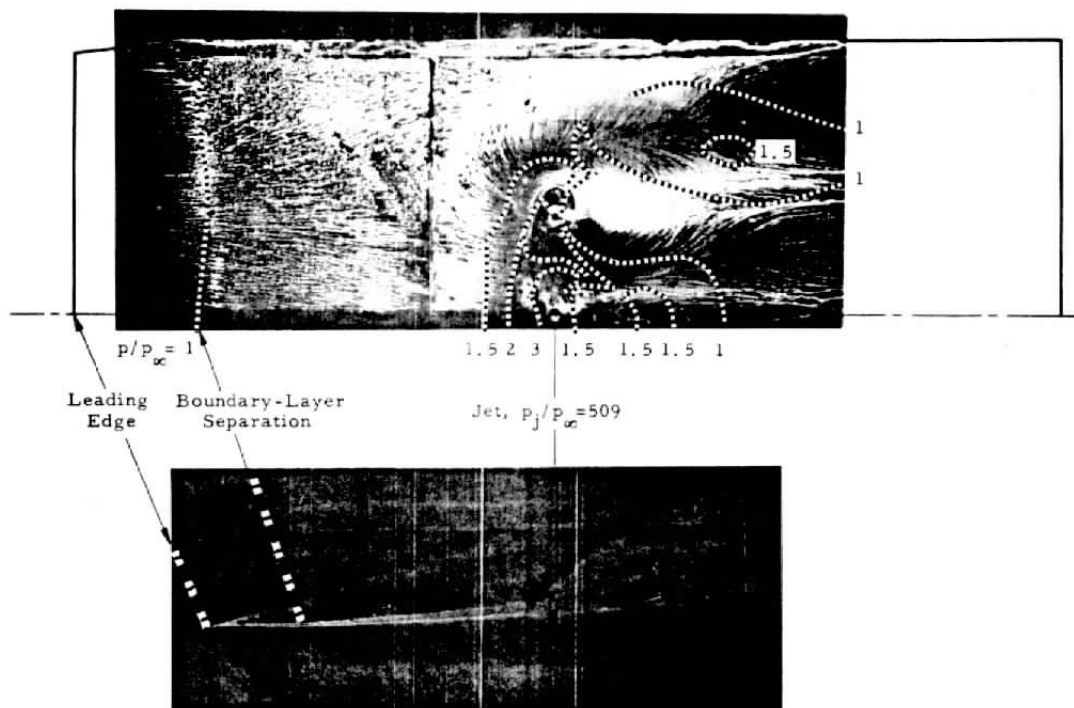
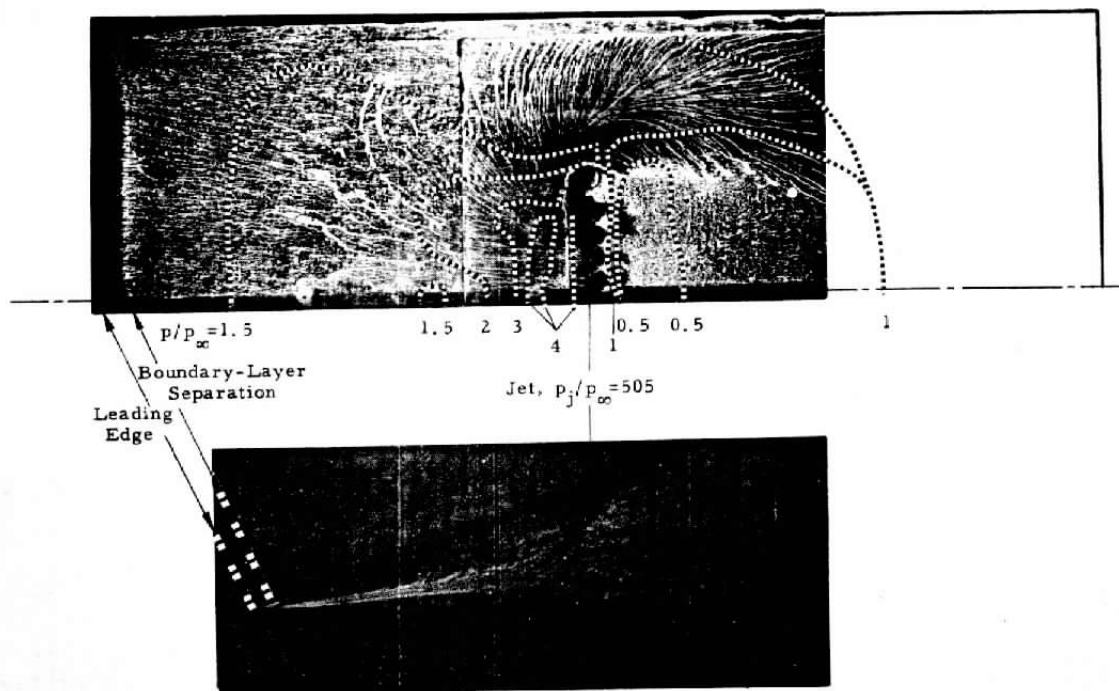
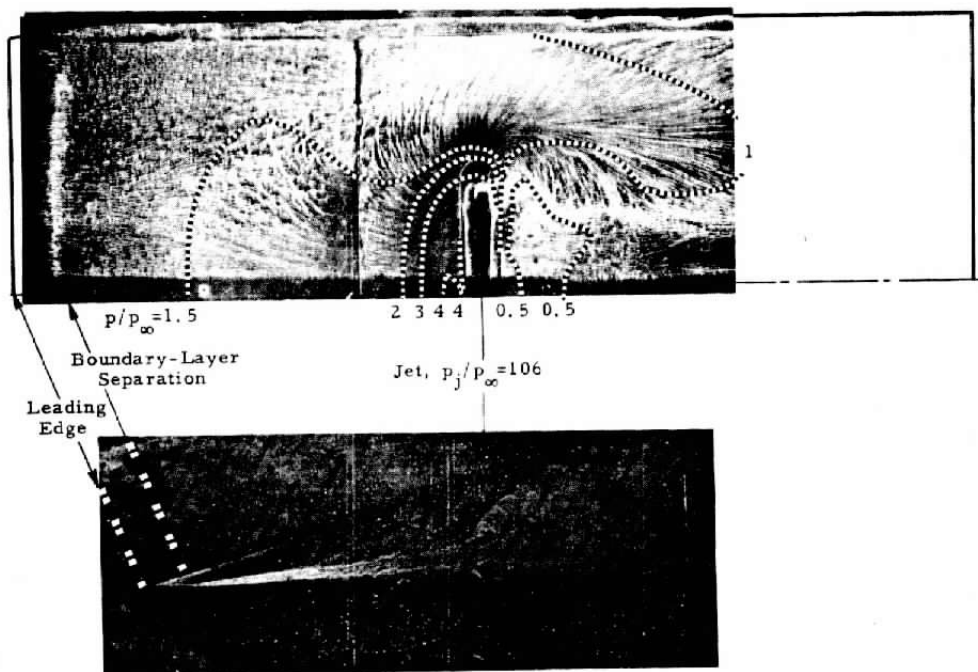

b. 0.125-in.-diam Multiple Circular Nozzles, $e/d_j = 12.3$

Fig. 10 Flow Patterns with Isobars at $M_{\infty} = 3.98$, $Re_x = 0.6 \times 10^6$



c. 0.125-in.-diam Multiple Circular Nozzles, $e/d_j = 3.1$



d. 0.131 by 3-in. Rectangular Nozzle

Fig. 10 Concluded

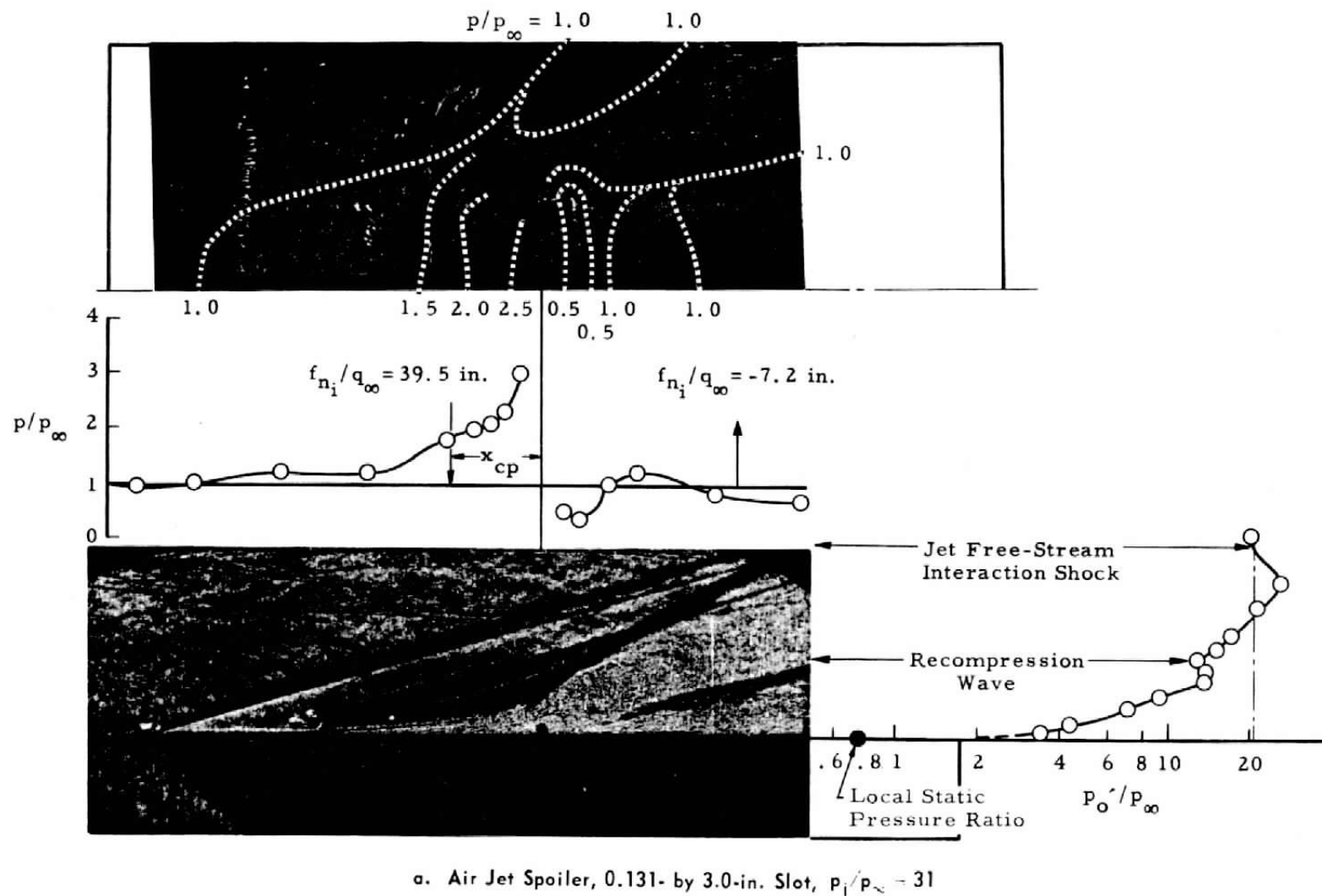
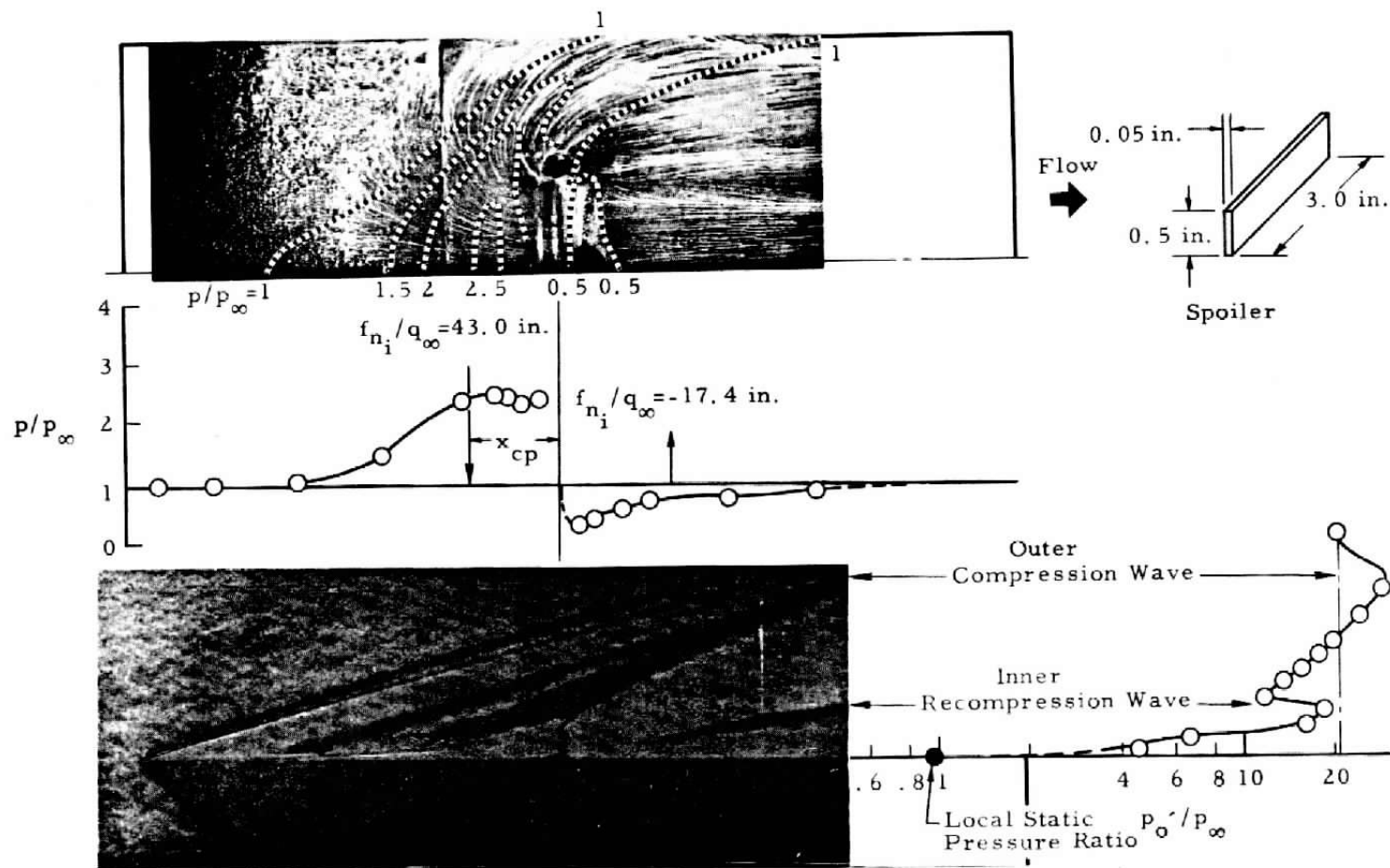
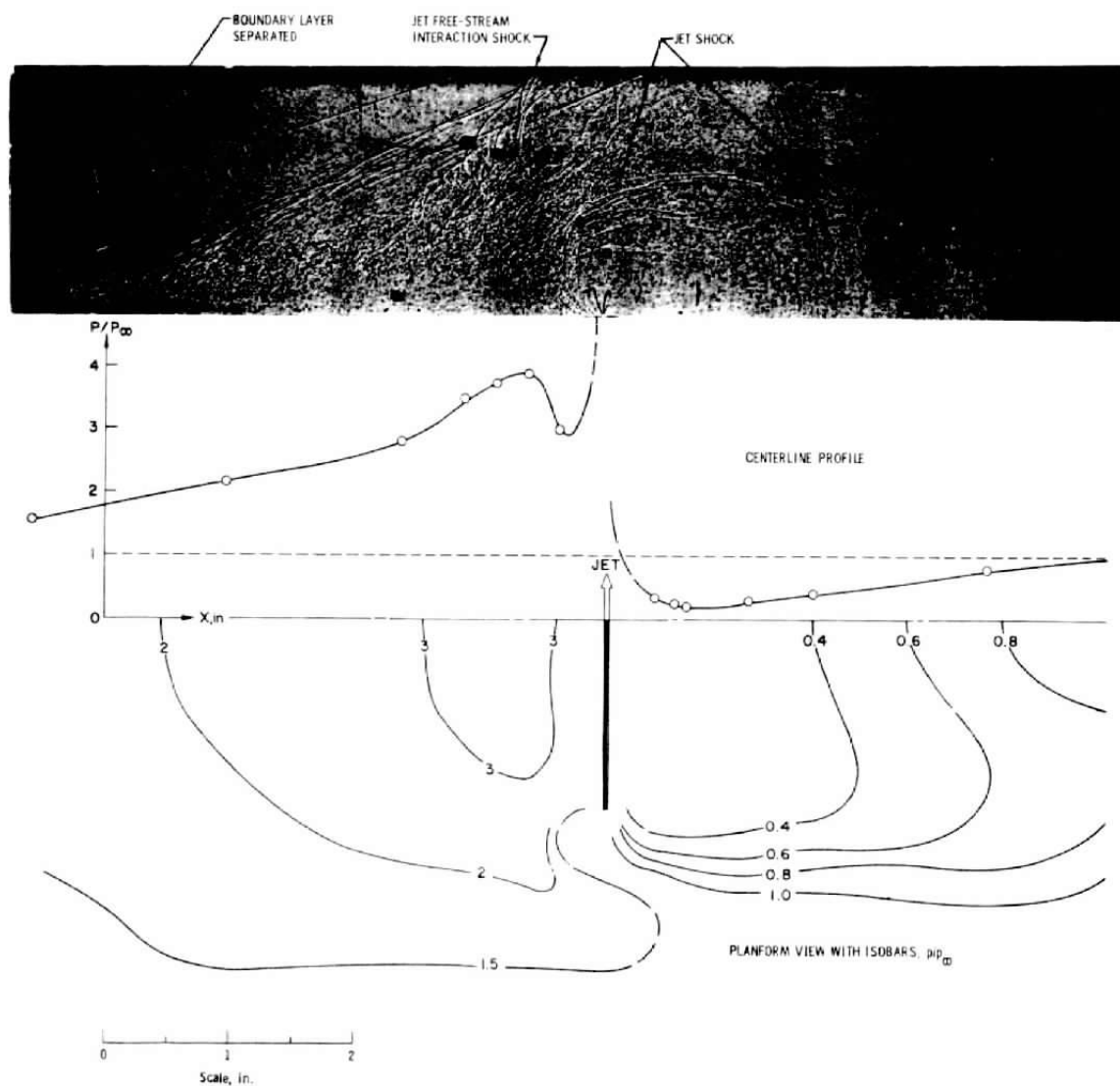


Fig. 11 Comparison of the Flow Field and Pressure Distribution Generated by an Air Jet and a Vertical Spoiler at $M_\infty = 3.98$, $Re_x = 2.0 \times 10^6$



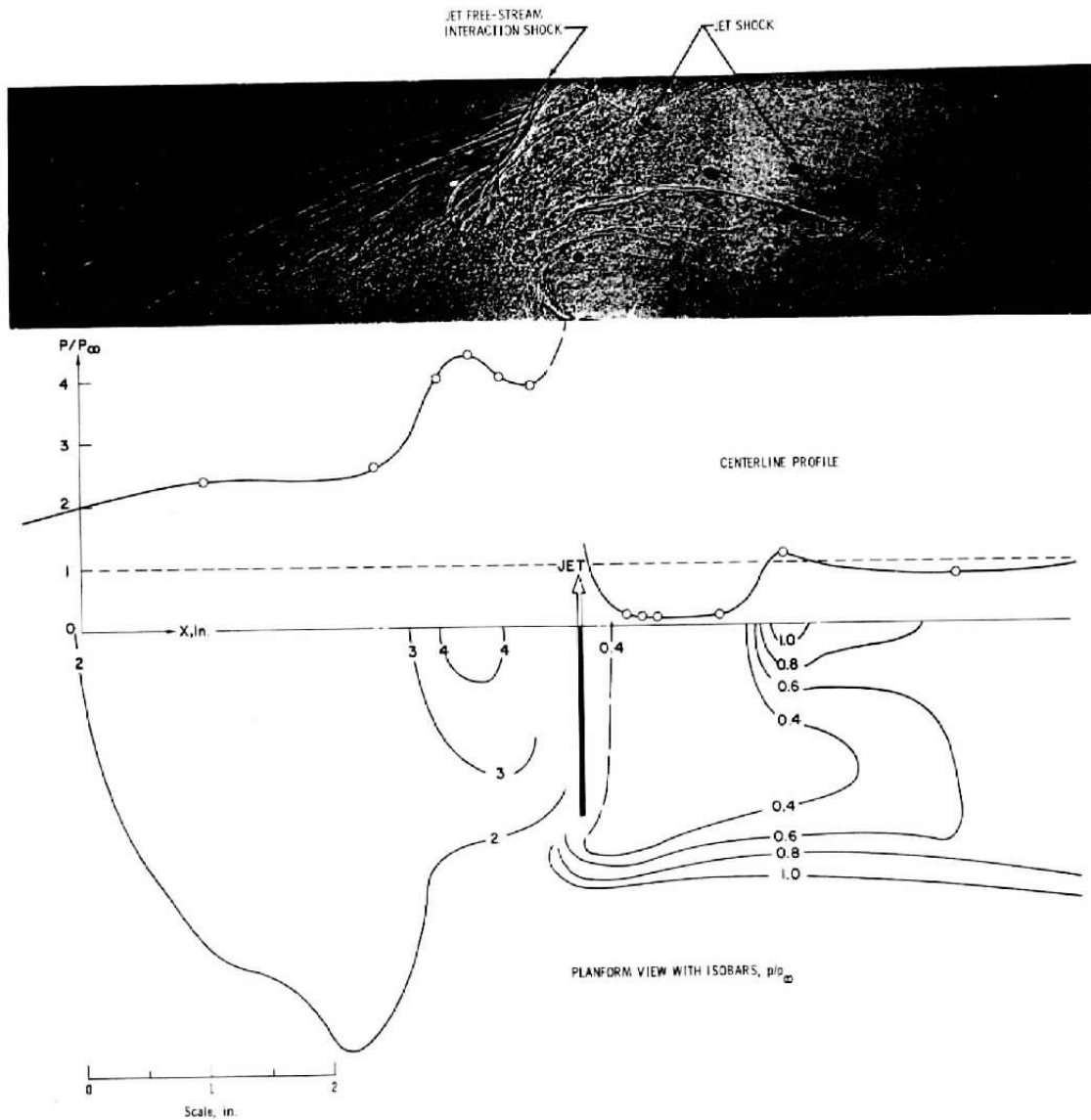
b. Vertical Spoiler, Height = 0.5 in. and Width = 3 in.

Fig. 11 Concluded



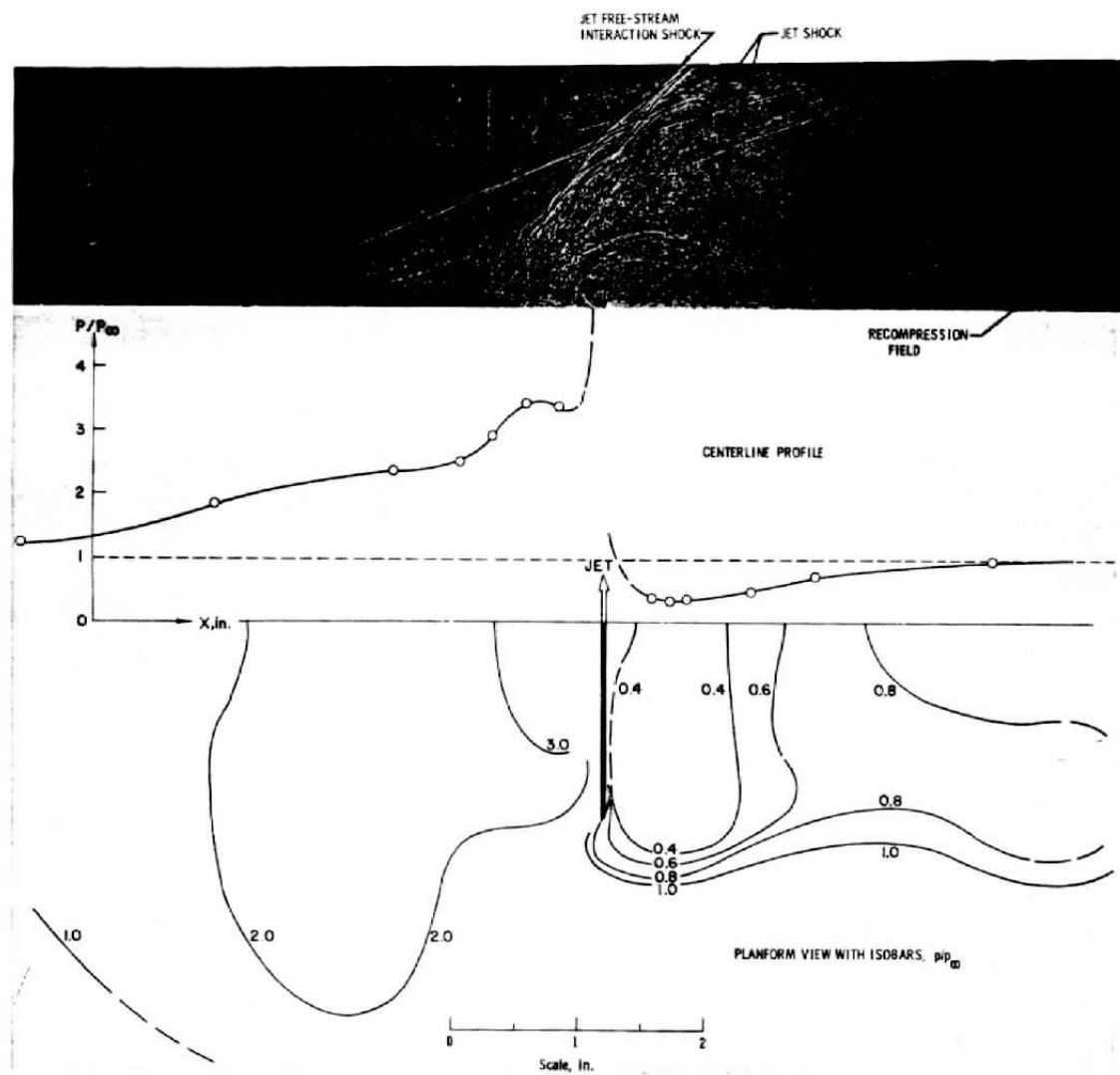
$$a. Re_X = 1.7 \times 10^6, p_i/p_\infty \approx 480, F_{N0}/q_\infty = 3.5 \text{ in.}^2$$

Fig. 12 Typical Pressure Distribution Generated by the Interaction of a Lateral Jet from 0.028-by 3-in. Slot into a Supersonic Stream, $M_\infty = 3.98$



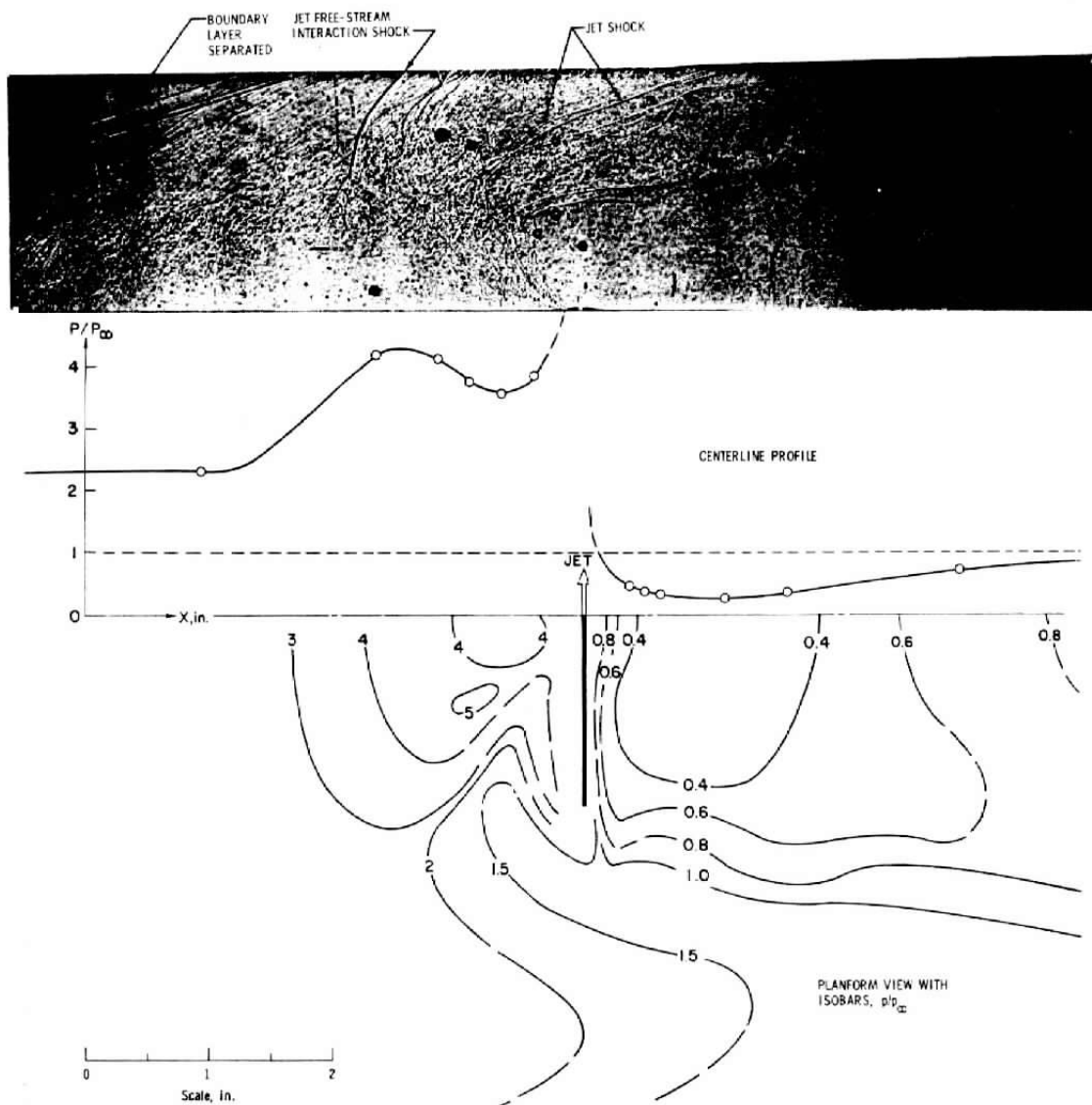
b. $Re_X = 3.5 \times 10^6$, $p_i/p_\infty = 480$, $F_{N_o}/q_\infty = 3.8 \text{ in.}^2$

Fig. 12 Continued



c. $Re_X = 3.5 \times 10^6$, $p_i/p_\infty = 231$, $F_{N_o}/q_\infty = 2.7 \text{ in.}^2$

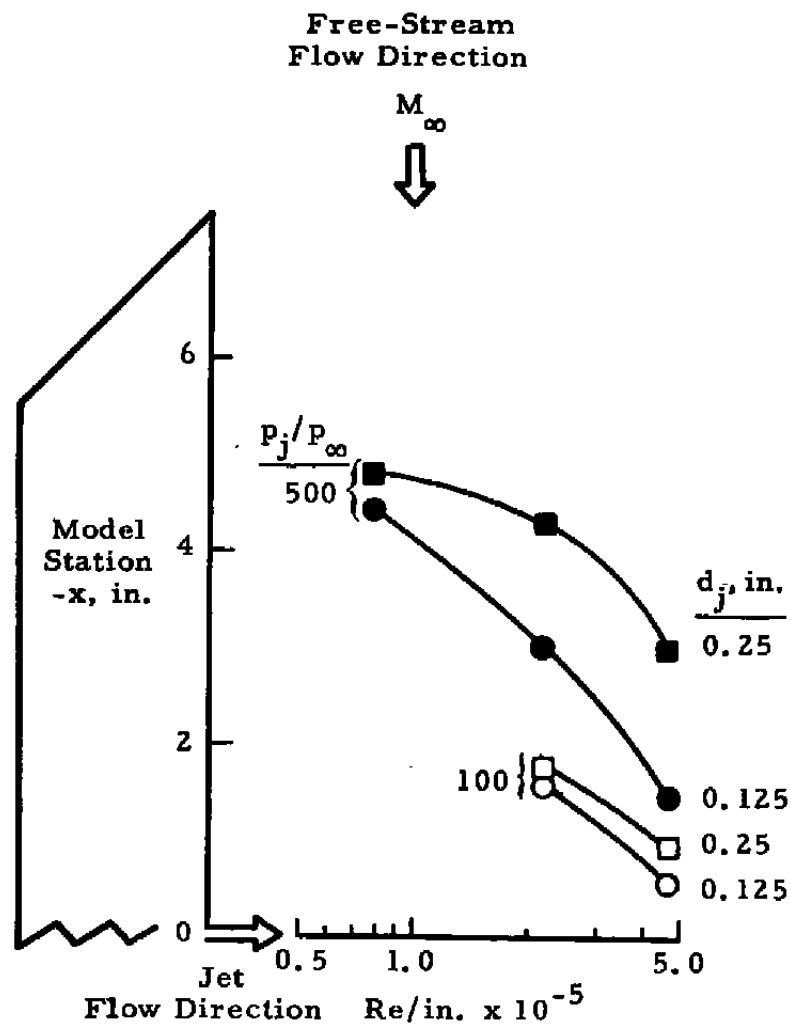
Fig. 12 Continued



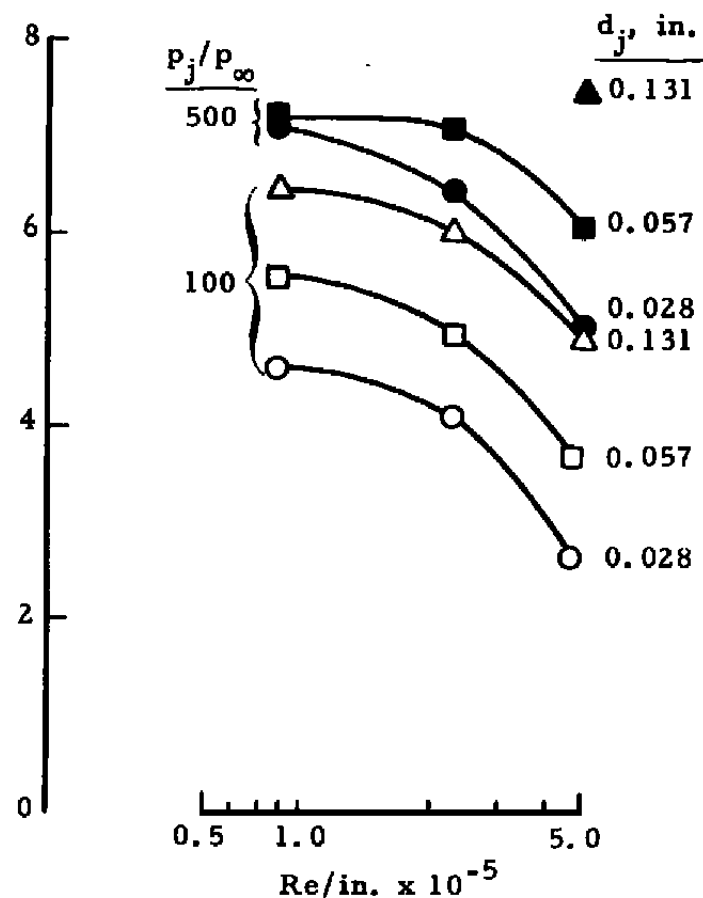
d. $Re_X = 1.8 \times 10^6$, $p_i/p_\infty = 934$, $F_{N-}/q_\infty = 5.9 \text{ in.}^2$

Fig. 12 Concluded

58



a. Circular Nozzle



b. Rectangular Nozzle

Fig. 13 Influence of Jet Nozzle Configuration and Pressure Ratio on Boundary-Layer Separation Location, $M_\infty = 3.98$

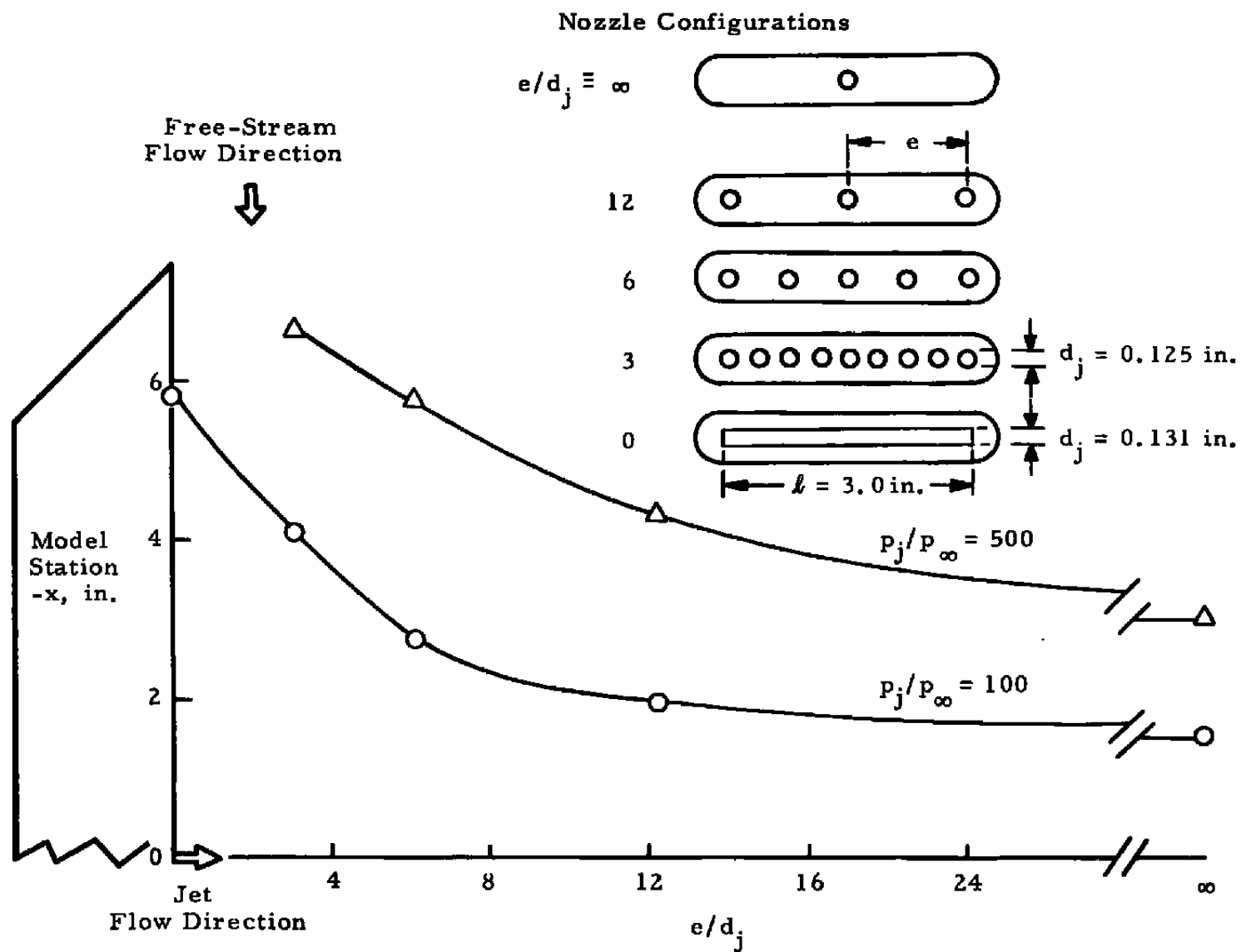


Fig. 14 Influence of Multiple Circular Nozzle Configurations on Boundary-Layer Separation Location,
 $Re_x = 1.8 \times 10^6$, $M_\infty = 3.98$

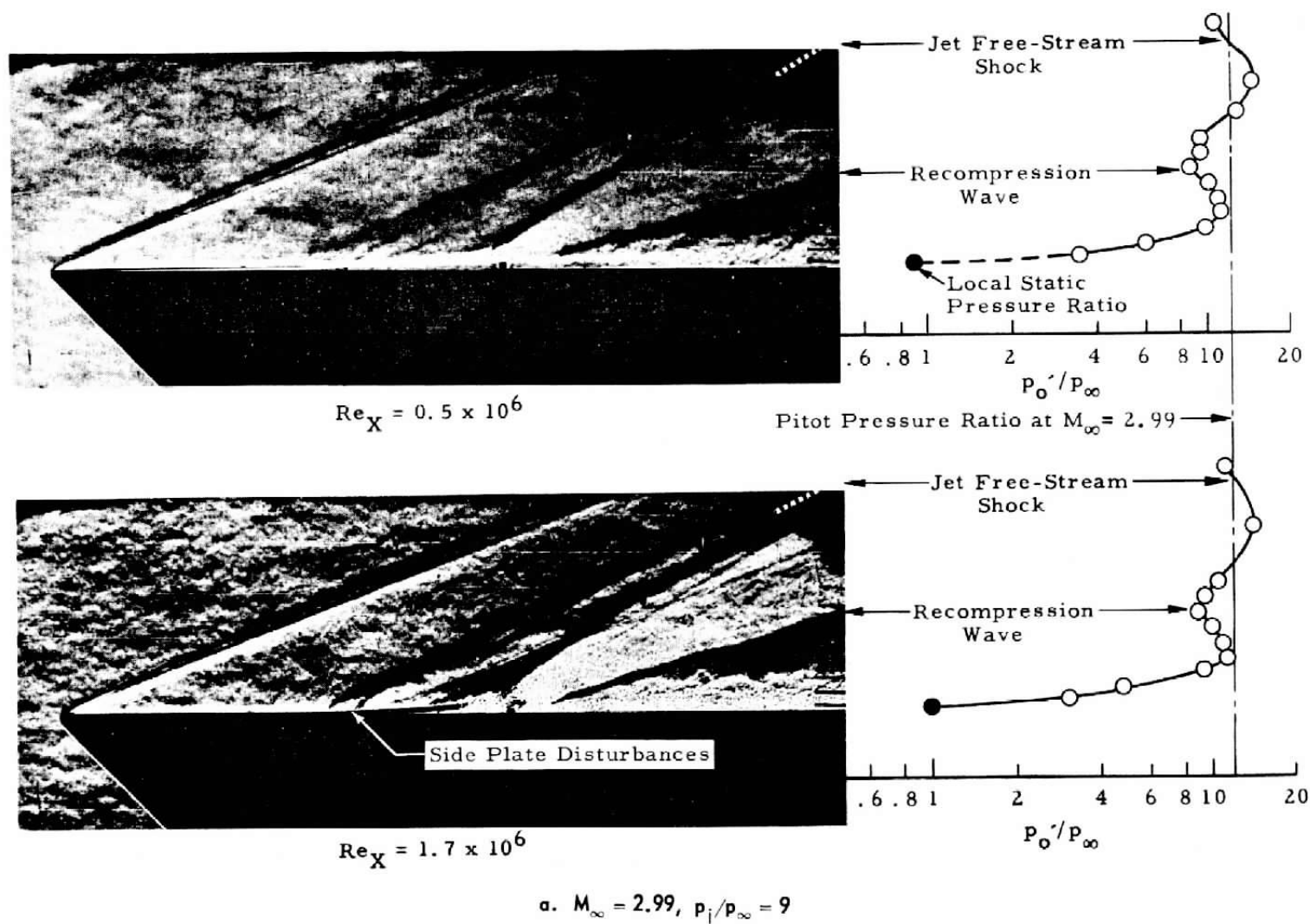
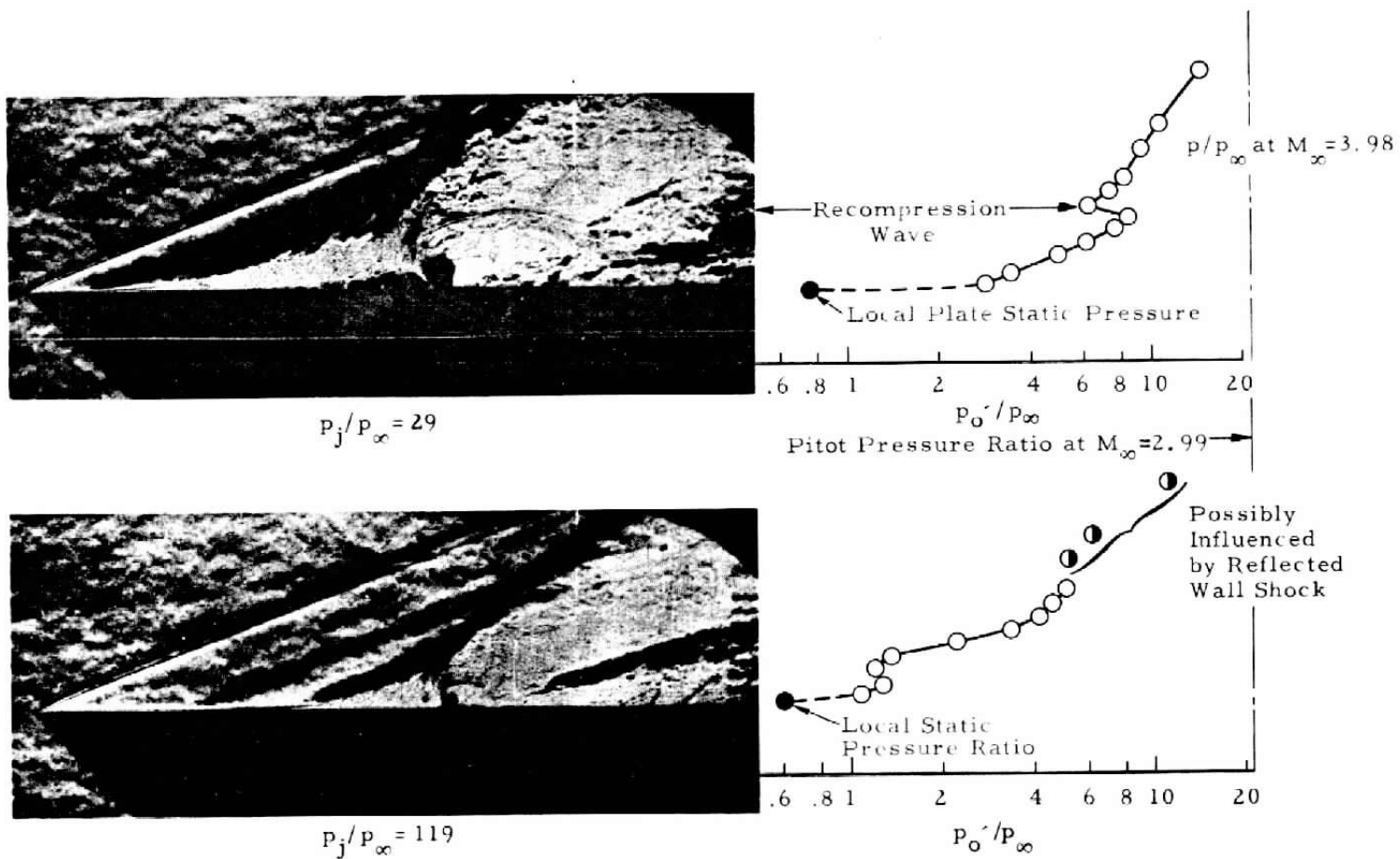
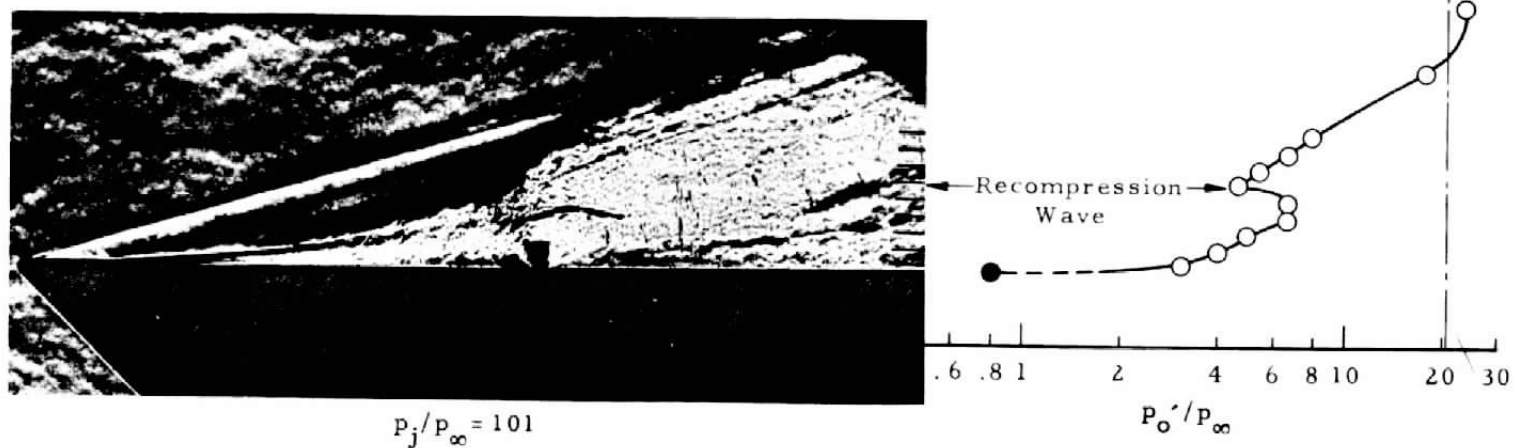
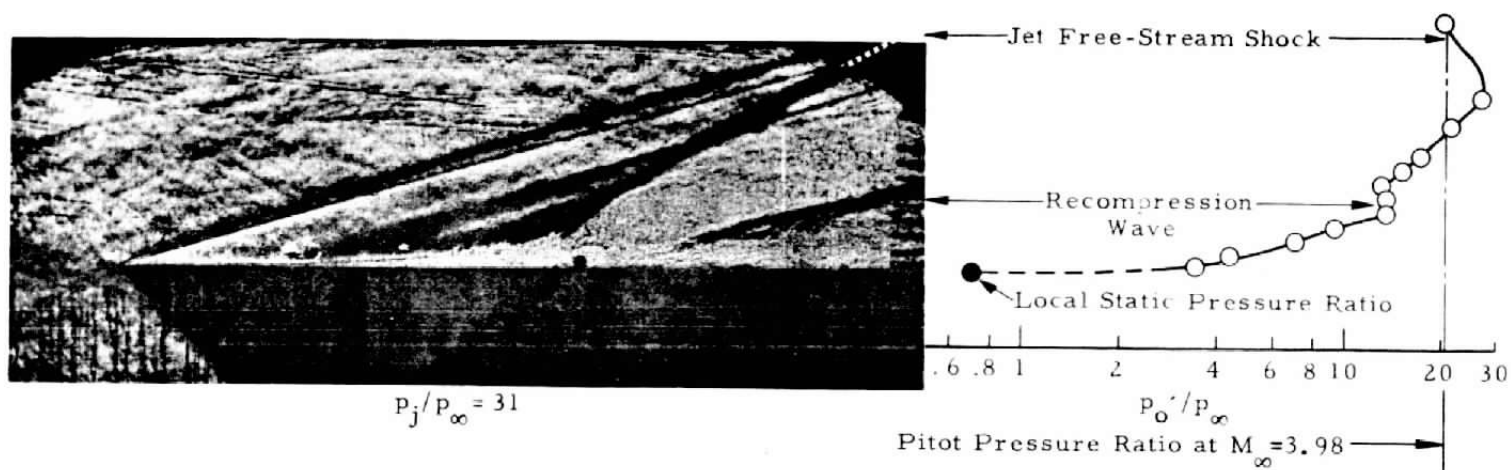


Fig. 15 Pitot Pressure Distribution Downstream of a Jet from a 0.131- by 3-in. Rectangular Slot



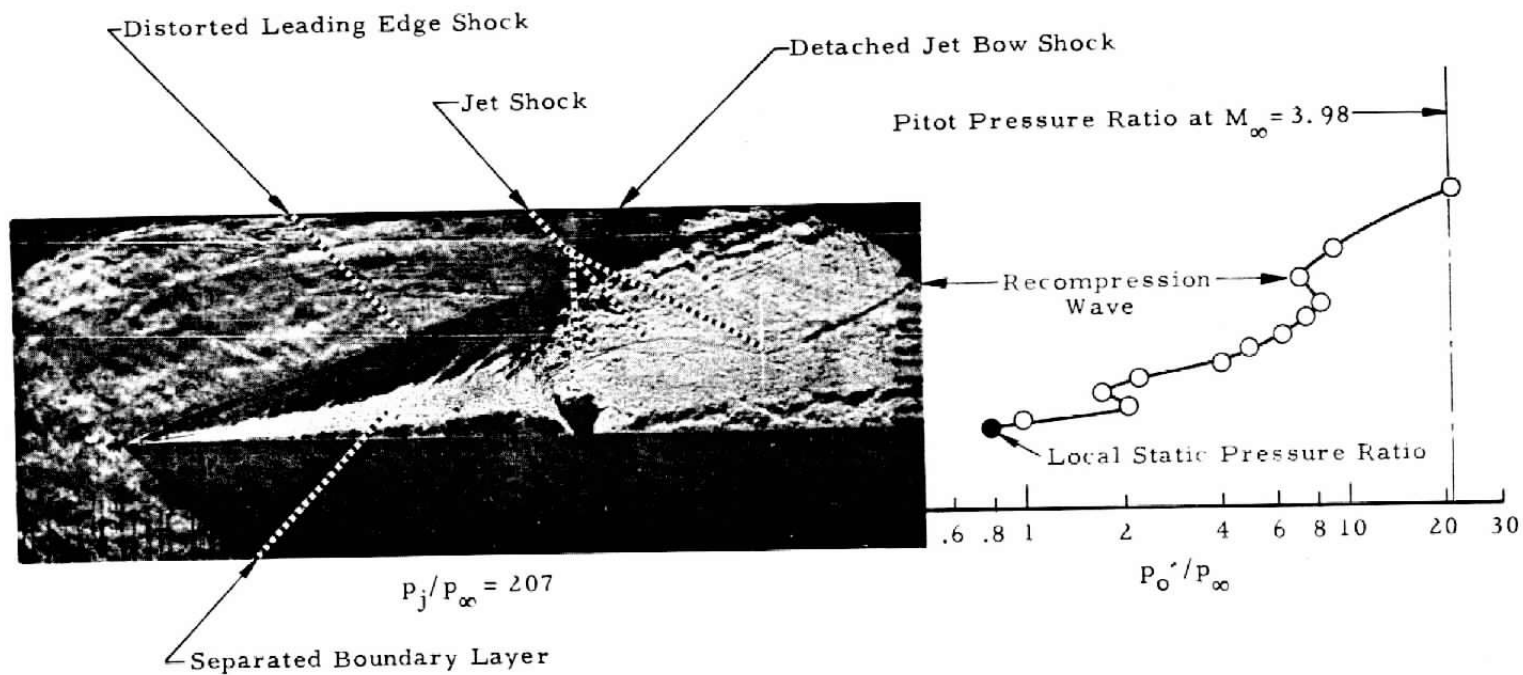
b. $M_\infty = 2.99$, $Re_x = 1.9 \times 10^6$, $p_i/p_\infty = 29, 119$

Fig. 15 Continued



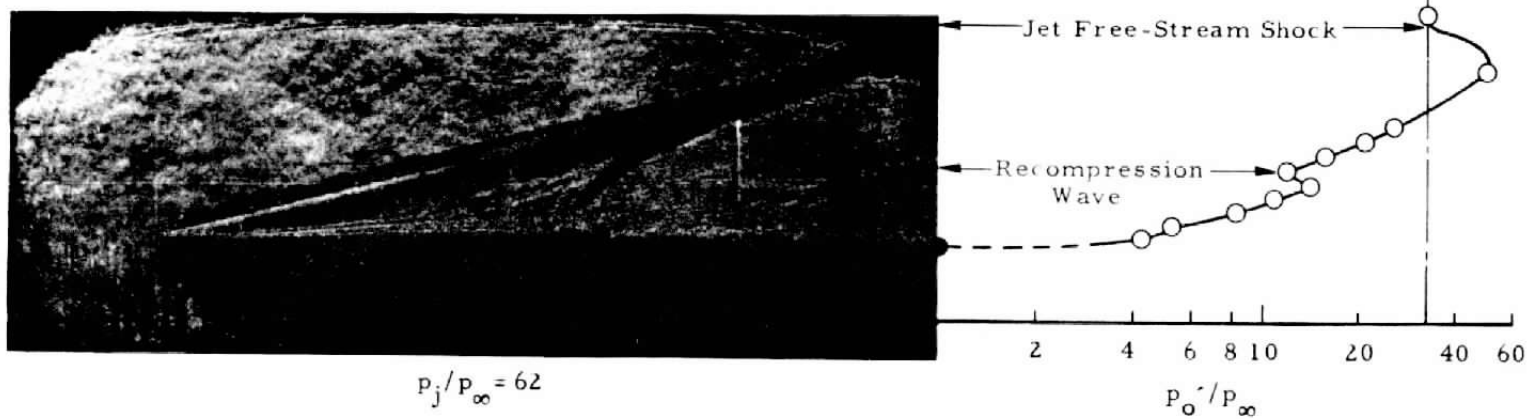
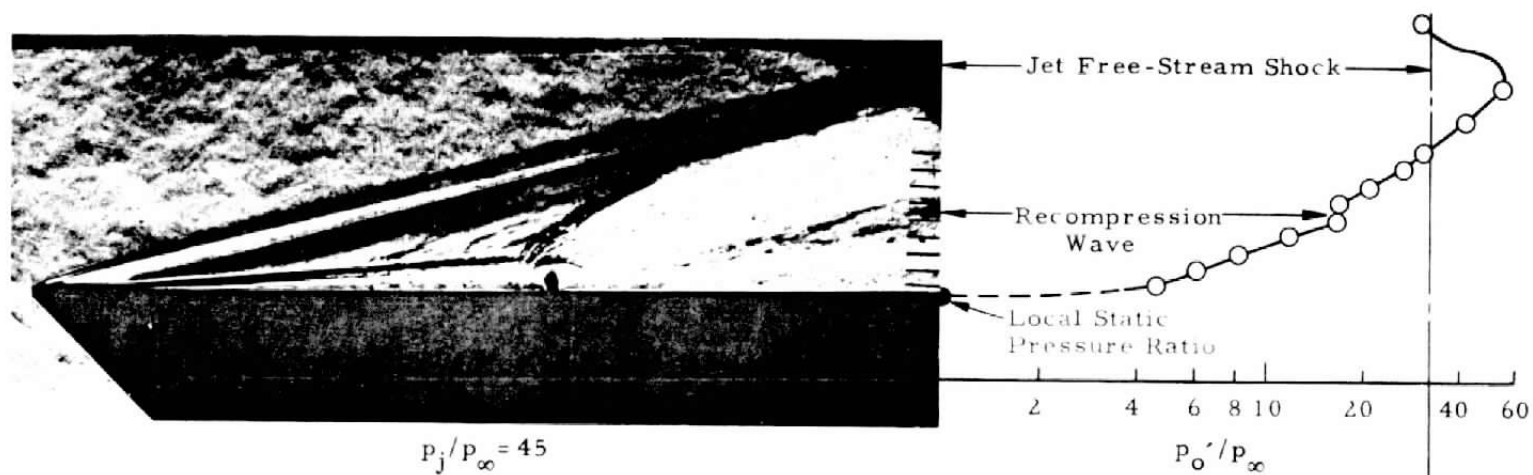
c. $M_\infty = 3.98$, $Re_X = 1.9 \times 10^6$, $p_j/p_\infty = 31, 101$

Fig. 15 Continued



d. $M_\infty = 3.98$, $Re_x = 1.9 \times 10^6$, $p_j/p_\infty = 207$

Fig. 15 Continued



e. $M_\infty = 5.01$, $Re_x = 2.2 \times 10^6$, $p_j/p_\infty = 45, 62$

Fig. 15 Continued

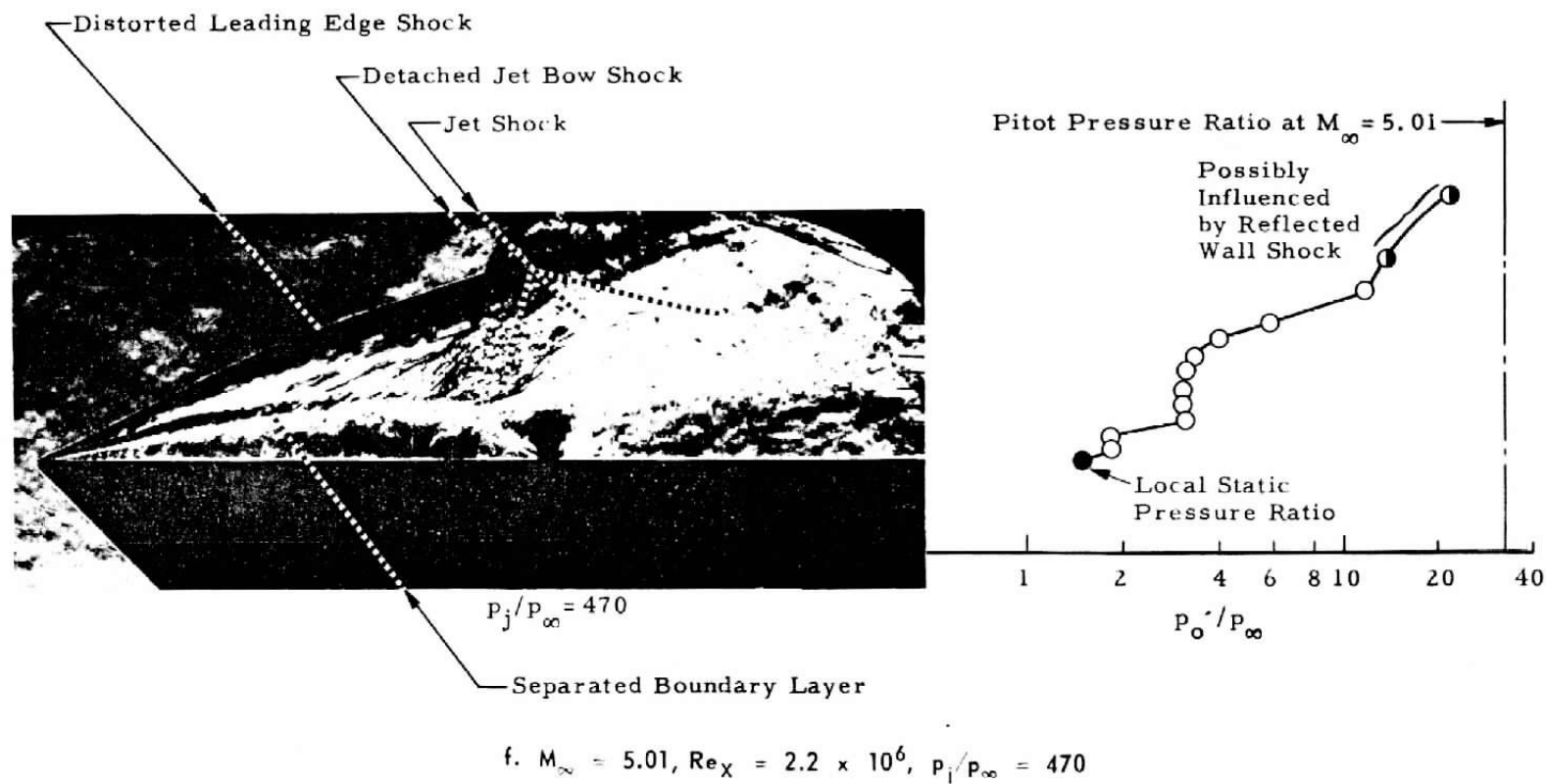
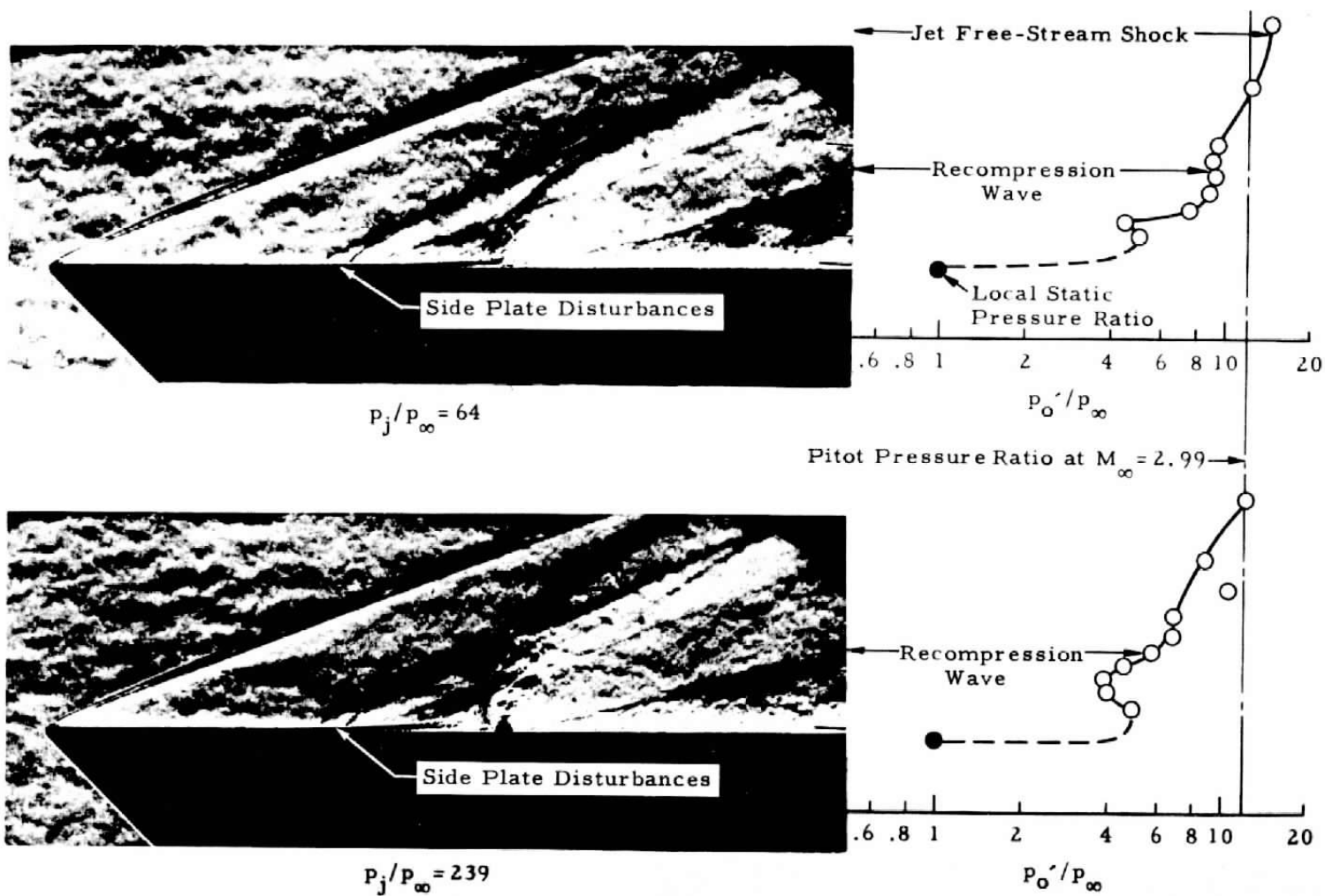
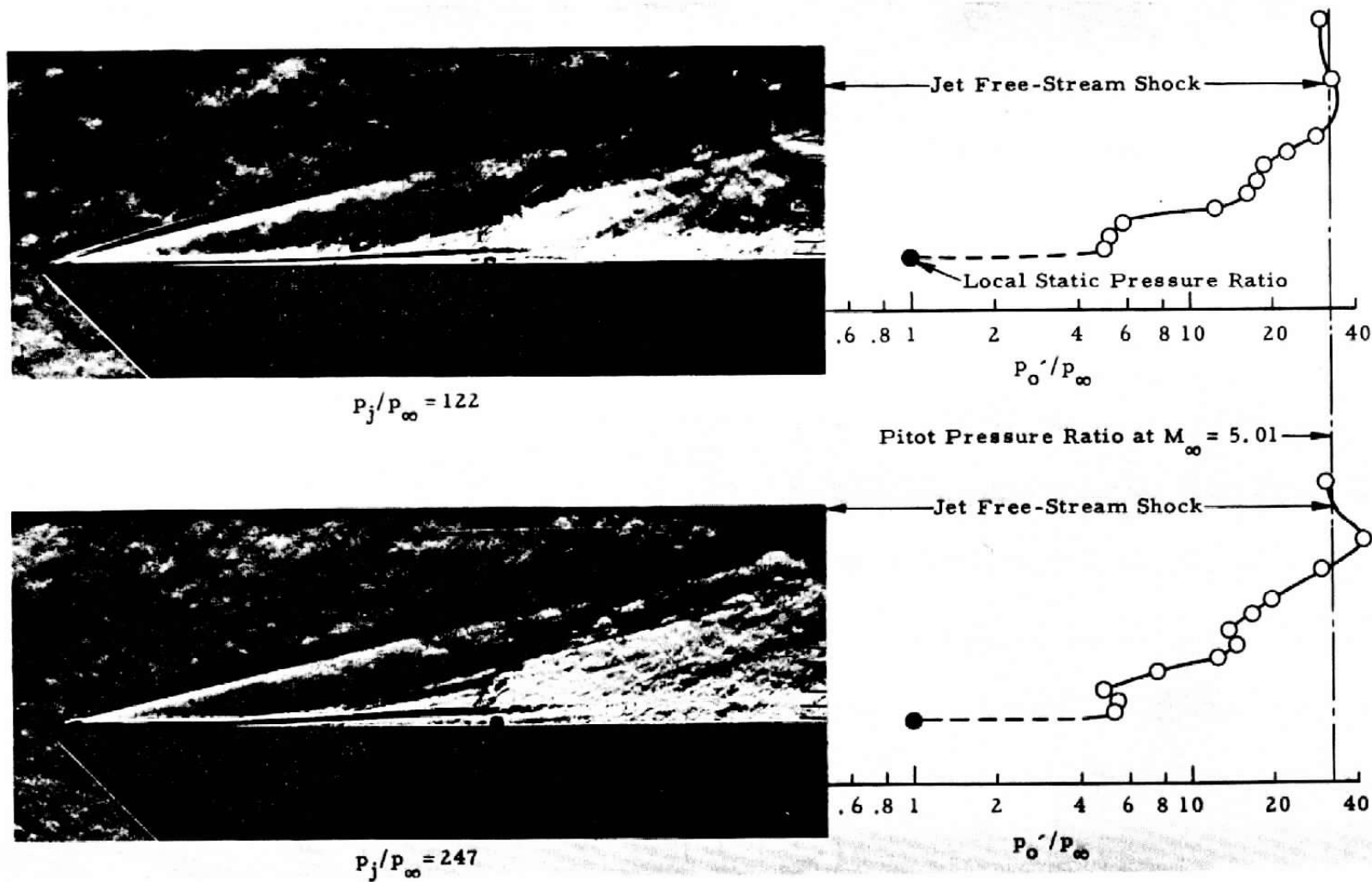


Fig. 15 Concluded



a. $M_\infty = 2.99$, $Re_x = 1.7 \times 10^6$

Fig. 16 Pitot Pressure Distribution Downstream of a Jet from a Circular Nozzle, $d_j = 0.25$ in.



b. $M_\infty = 5.01$, $Re_x = 2.1 \times 10^6$

Fig. 16 Concluded

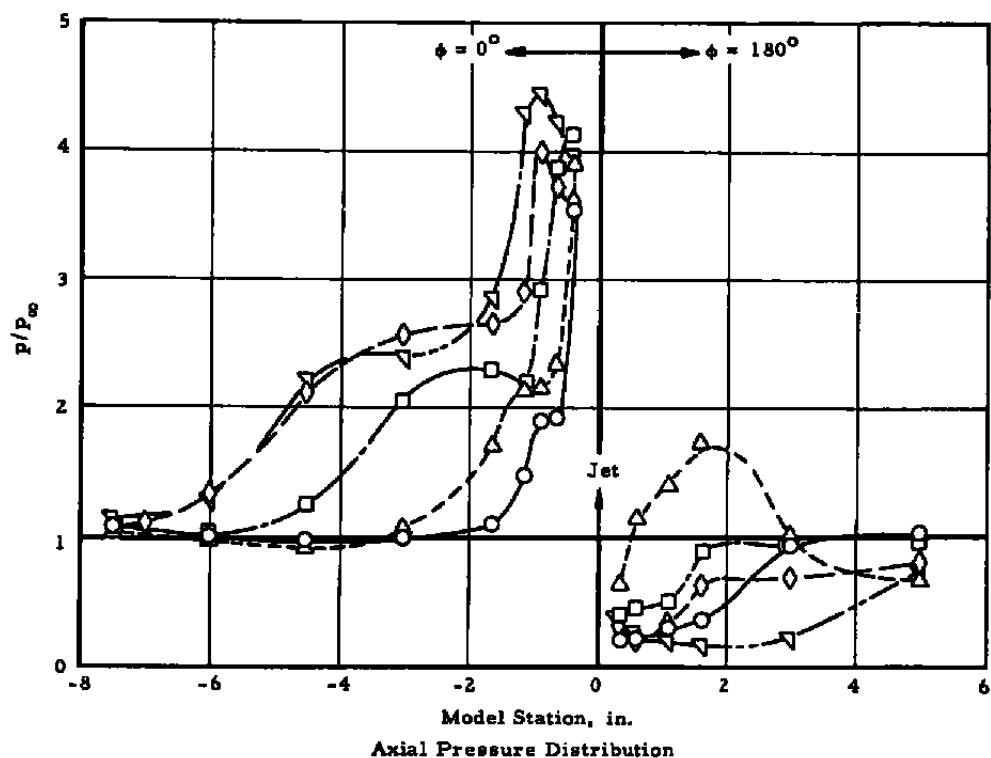
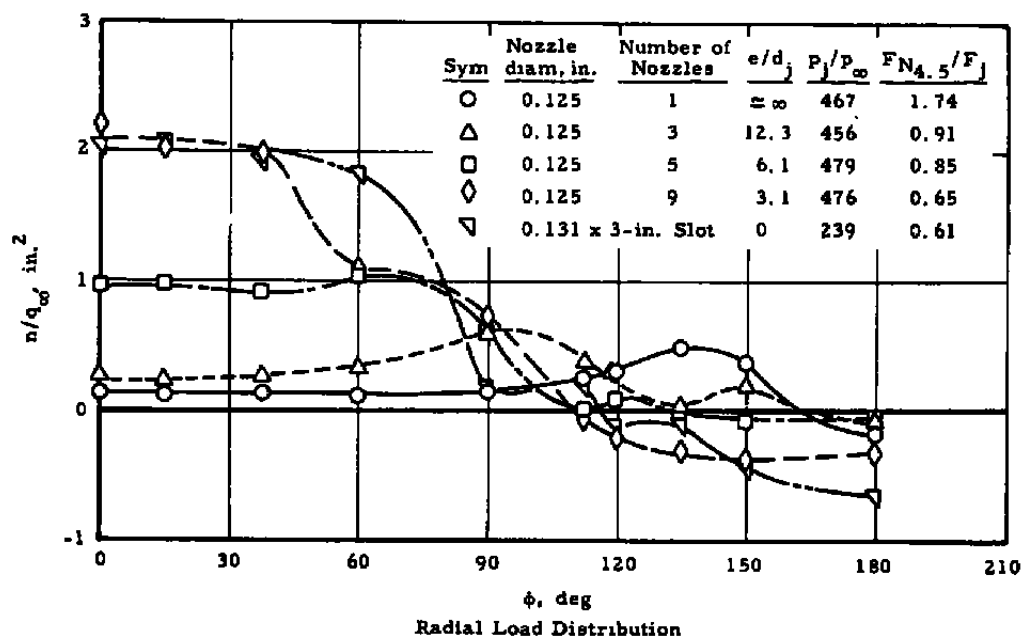


Fig. 17 Influence of Nozzle Configuration on the Radial Load and Pressure Distribution, $M_\infty = 3.98$, $Re_x = 3.6 \times 10^6$

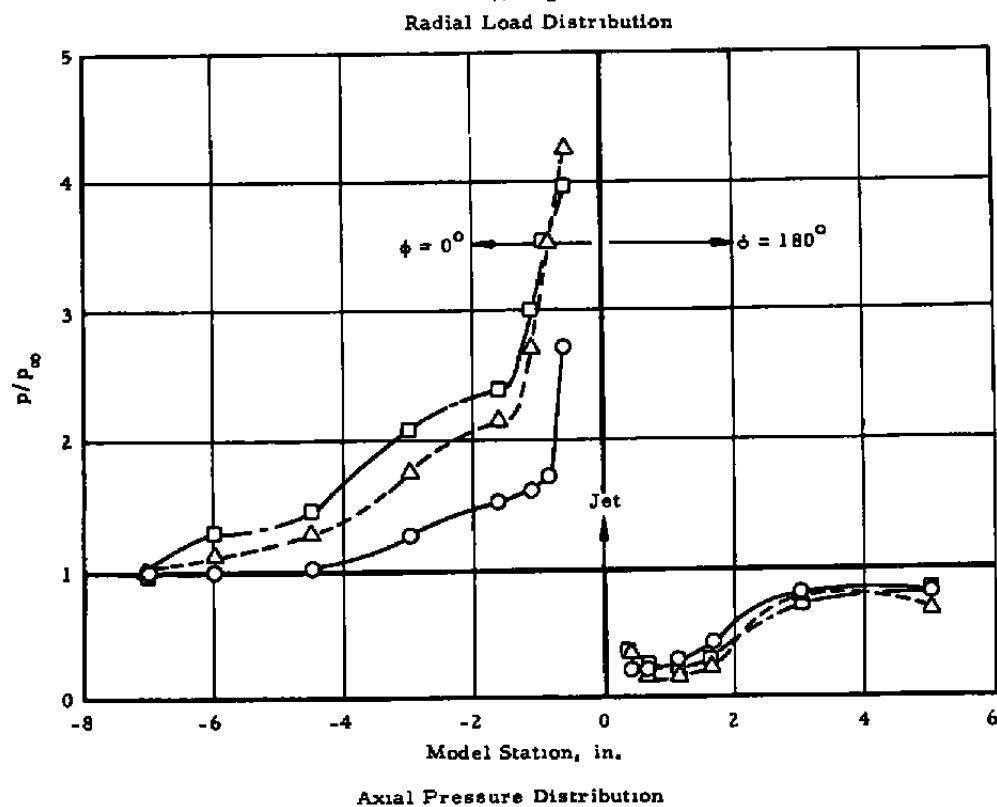
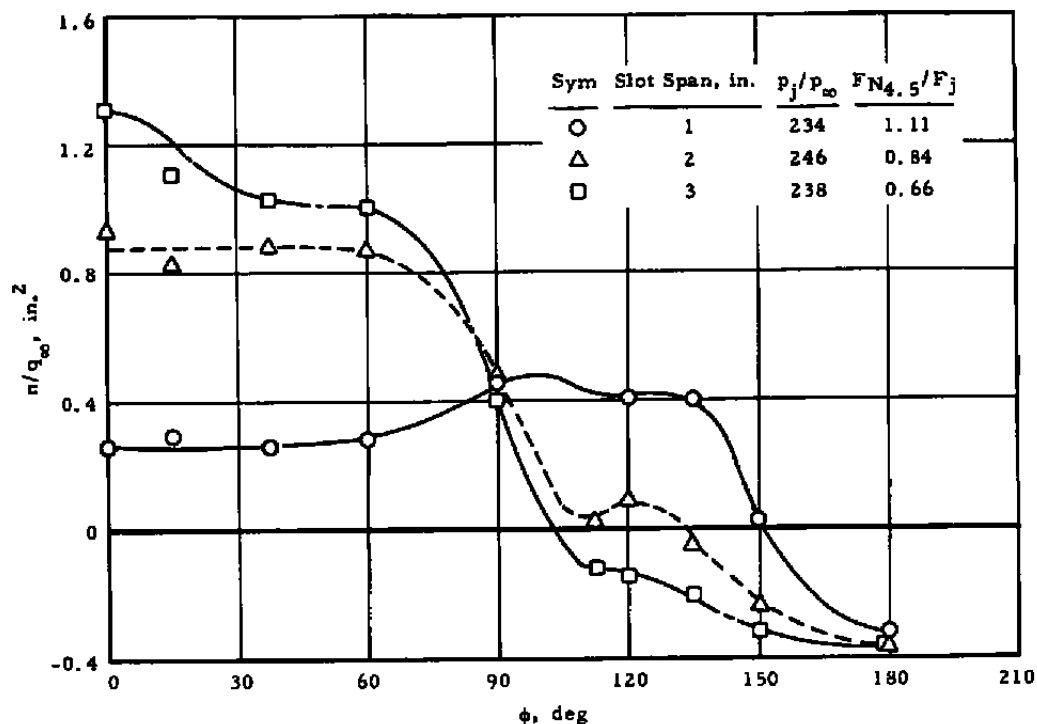


Fig. 18 Influence of Slot Span on the Radial Load and Axial Pressure Distribution of a 0.057-by 3-in. Slot, $M_\infty = 3.98$, $Re_x = 1.8 \times 10^6$

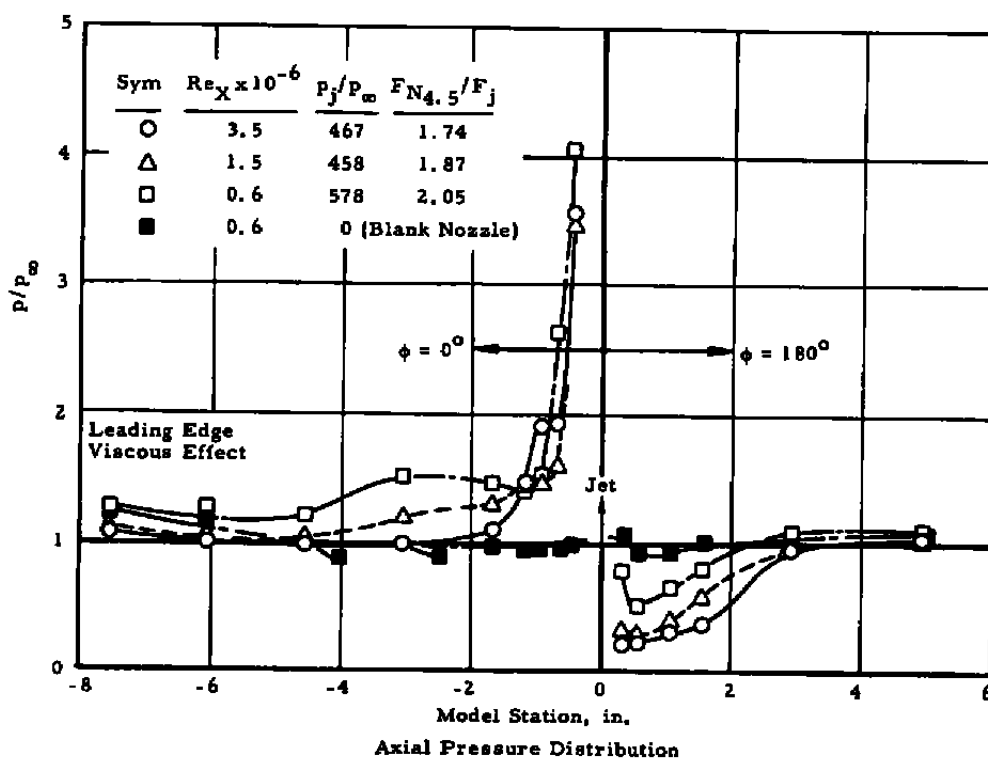
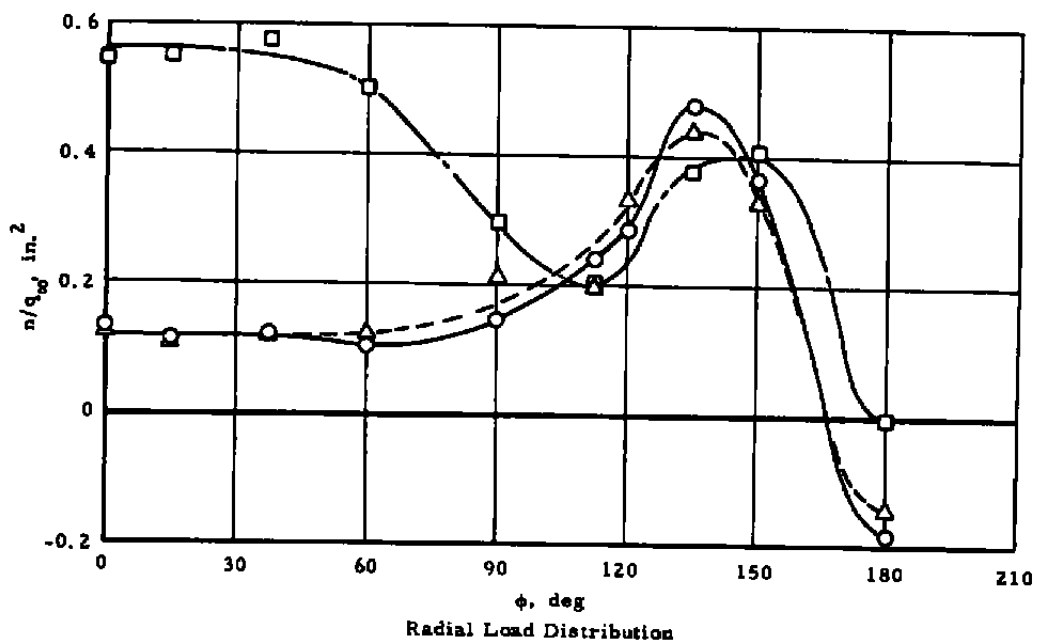


Fig. 19 Influence of Reynolds Number on the Radial Load and Pressure Distribution of a 0.125-in.-diam Circular Nozzle, $M_\infty = 3.98$

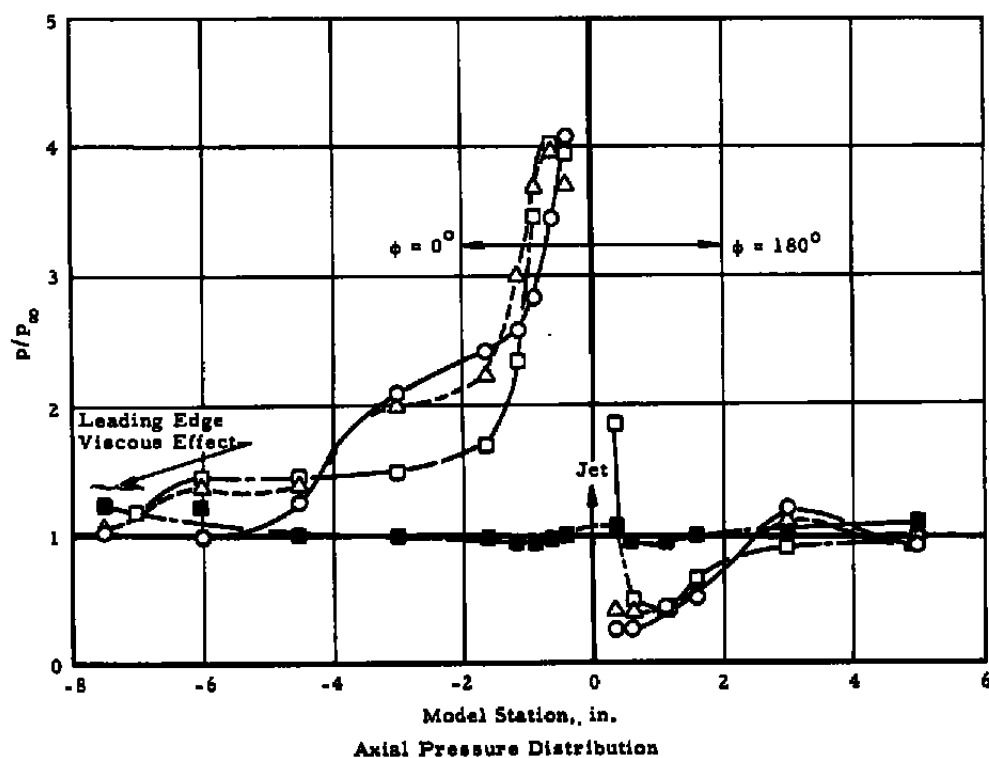
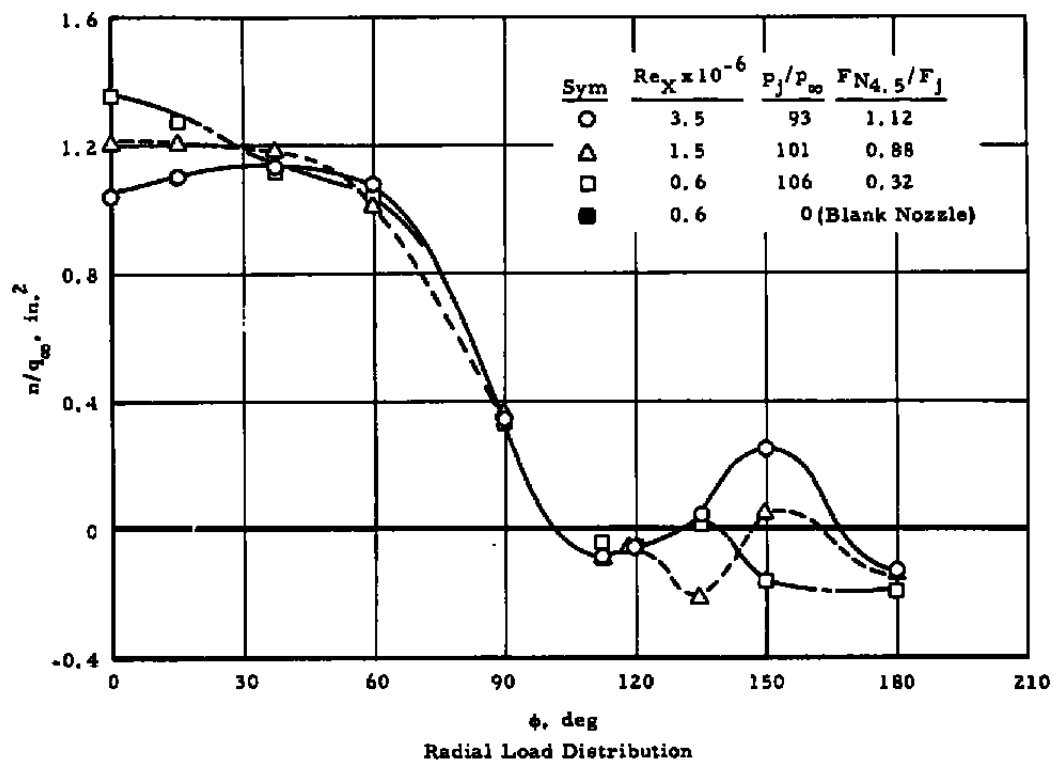


Fig. 20 Influence of Reynolds Number on the Radial Load and Pressure Distribution of a 0.131-by 3-in. Slot, $M_\infty = 3.98$

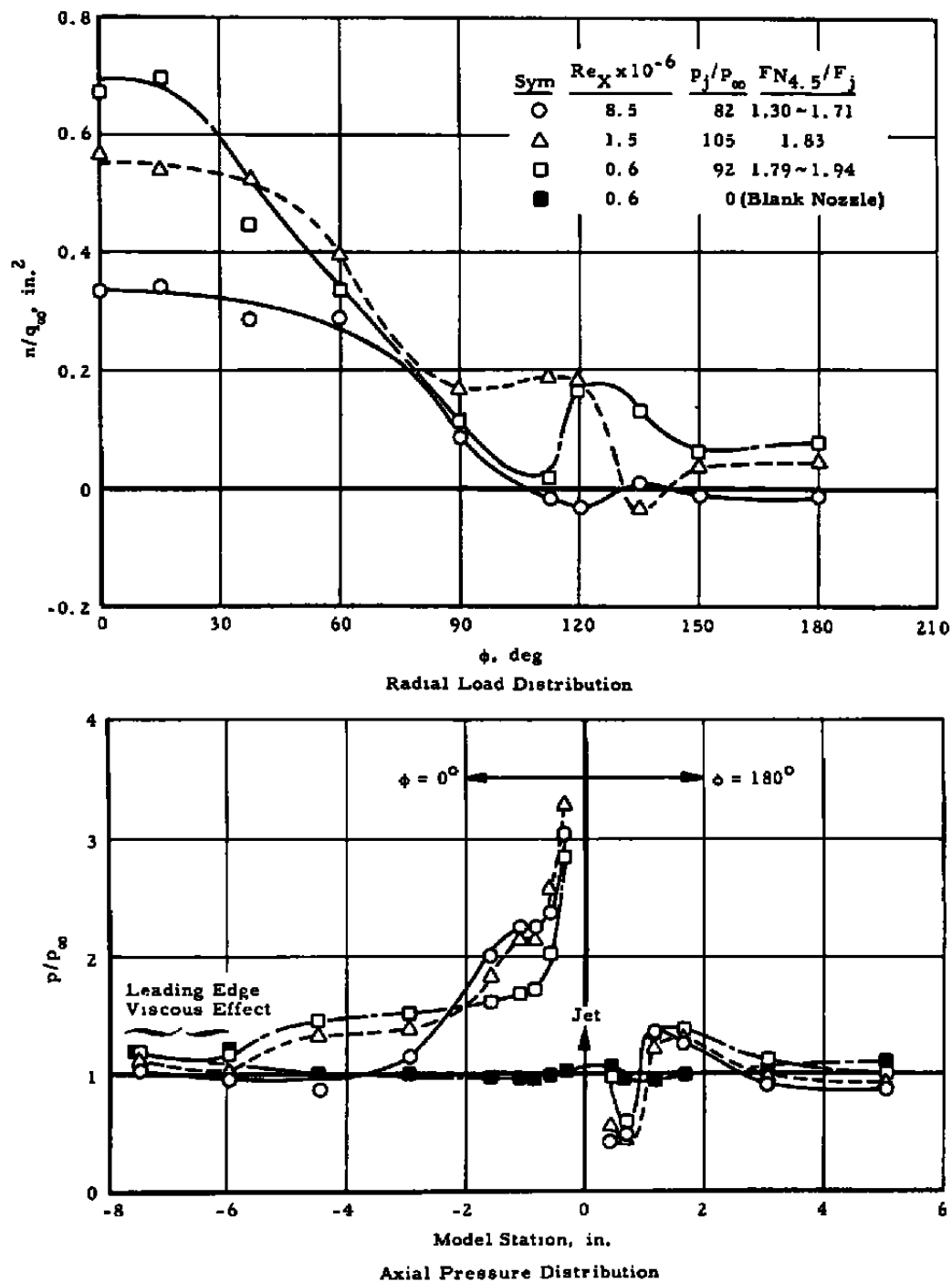


Fig. 21 Influence of Reynolds Number on the Radial Load and Axial Pressure Distribution of a 0.028-by 3-in. Slot, $M_\infty = 3.98$

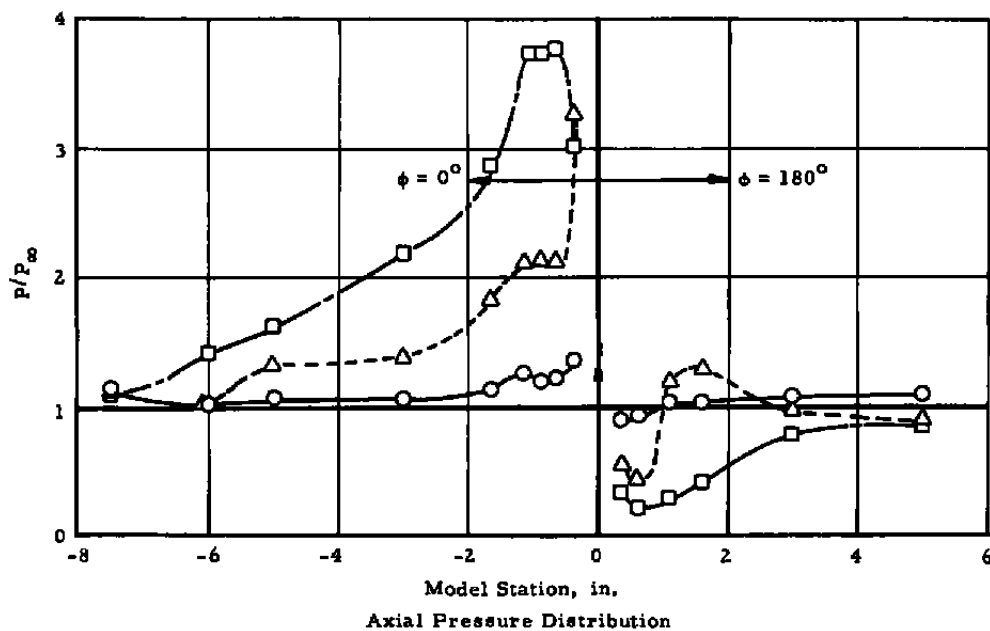
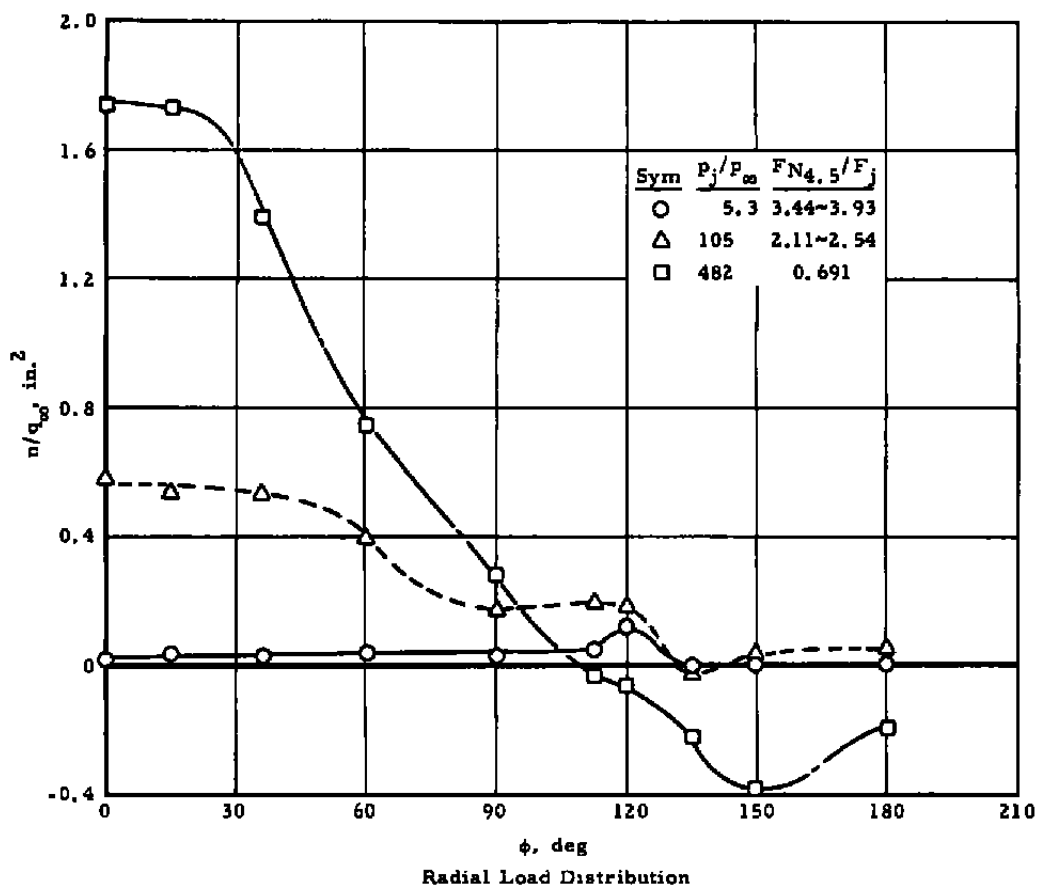


Fig. 22 Influence of Jet Pressure on the Radial Load and Axial Pressure Distribution of a 0.028-by 3-in. Slot, $Re_x = 1.8 \times 10^6$, $M_\infty = 3.98$

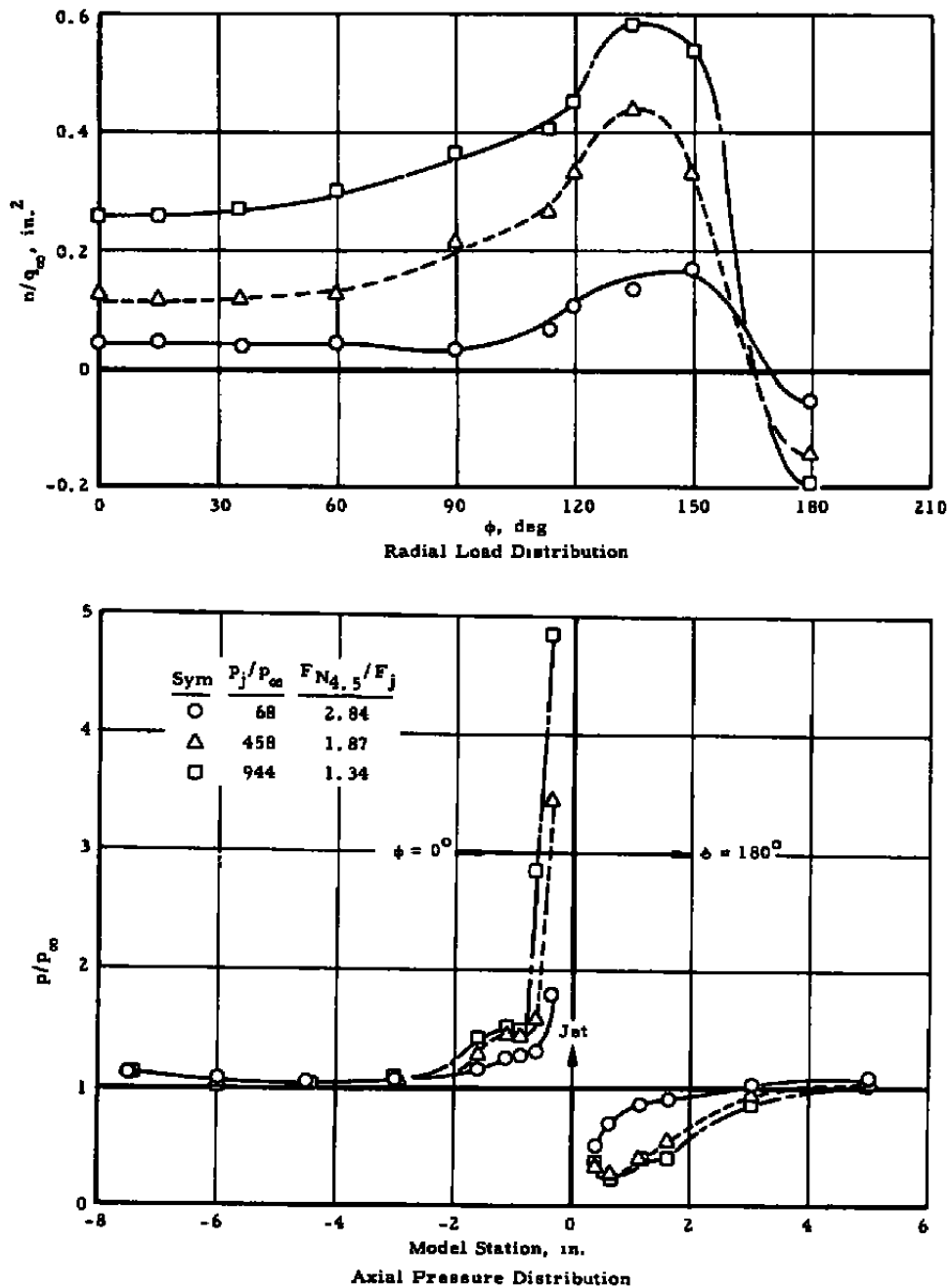


Fig. 23 Influence of Jet Pressure on the Radial Load and Axial Pressure Distribution of a 0.125-in.-diam Nozzle, $Re_x = 1.8 \times 10^6$, $M_\infty = 3.98$

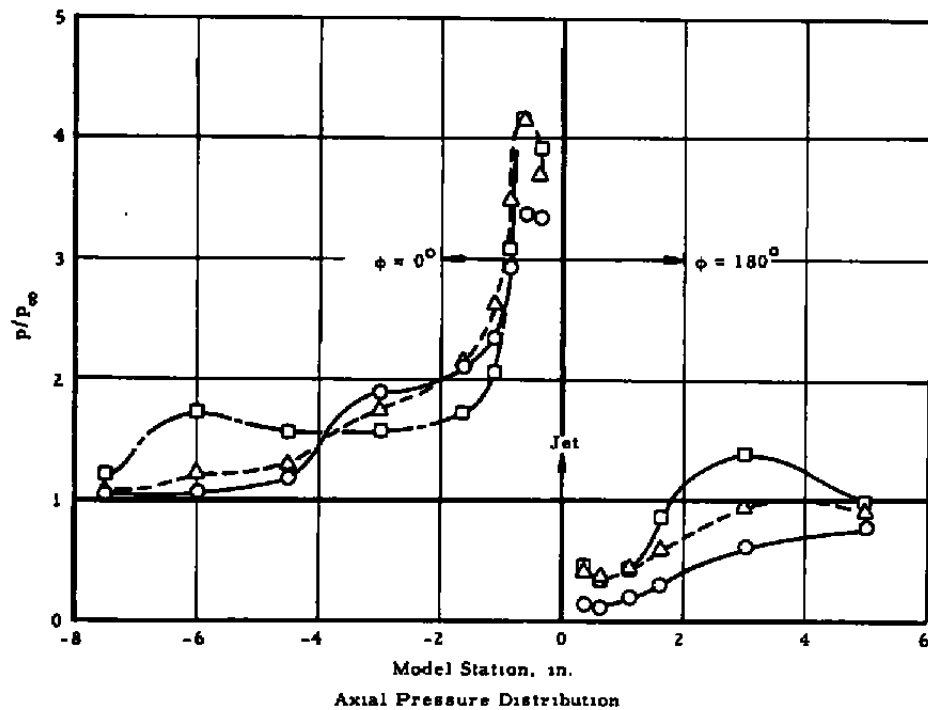
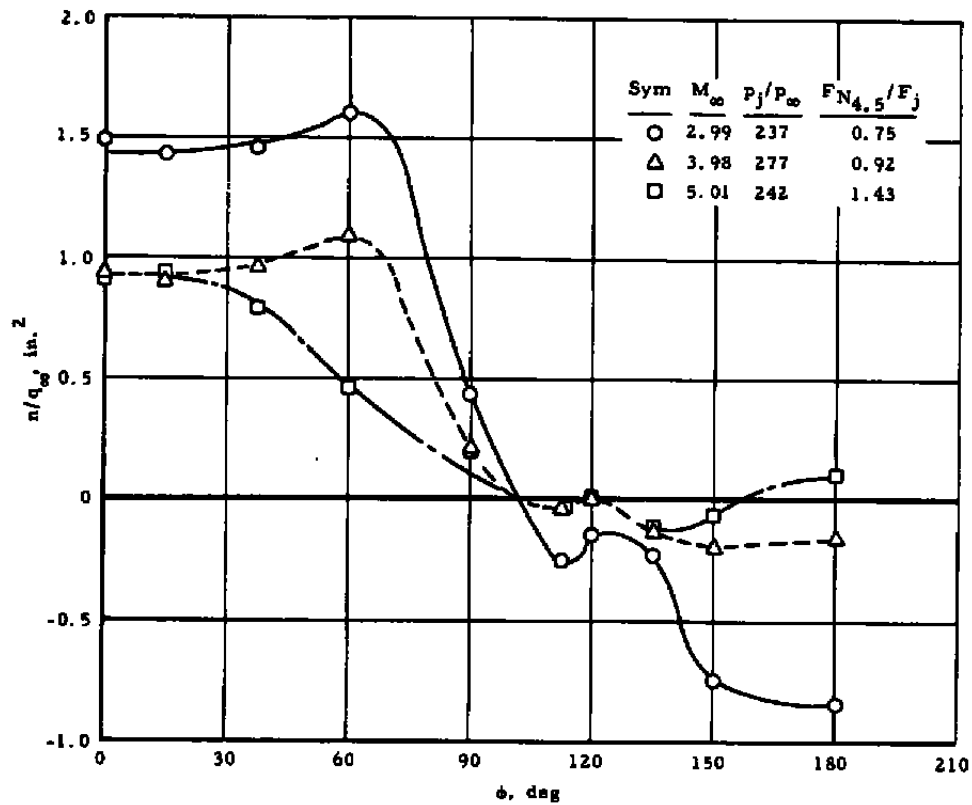


Fig. 24 Influence of Mach Number on the Radial Load and Axial Pressure Distributions of a 0.028-by 3-in. Slot, $Re_x = 1.5$ to 2.2×10^6

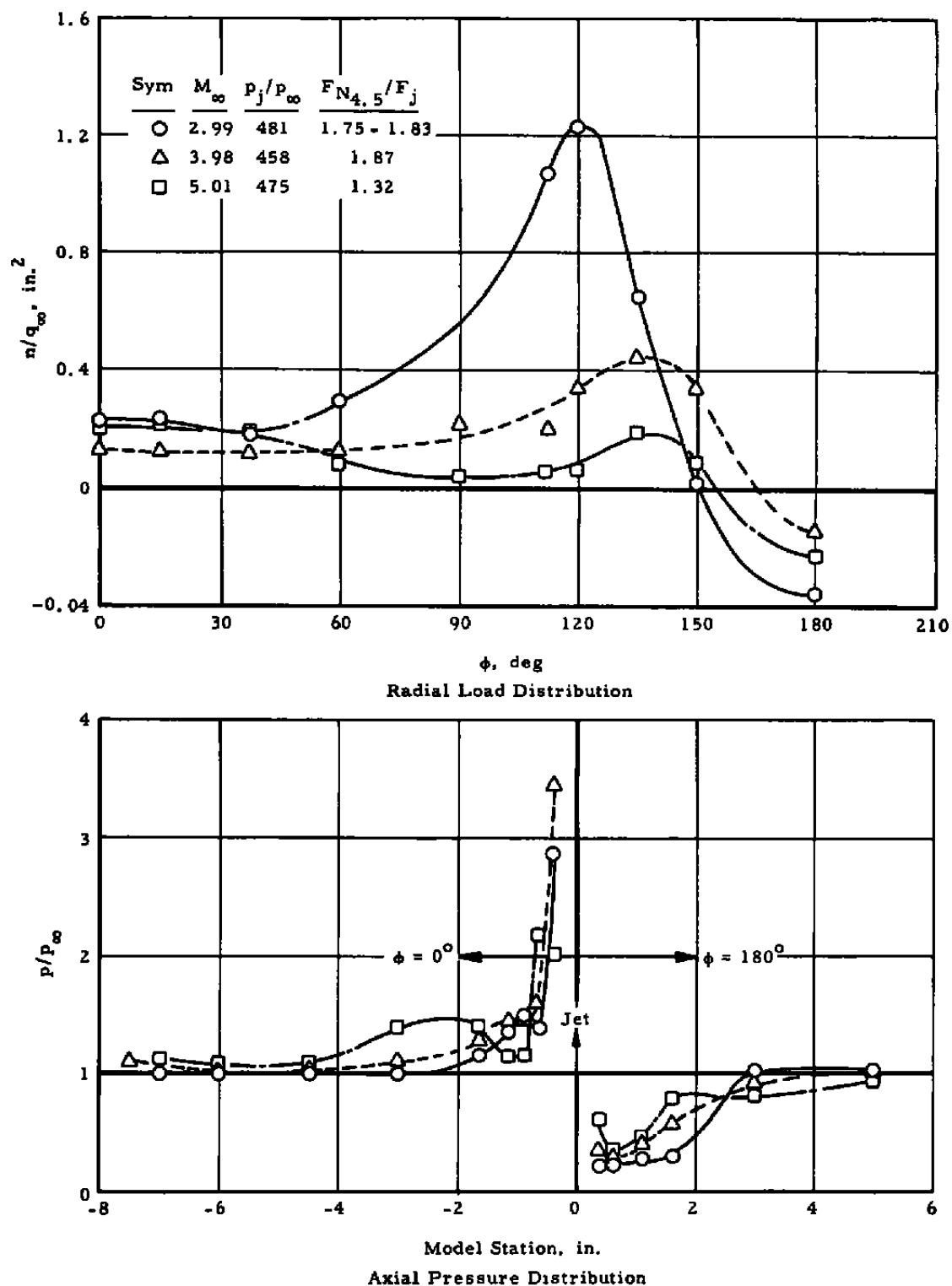


Fig. 25 Influence of Mach Number on the Radial Load and Axial Pressure Distribution of a 0.125-in.-diam Circular Nozzle, $Re_x = 1.5$ to 2.2×10^6

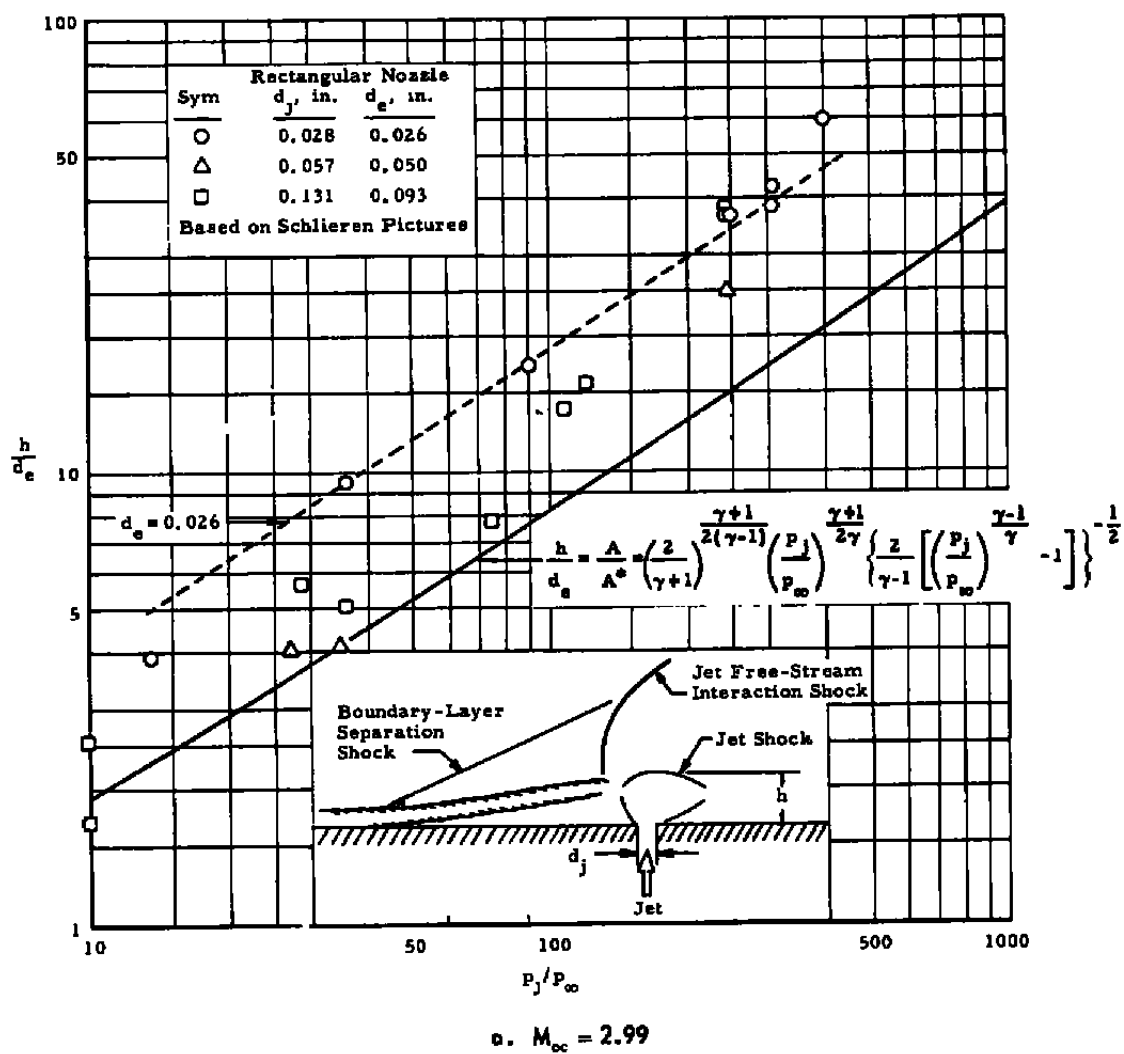


Fig. 26 The Effective Spoiler Height Generated by Rectangular Sonic Nozzle Jets

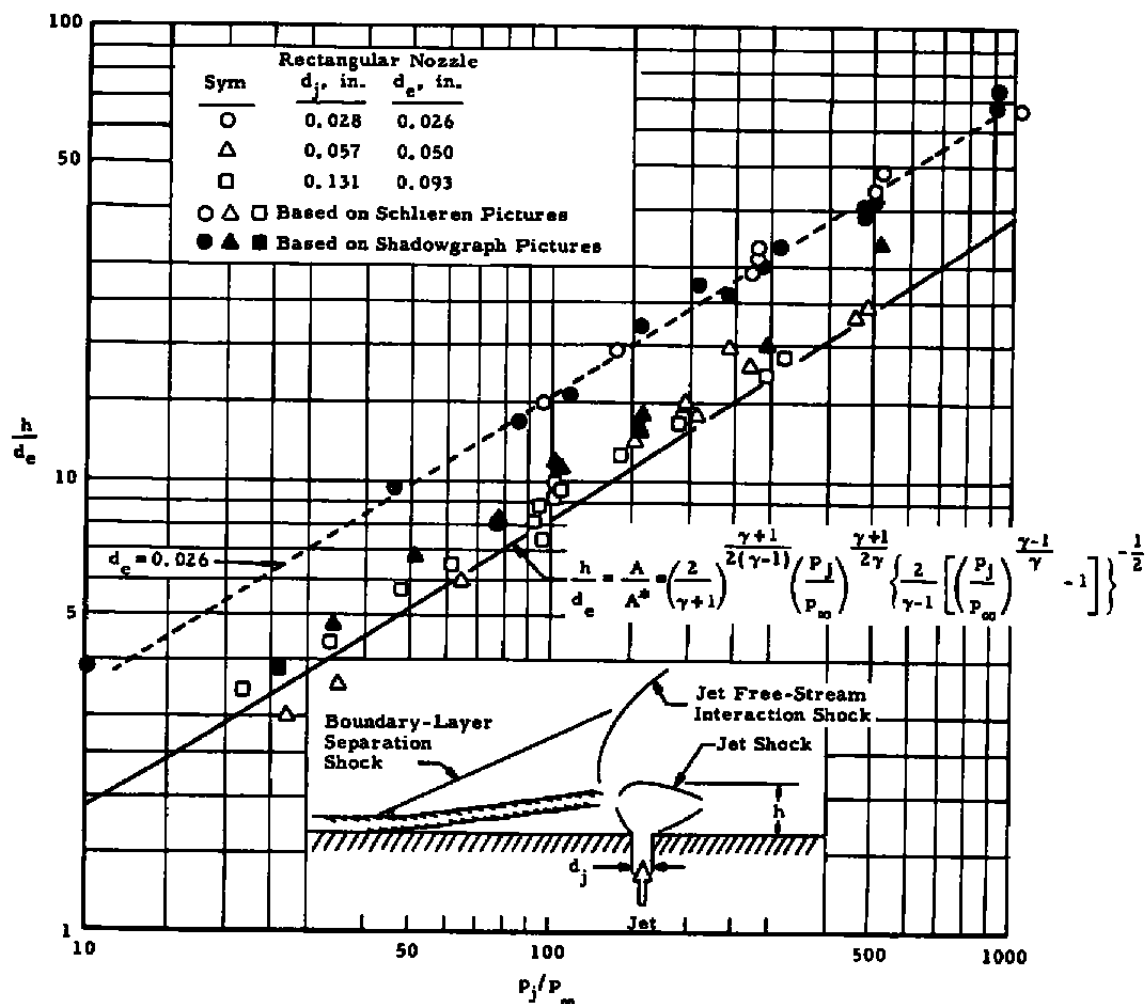
b. $M_\infty = 3.98$

Fig. 26 Continued

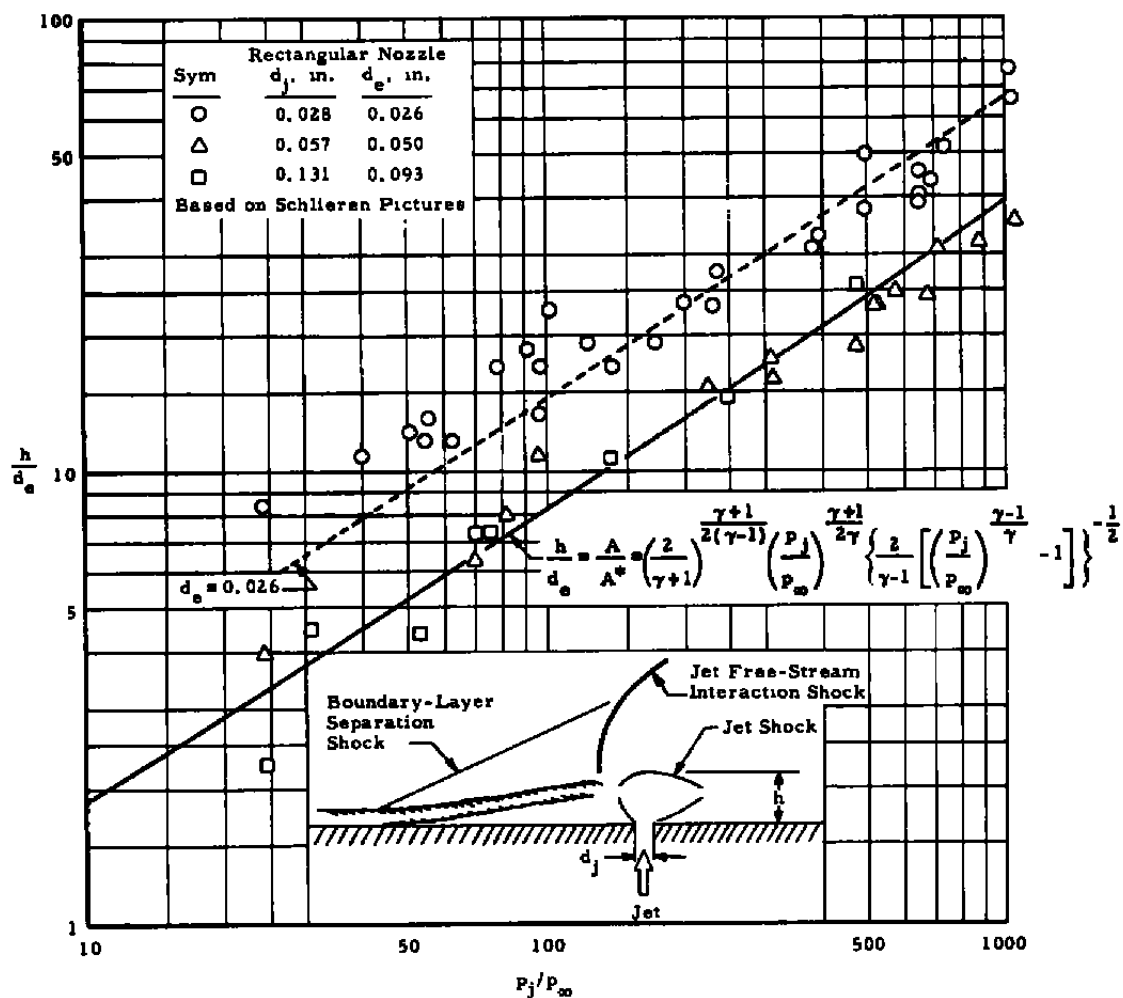
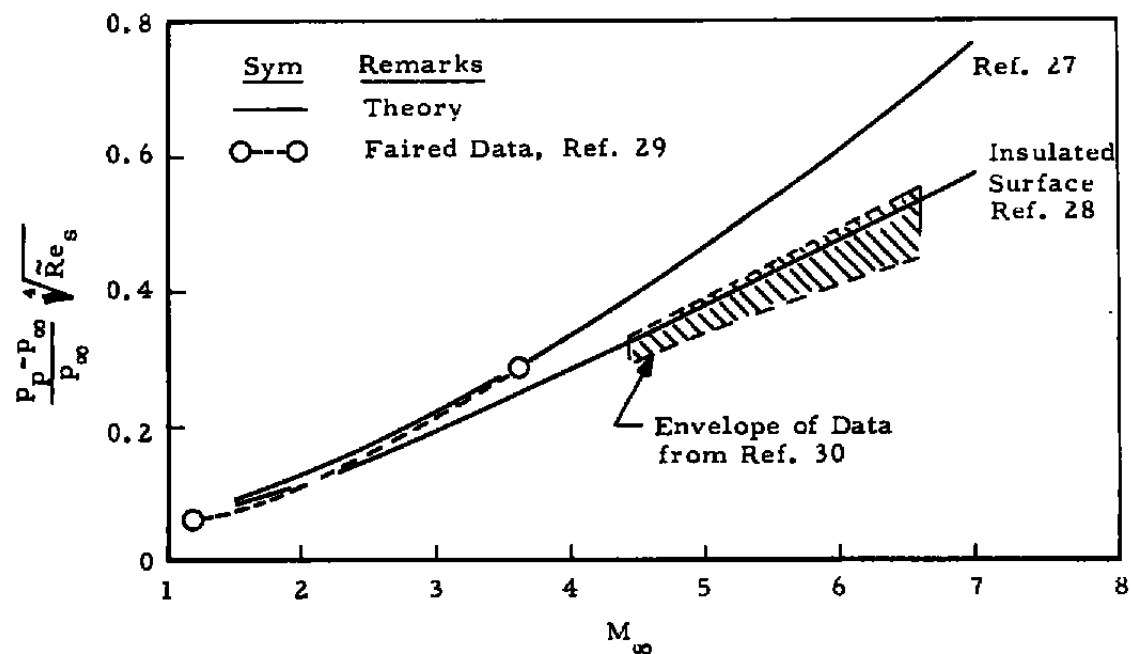
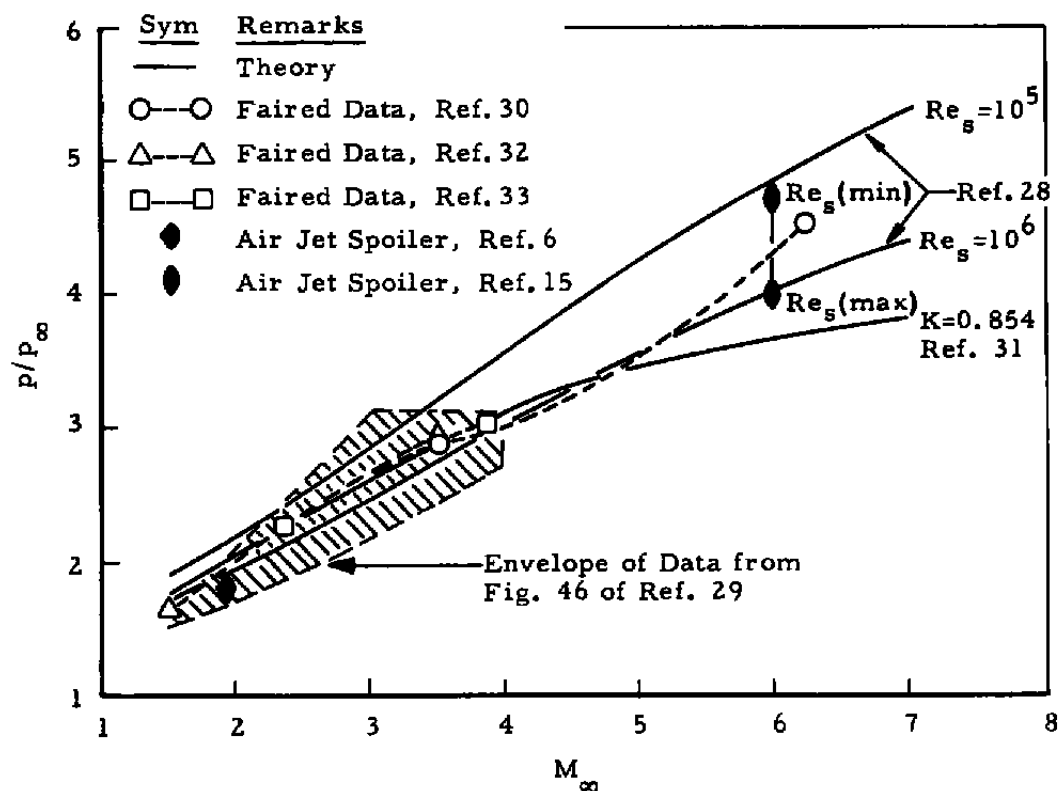
c. $M_\infty = 5.01$

Fig. 26 Concluded

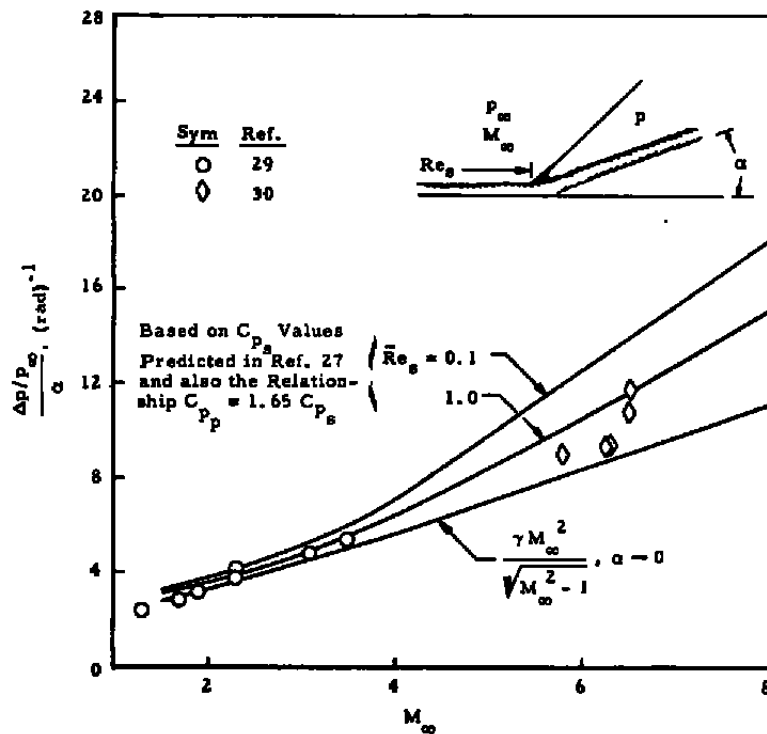


a. Laminar Separation

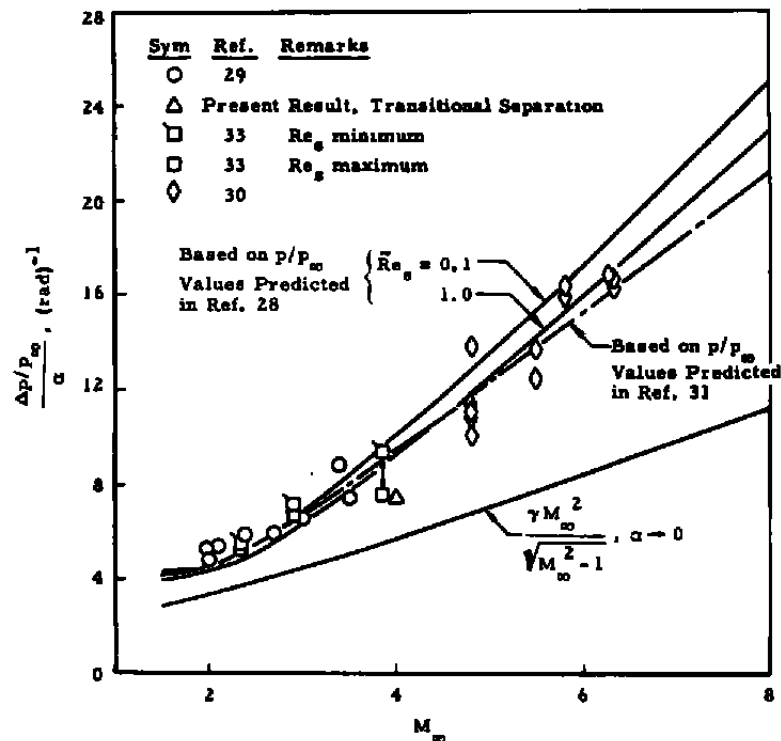


b. Turbulent Separation

Fig. 27 Plateau Pressure Produced by a Separated Boundary Layer at Various Mach Numbers



a. Laminar Boundary-Layer Separation



b. Turbulent Boundary-Layer Separation

Fig. 28 Theoretical and Experimental Correlation of the Pressure Loading Factor Generated by Separated Boundary Layers

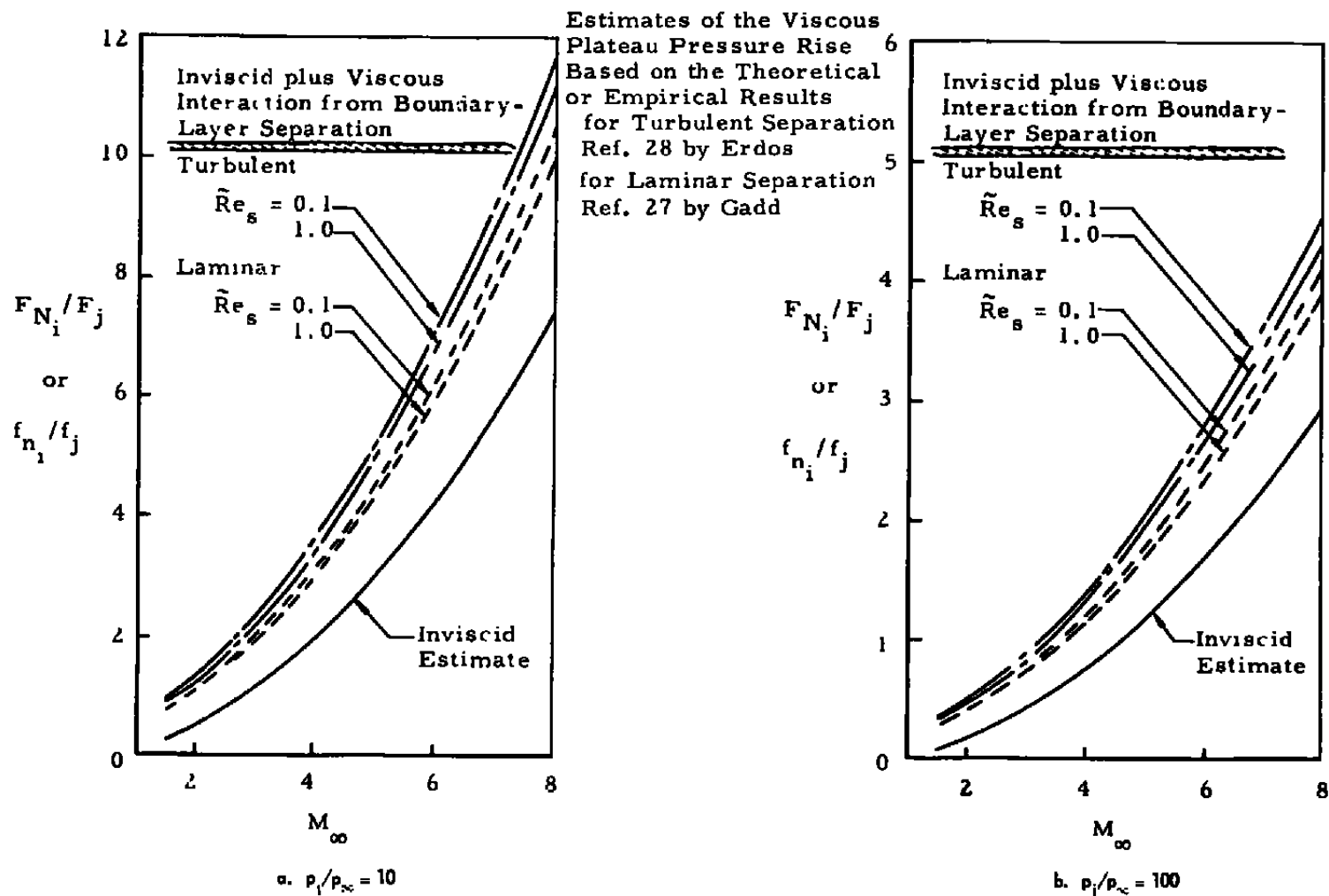


Fig. 29 Estimated Ratio of Interaction Force to Jet Reaction Force of a Sonic, Two-Dimensional Lateral Jet

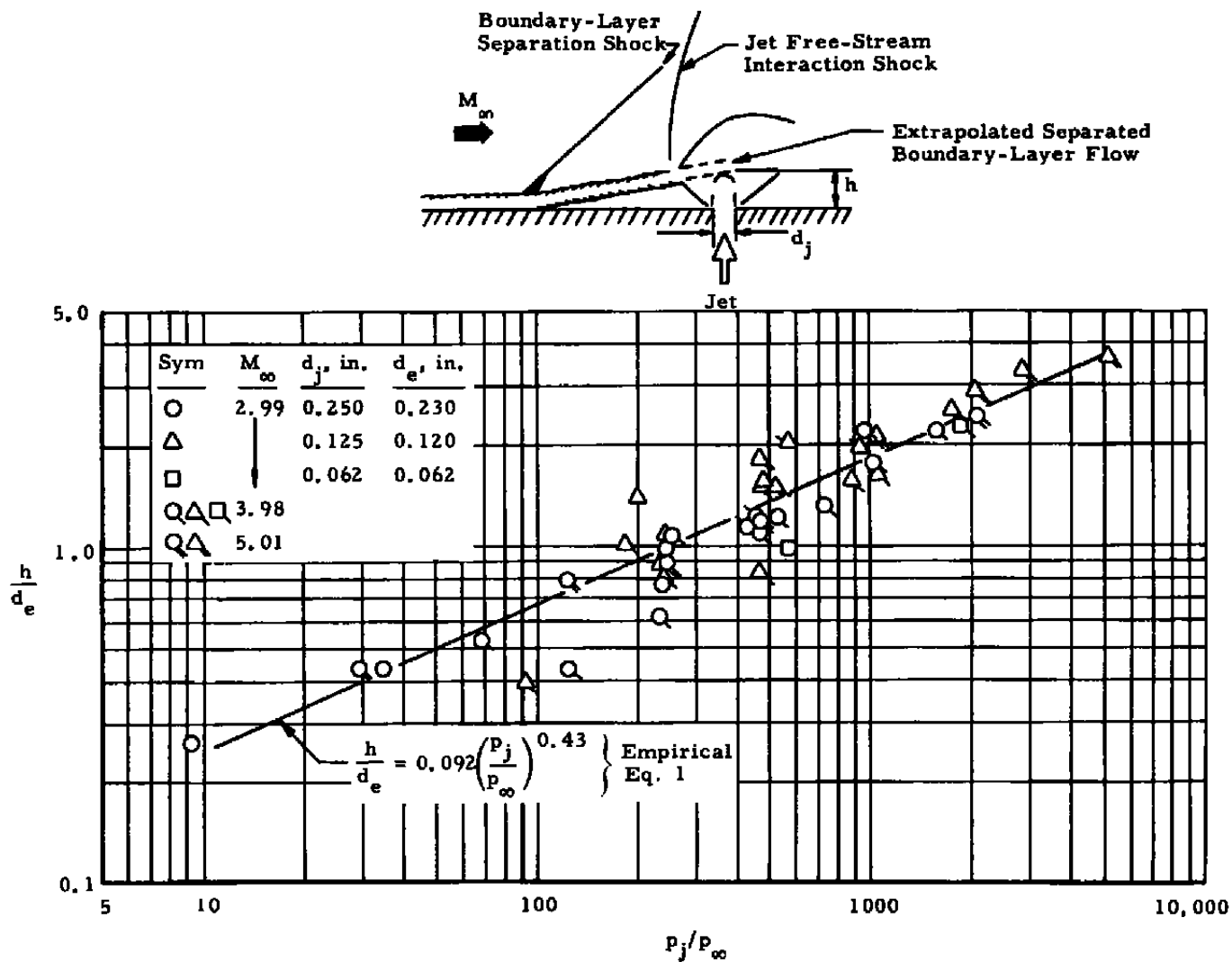
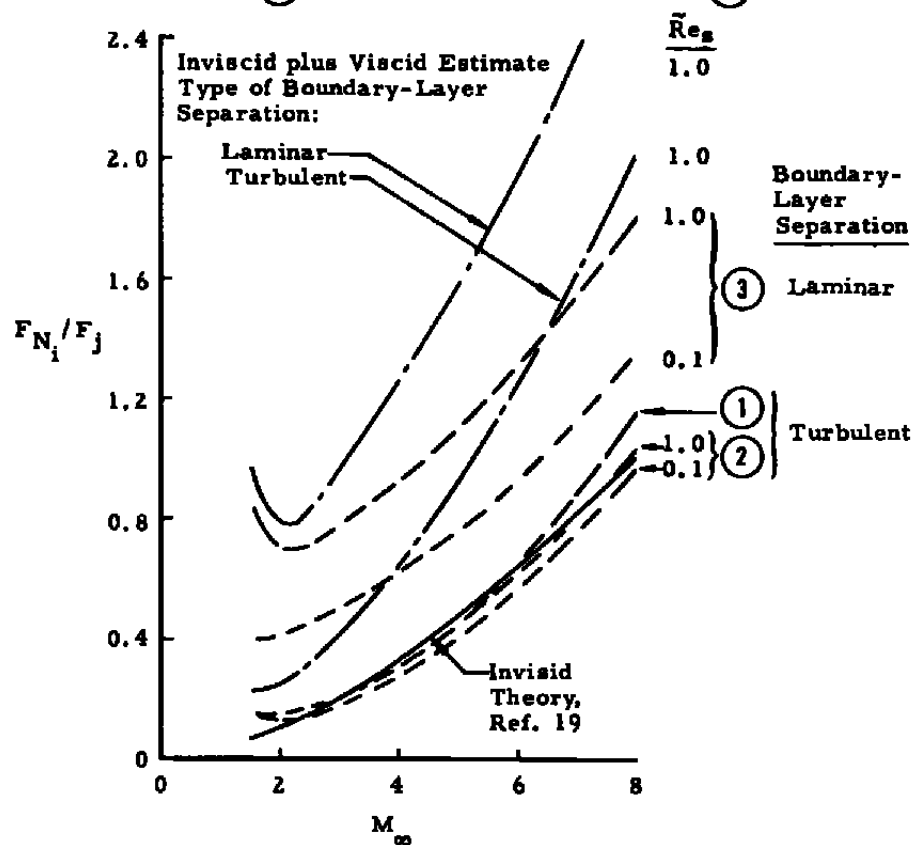


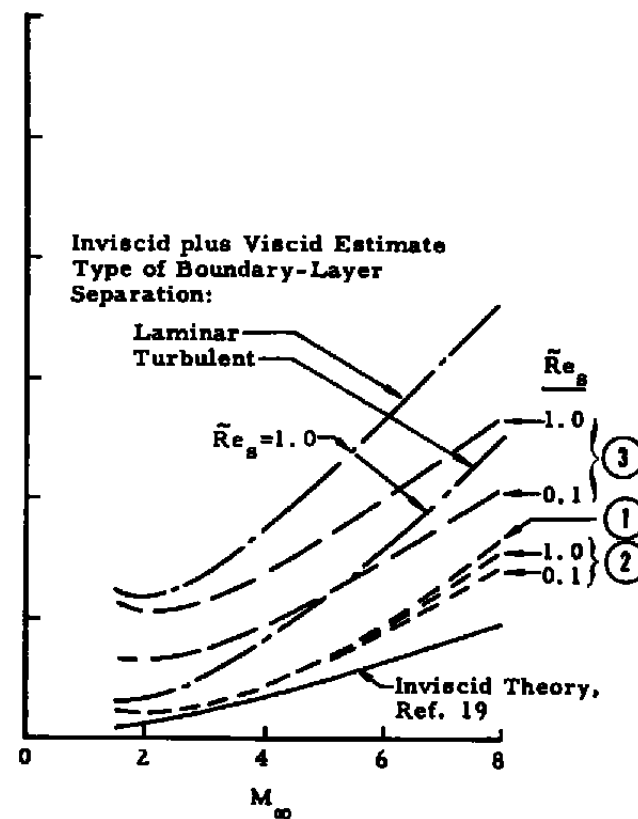
Fig. 30 The Effective Spoiler Height Generated by Circular Sonic Nozzle Jets

Based on Theoretical or Empirical Estimates of the Separated
Boundary-Layer Plateau Pressure Rise of Reference

① Crocco and Probstein, Ref. 31 ② Erdos, Ref. 28 ③ Gadd, Ref. 27



a. $p_i/p_\infty = 100$



b. $p_i/p_\infty = 1000$

Fig. 31 Estimated Ratio of Interaction Force to Jet Reaction Force of a Circular Sonic Lateral Jet

Sym	d_j , in.	l/d_j
○	0.028	107
△	0.057	53
□	↓	35
◇	↓	18
▽	0.131	23

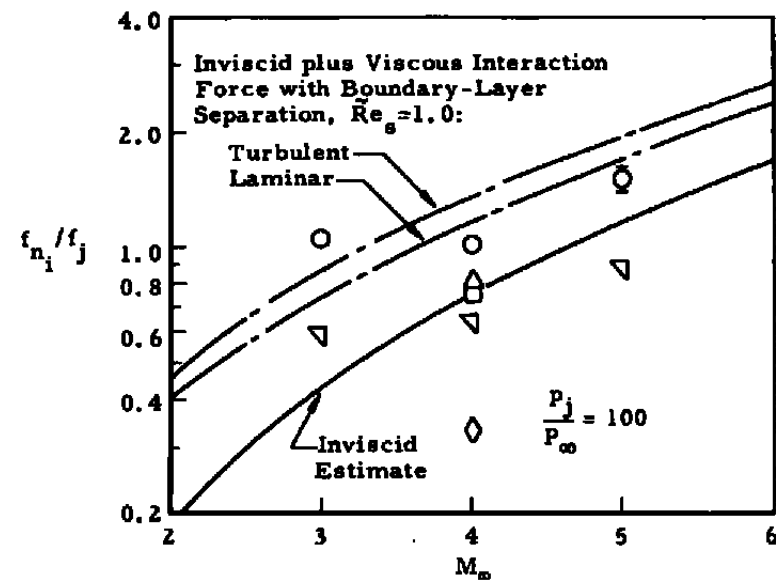
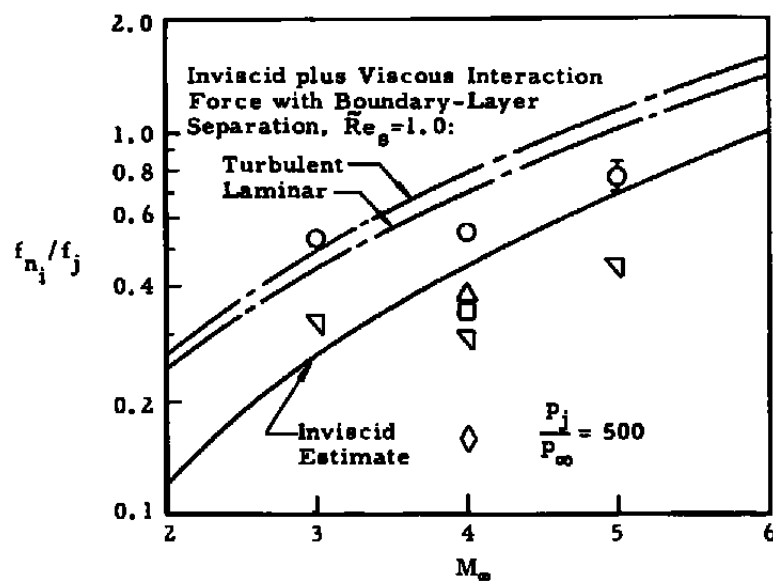


Fig. 32 Comparison of the Theoretical Interaction Force Ratio, f_{n_i}/f_j , with the Experimental Values of Rectangular Nozzles

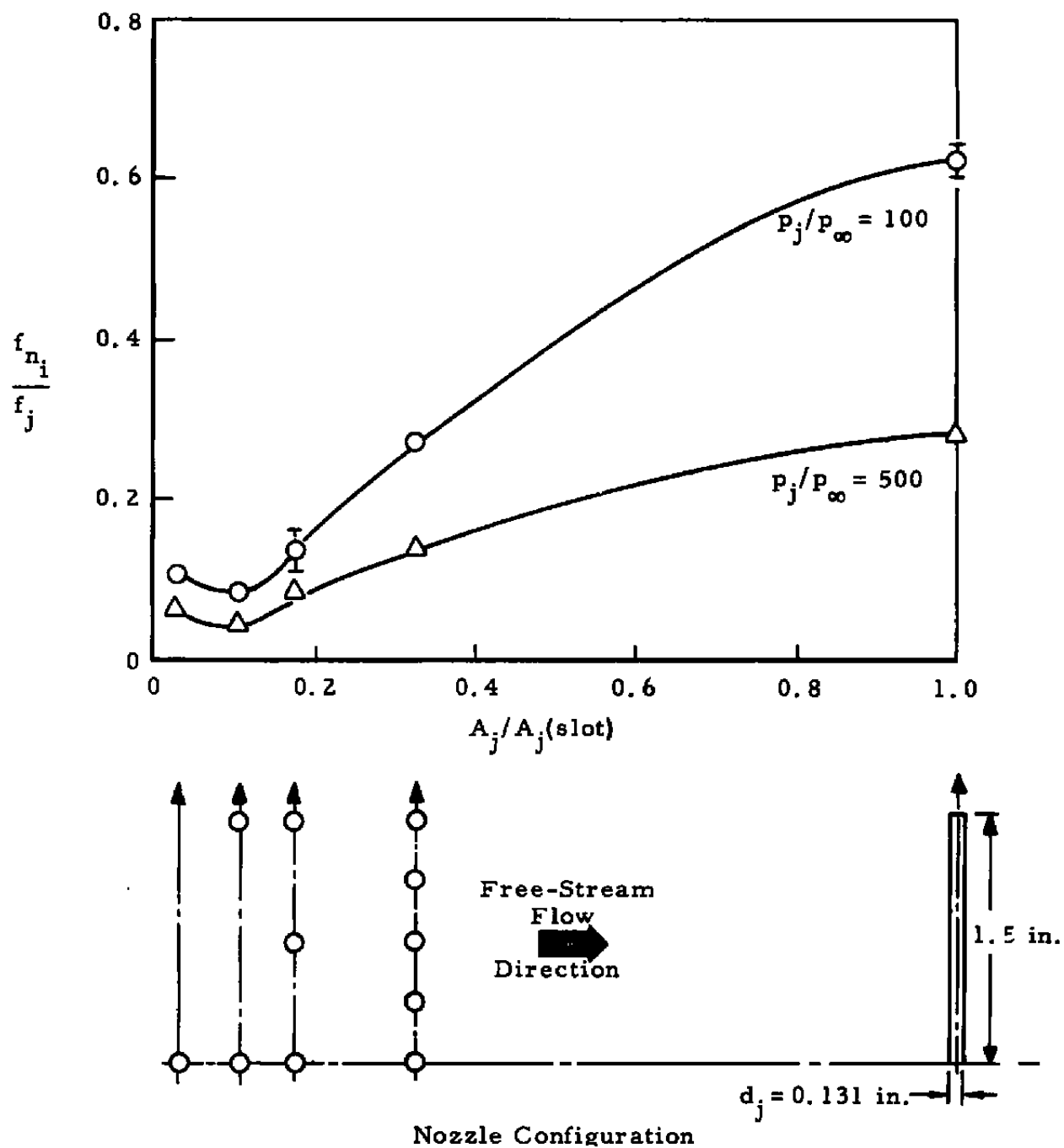


Fig. 33 The Two- and Three-Dimensional Effects of Circular Nozzle Configurations at $M_\infty = 3.98$, $Re_x = 0.6$ to 3.6×10^6

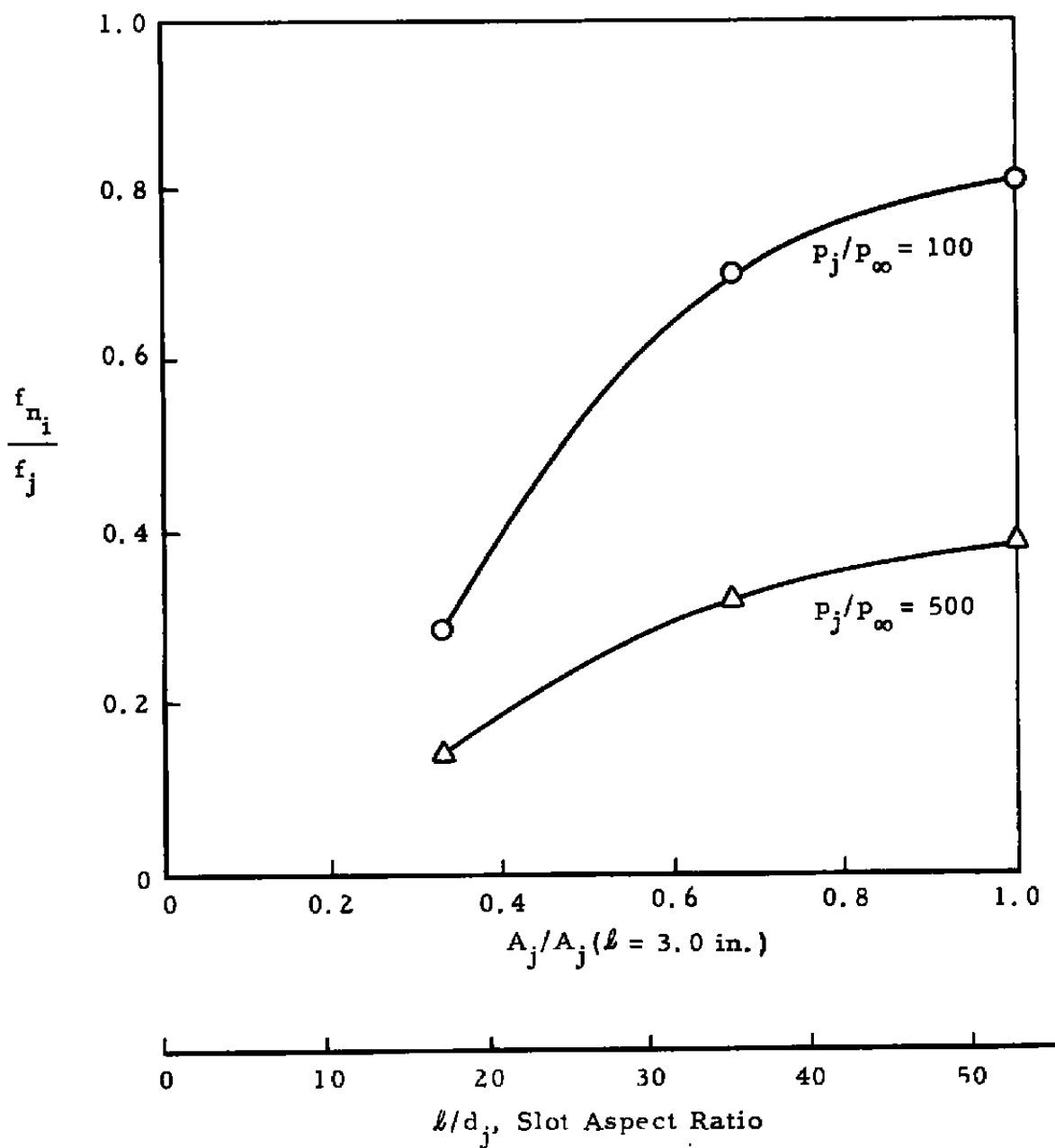
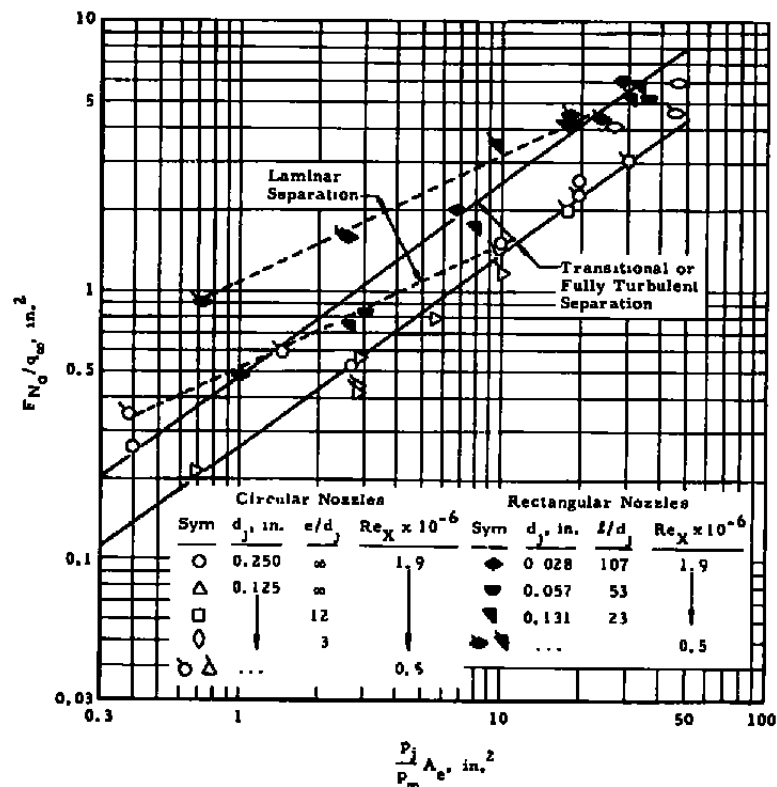
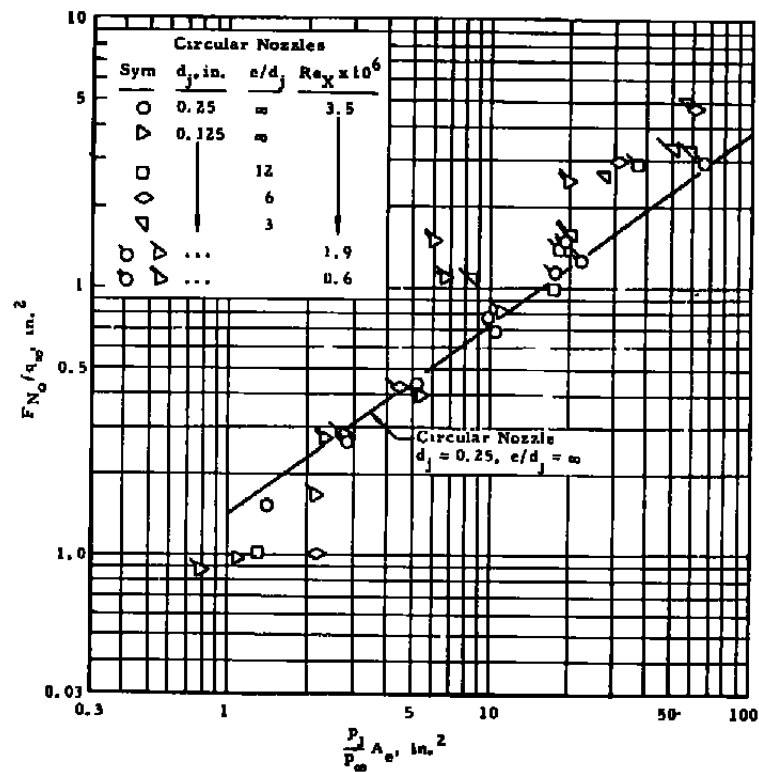


Fig. 34 The Two- and Three-Dimensional Effects of 0.057-in.-width Slots of Various Aspect Ratios, $M_\infty = 3.98$, $Re_x = 0.6$ to 3.6×10^6

a. Circular and Rectangular Nozzles, $M_{\infty} = 2.99$ b. Circular Nozzles, $M_{\infty} = 3.98$ Fig. 35 Variation of Interaction Force, F_{N_0}/q_{∞} , Generated Upstream of the Jet versus $(p_i/p_{\infty}) A_e$

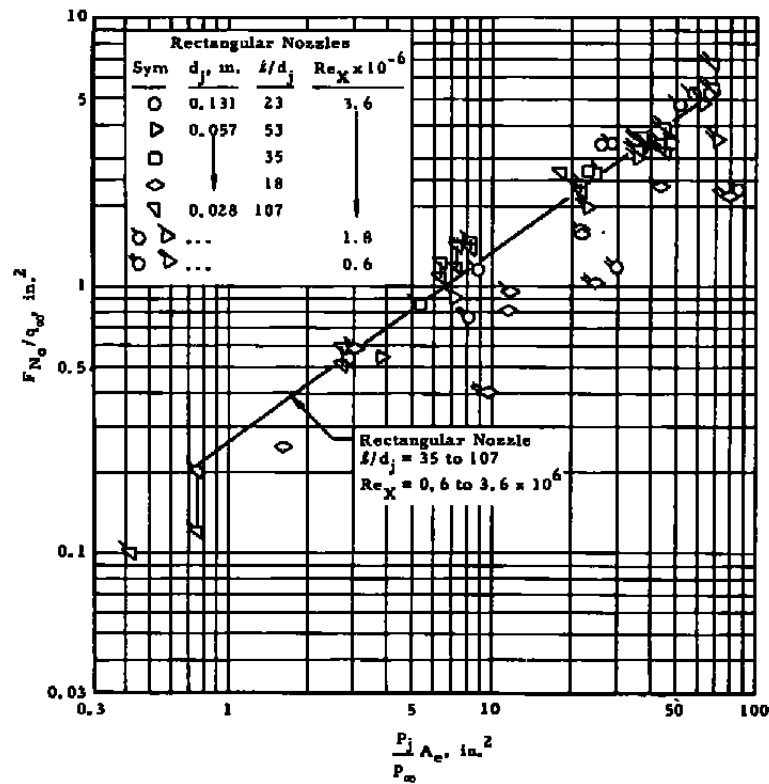
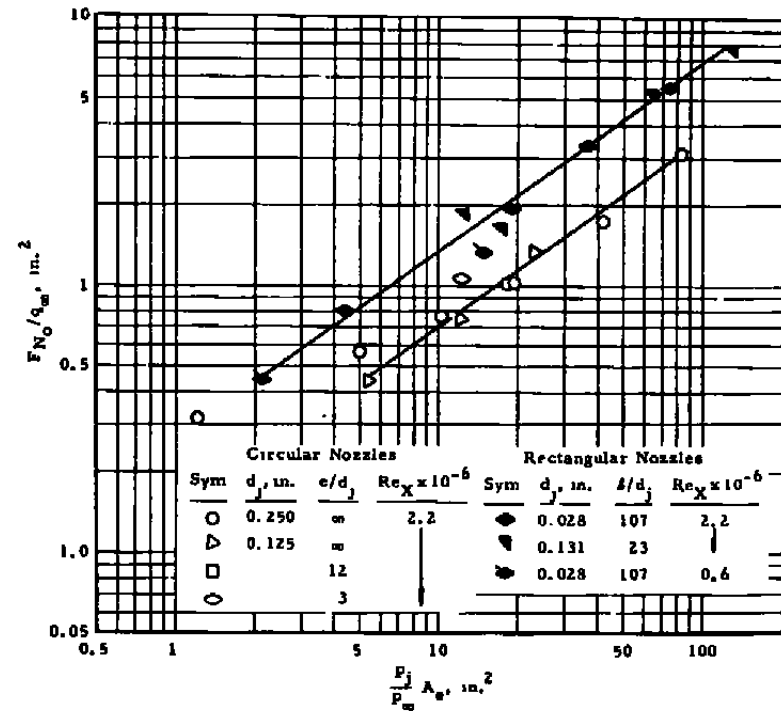
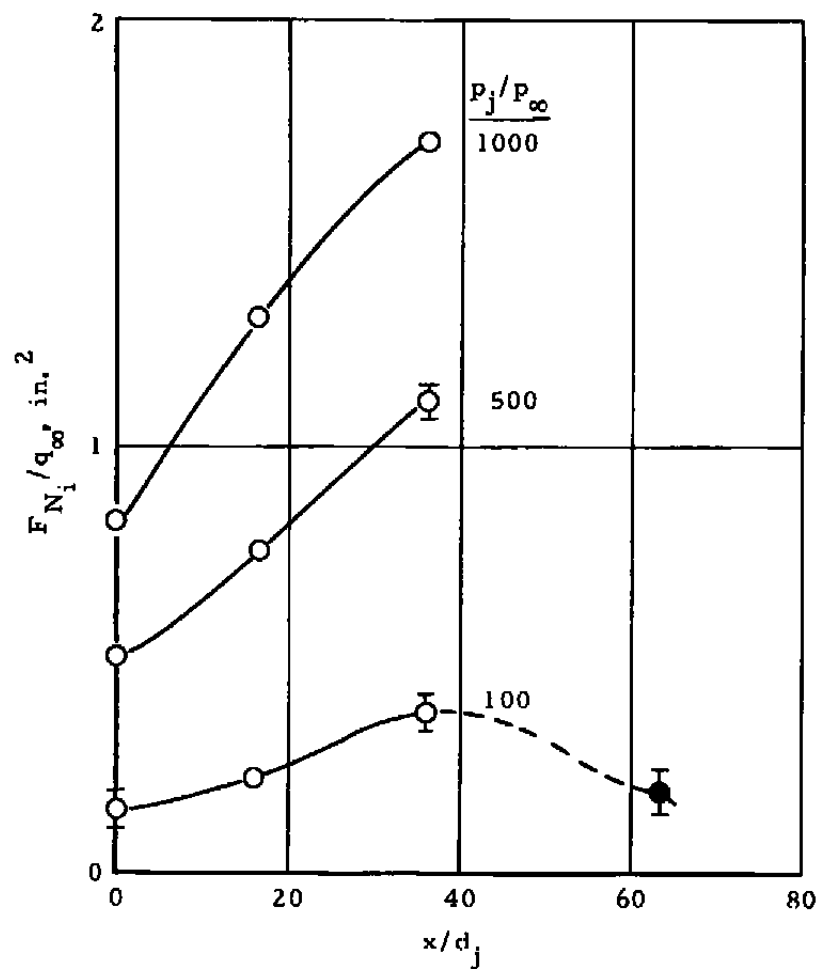
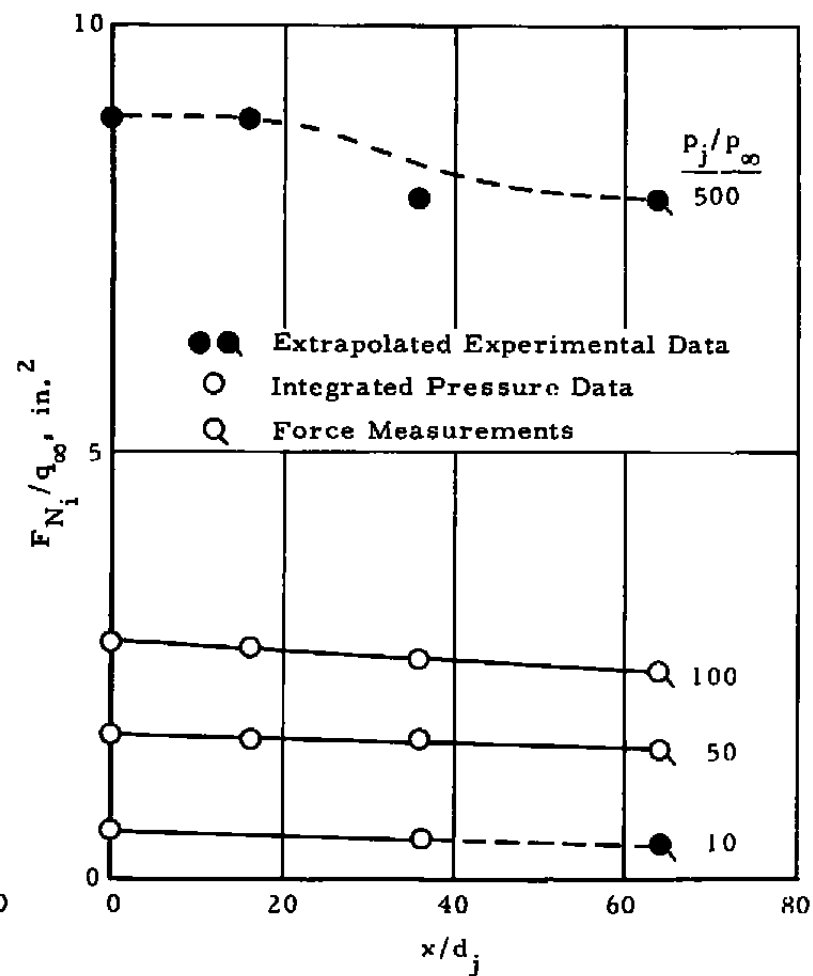
c. Rectangular Nozzles, $M_\infty = 3.98$ d. Circular and Rectangular Nozzles, $M_\infty = 5.01$

Fig. 35 Concluded

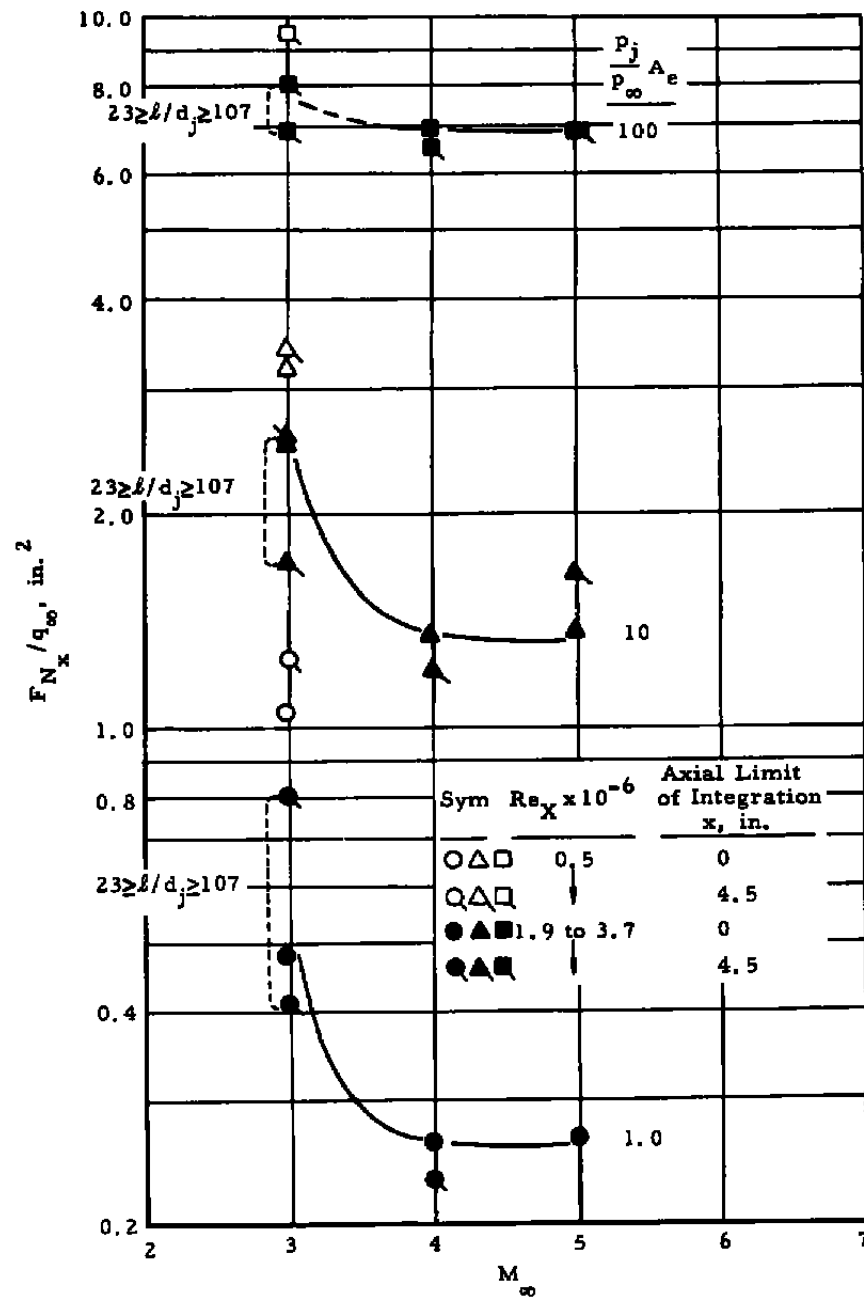


a. 0.125-in. Single Circular Nozzle



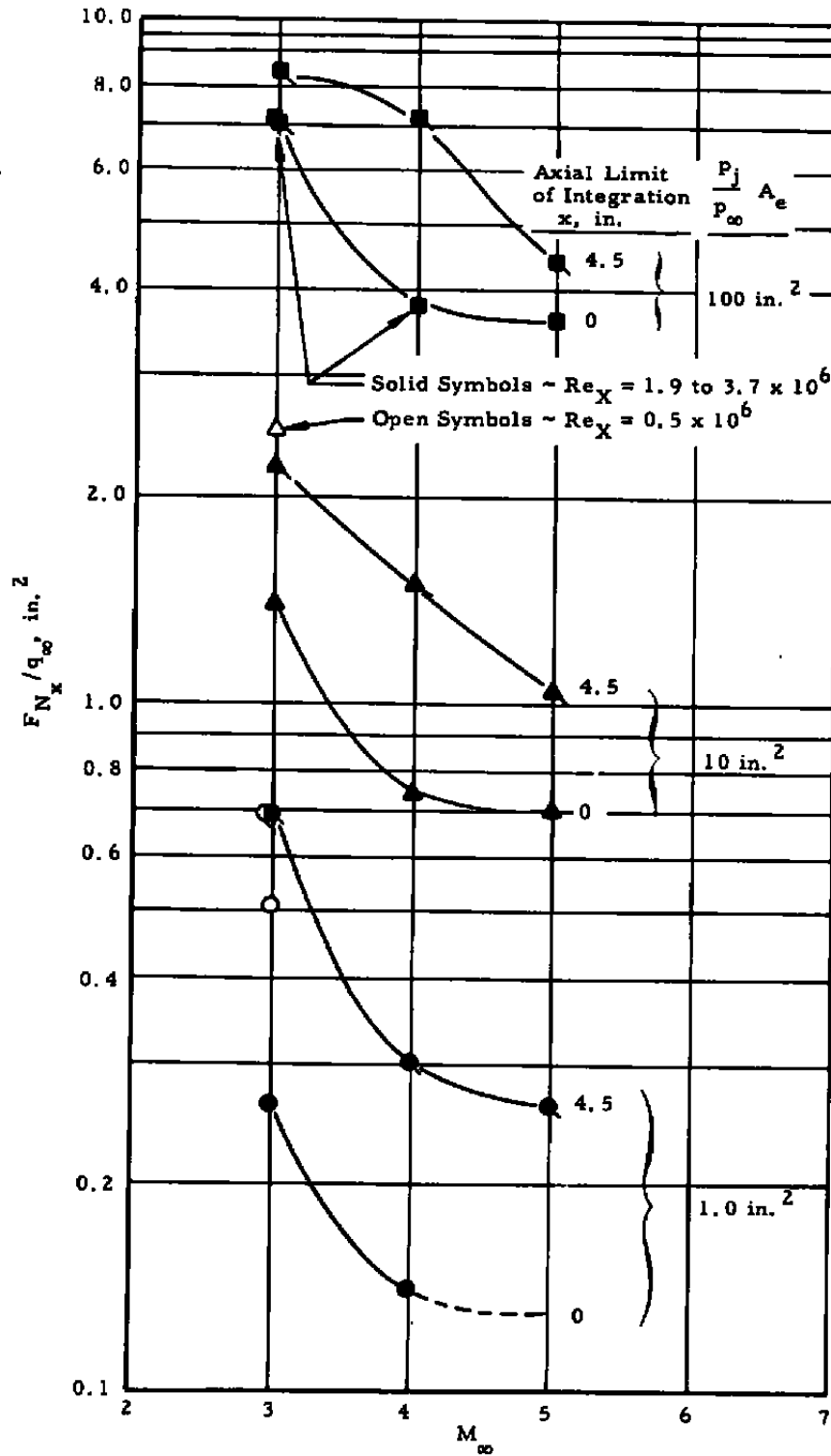
b. 0.131 by 3.0-in. Rectangular Nozzle

Fig. 36 Influence of the Pressure Field Aft of the Jet Nozzle on the Resultant Interaction Force, $M_{\infty} = 3.98$, $Re_x = 1.8$ to 3.6



a. Rectangular Nozzles

Fig. 37 The Effect of Mach Number on the Sonic Nozzle Jet Interaction Force



b. Circular Nozzles

Fig. 37 Concluded

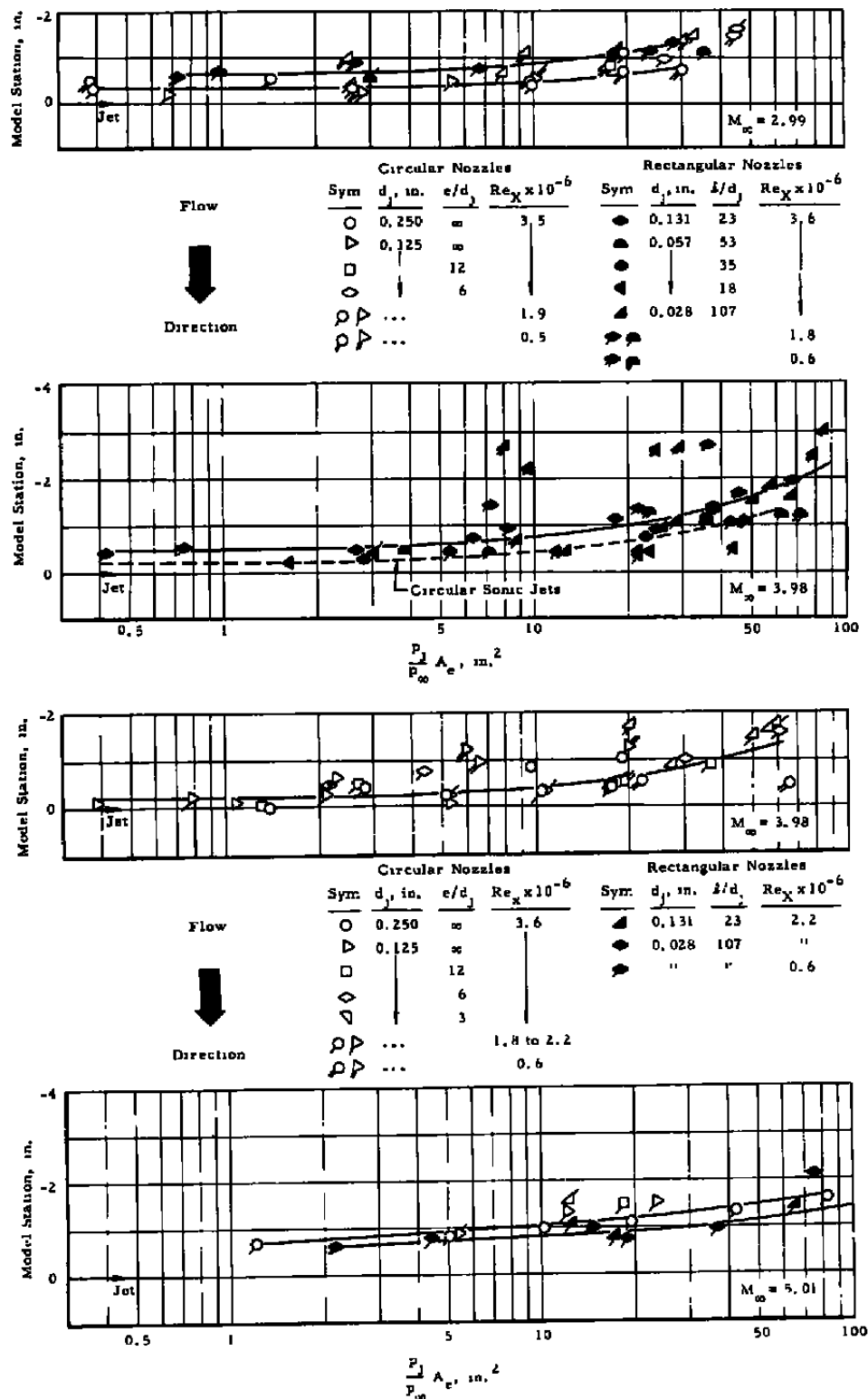
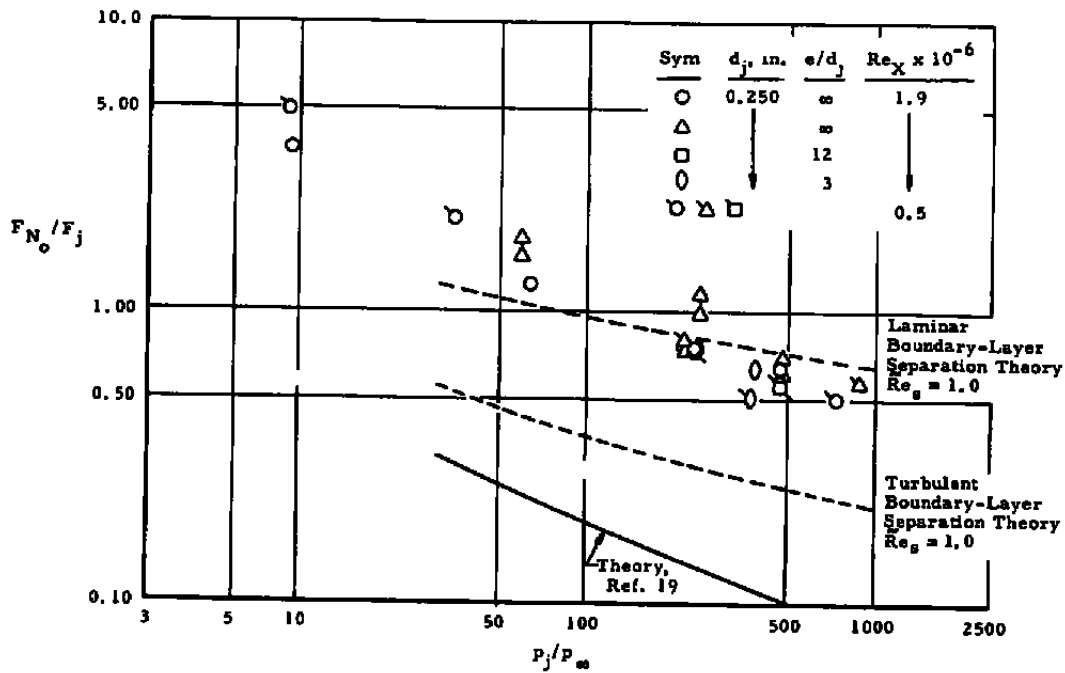
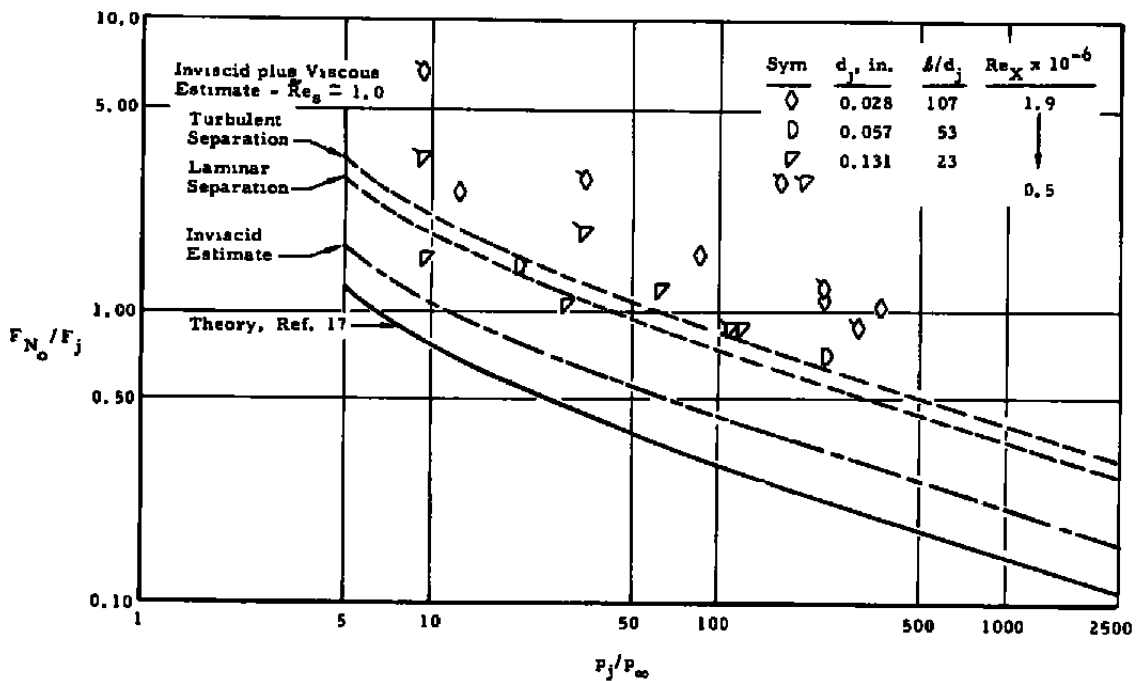


Fig. 38 Center of Pressure of the Interaction Load Ahead of the Nozzle Jet



a. $M_\infty = 2.99$, Circular Nozzles



b. $M_\infty = 2.99$, Rectangular Nozzles

Fig. 39 Influence of the Jet Pressure Ratio on the Ratio of the Interaction to Jet Reaction Force for Various Nozzle Configurations

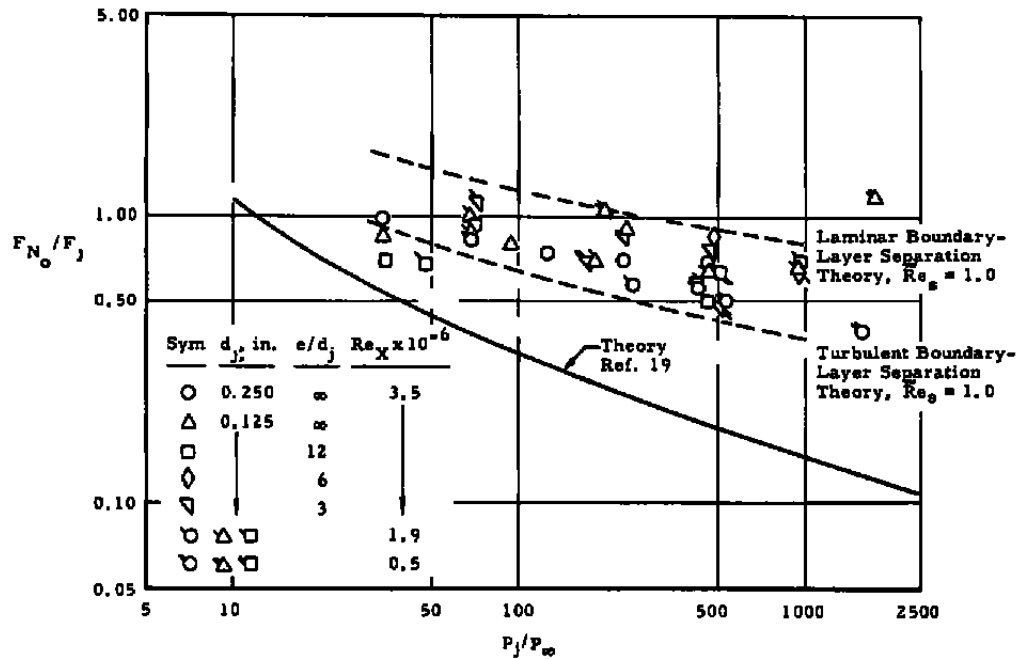
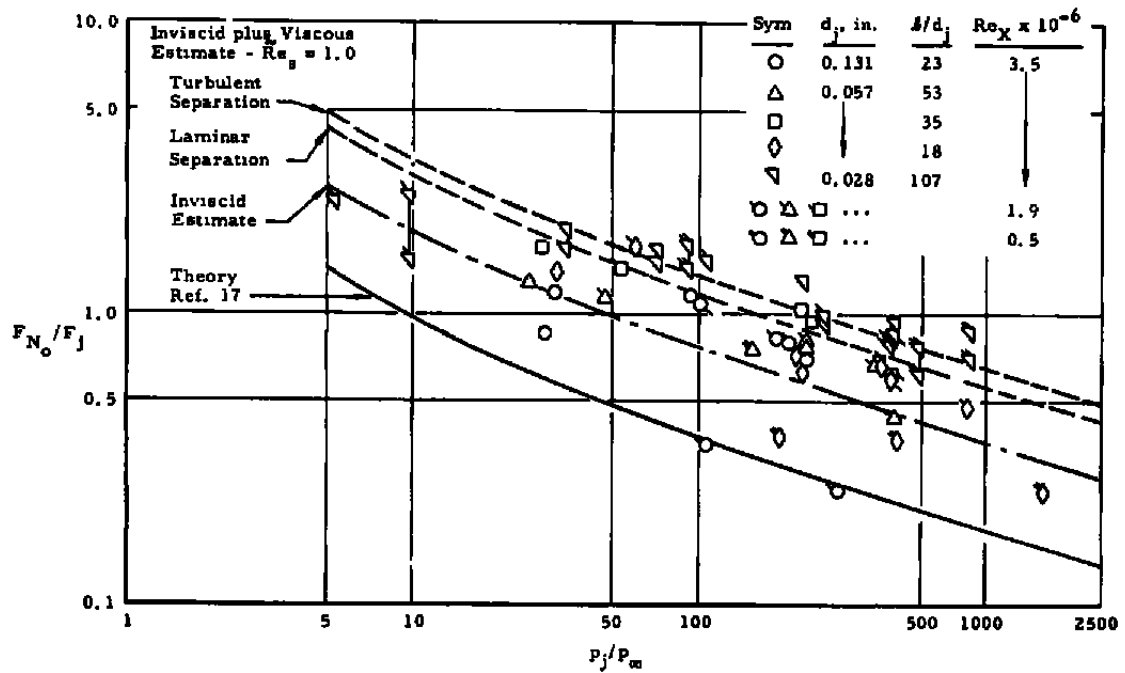
c. $M_{\infty} = 3.98$, Circular Nozzlesd. $M_{\infty} = 3.98$, Rectangular Nozzles

Fig. 39 Continued

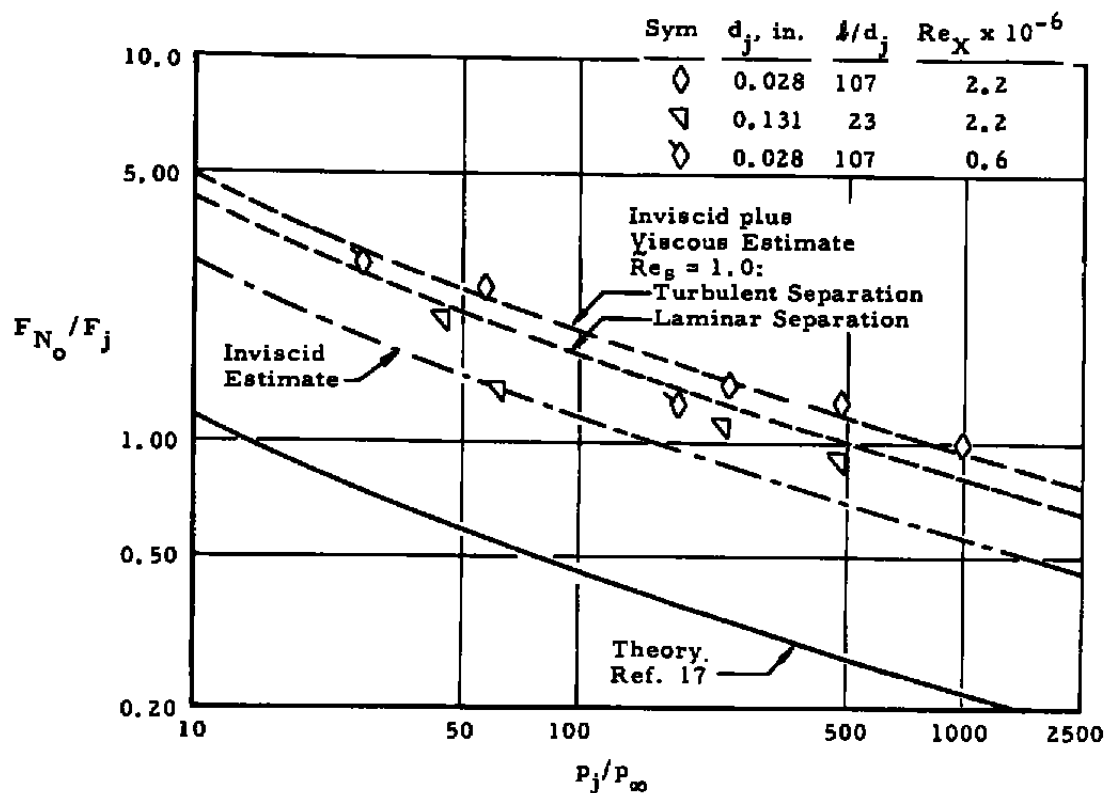
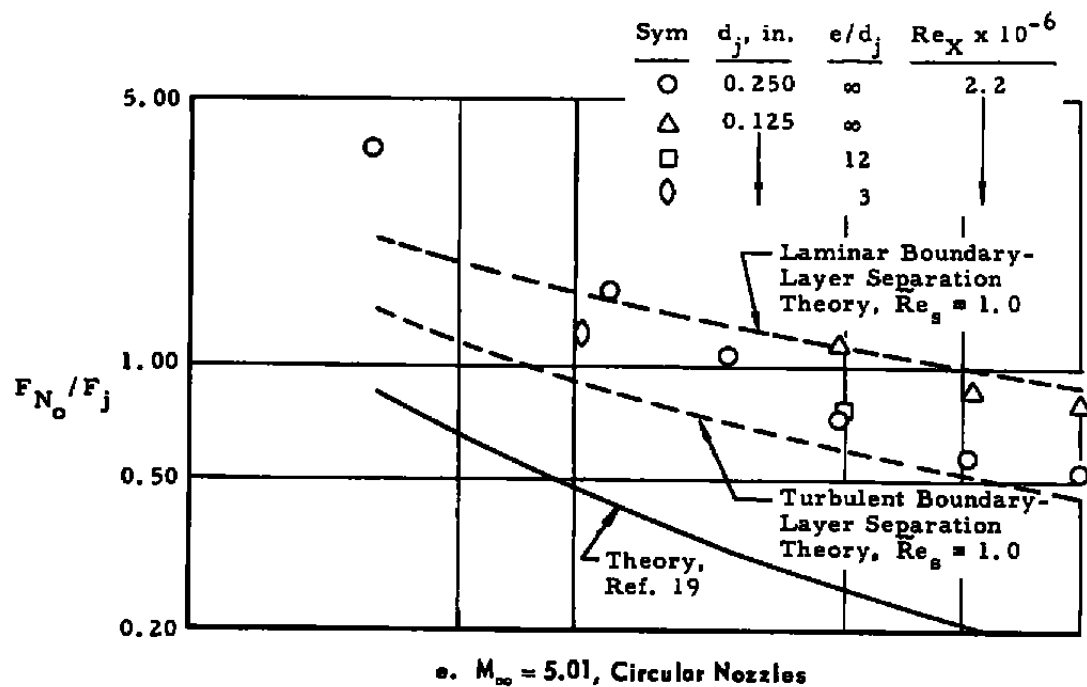
f. $M_\infty = 5.01$, Rectangular Nozzles

Fig. 39 Concluded

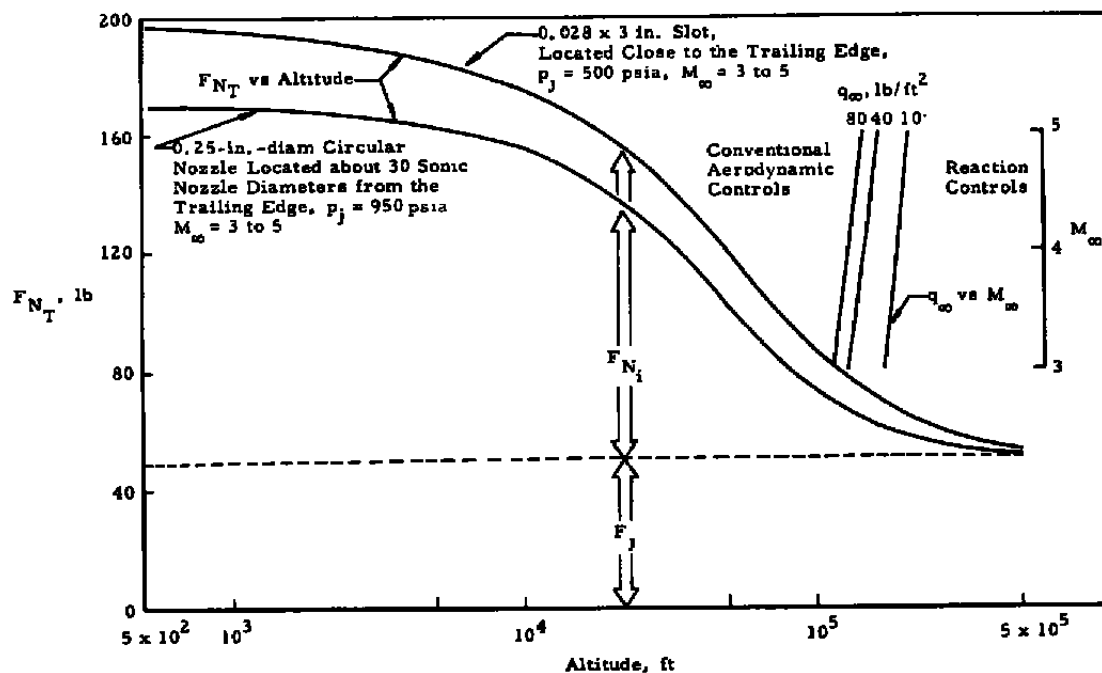


Fig. 40 Comparison of Resultant Force Produced by a Lateral Jet from a Circular Sonic Nozzle and a Slot at Various Altitudes

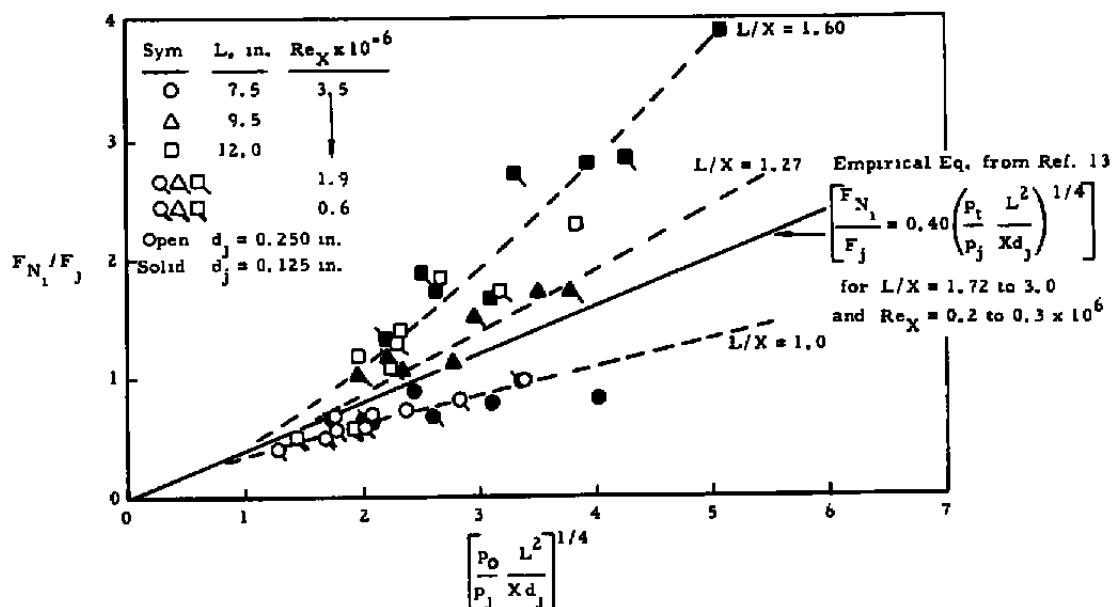
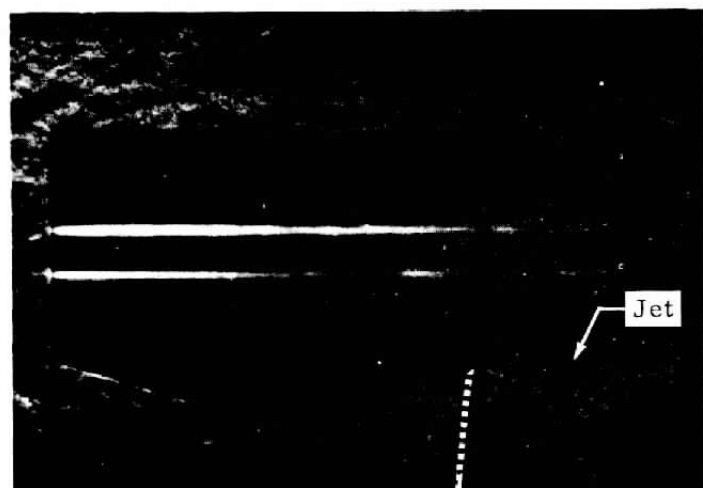


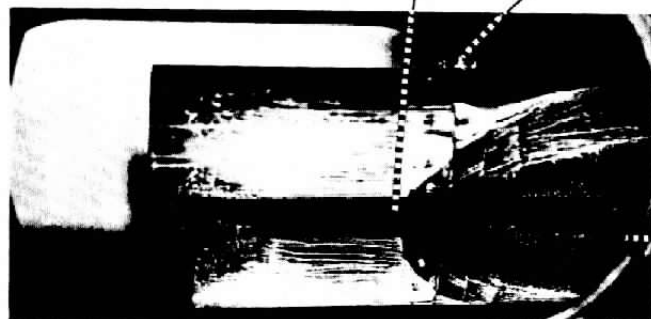
Fig. 41 Comparison of AEDC Results with Amick and Hays (Ref. 13) Empirical Relationship



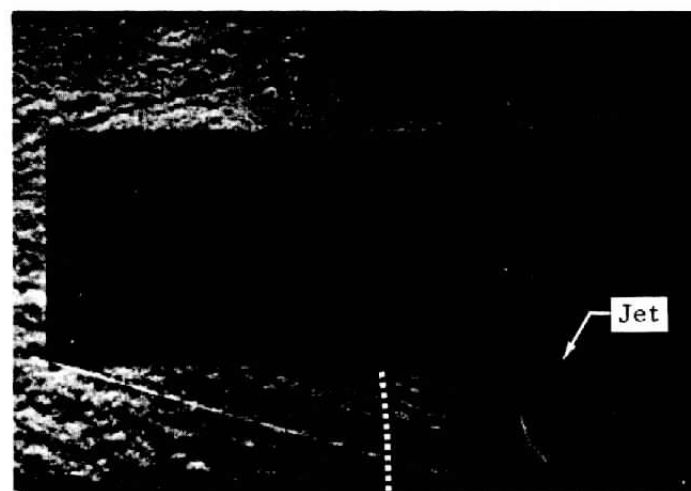
$$p_j/p_\infty = 480$$

$$A_e(p_j/p_\infty) \approx 20 \text{ in.}^2$$

Corresponding Points
of Separation



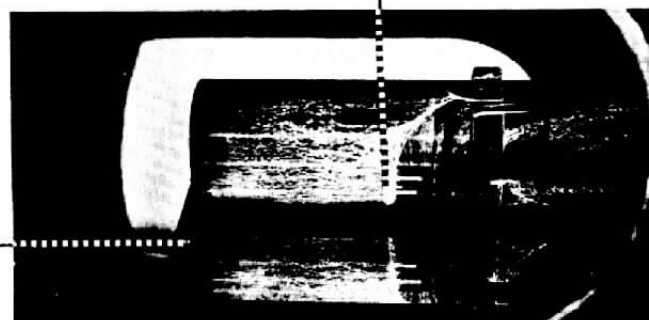
a. 0.25-in.-diam Circular Nozzle



$$p_j/p_\infty = 237$$

$$A_e(p_j/p_\infty) \approx 31 \text{ in.}^2$$

Corresponding Points
of Separation



b. 0.05-in. by 3-in. Rectangular Nozzle

Fig. 42 Typical Flow Patterns Generated about the Hollow Cylinder by Lateral Jets from Rectangular and Circular Nozzles,
 $Re_x = 3.9 \times 10^6$, $M_\infty = 3.98$

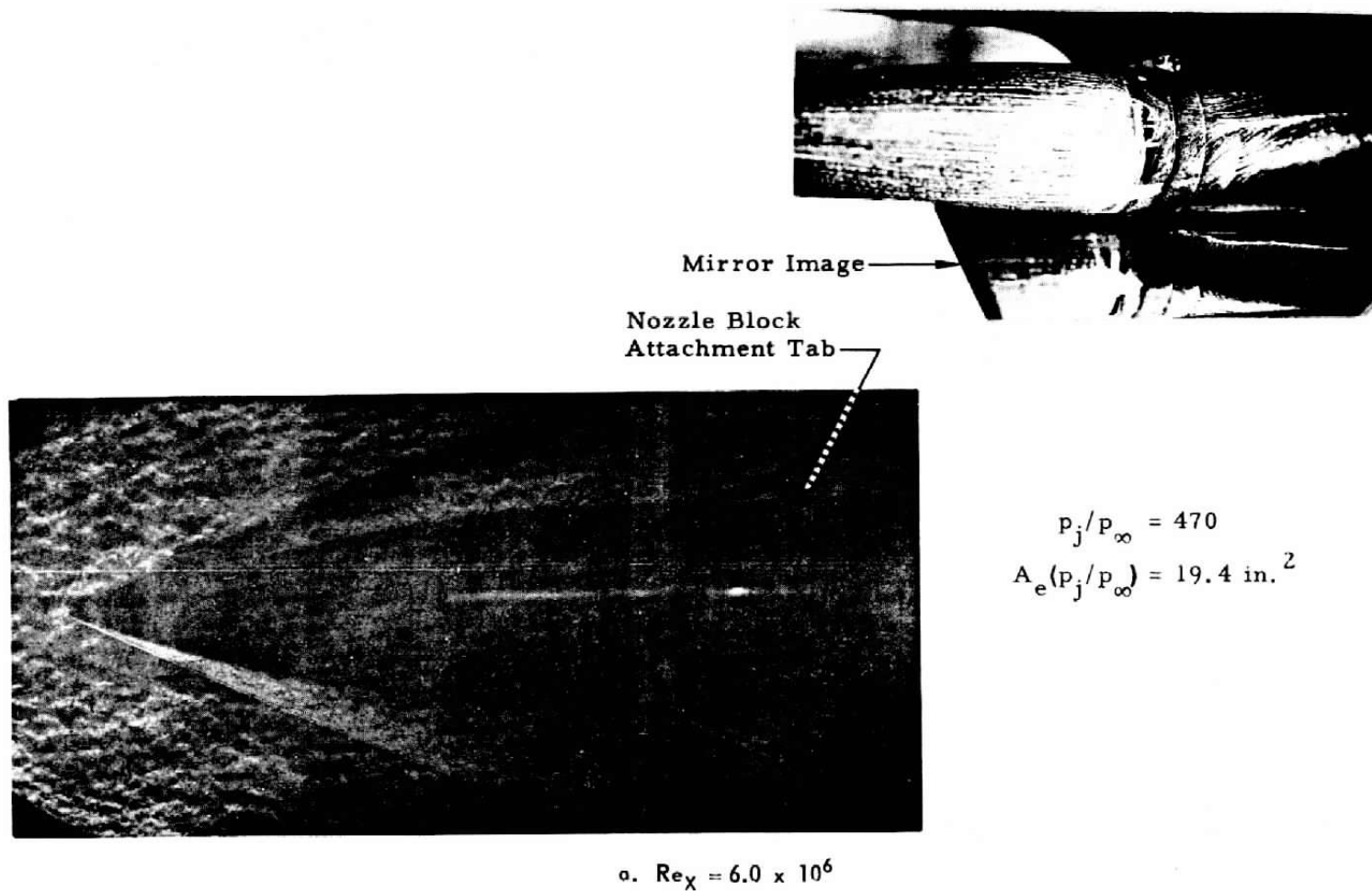
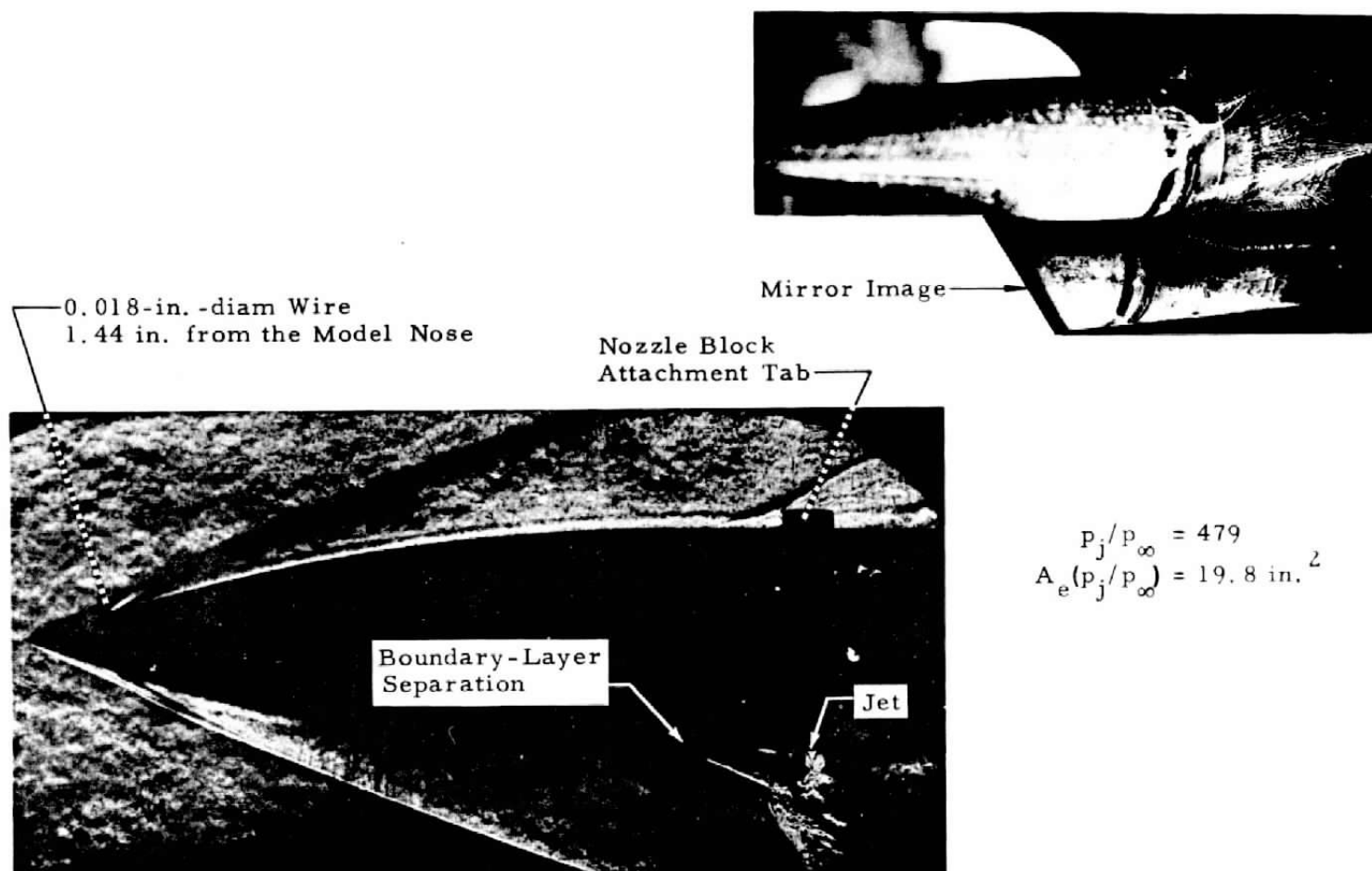
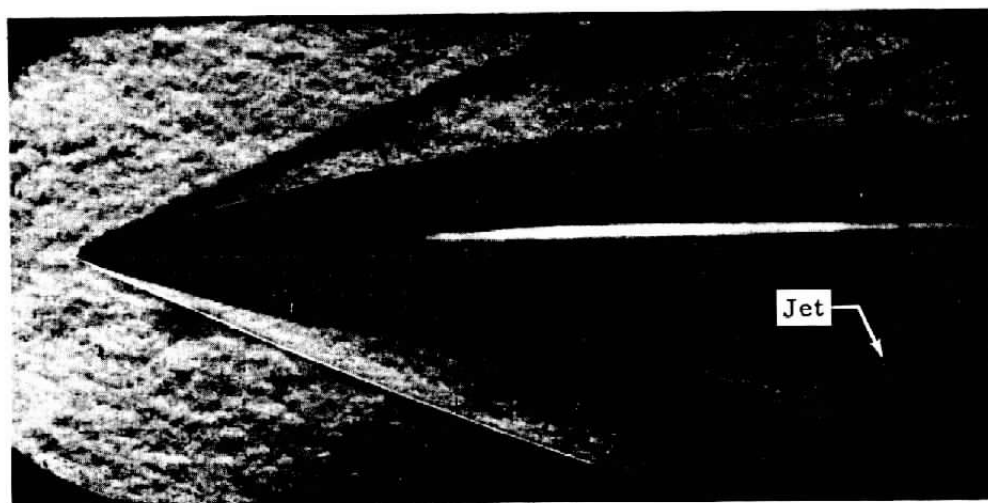


Fig. 43 Typical Flow Pattern about a Nine-Caliber Ogive Generated by a Lateral Jet from a 0.25-in.-diam Circular Nozzle, $M_\infty = 3.98$

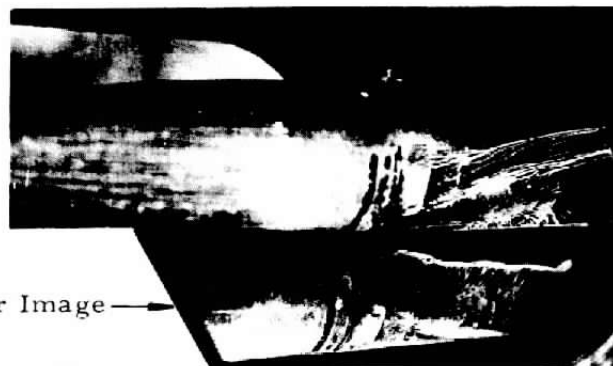


b. $Re_x = 3.2 \times 10^6$, with a Boundary-Layer Trip Mounted on the Model Nose

Fig. 43 Continued



Mirror Image →

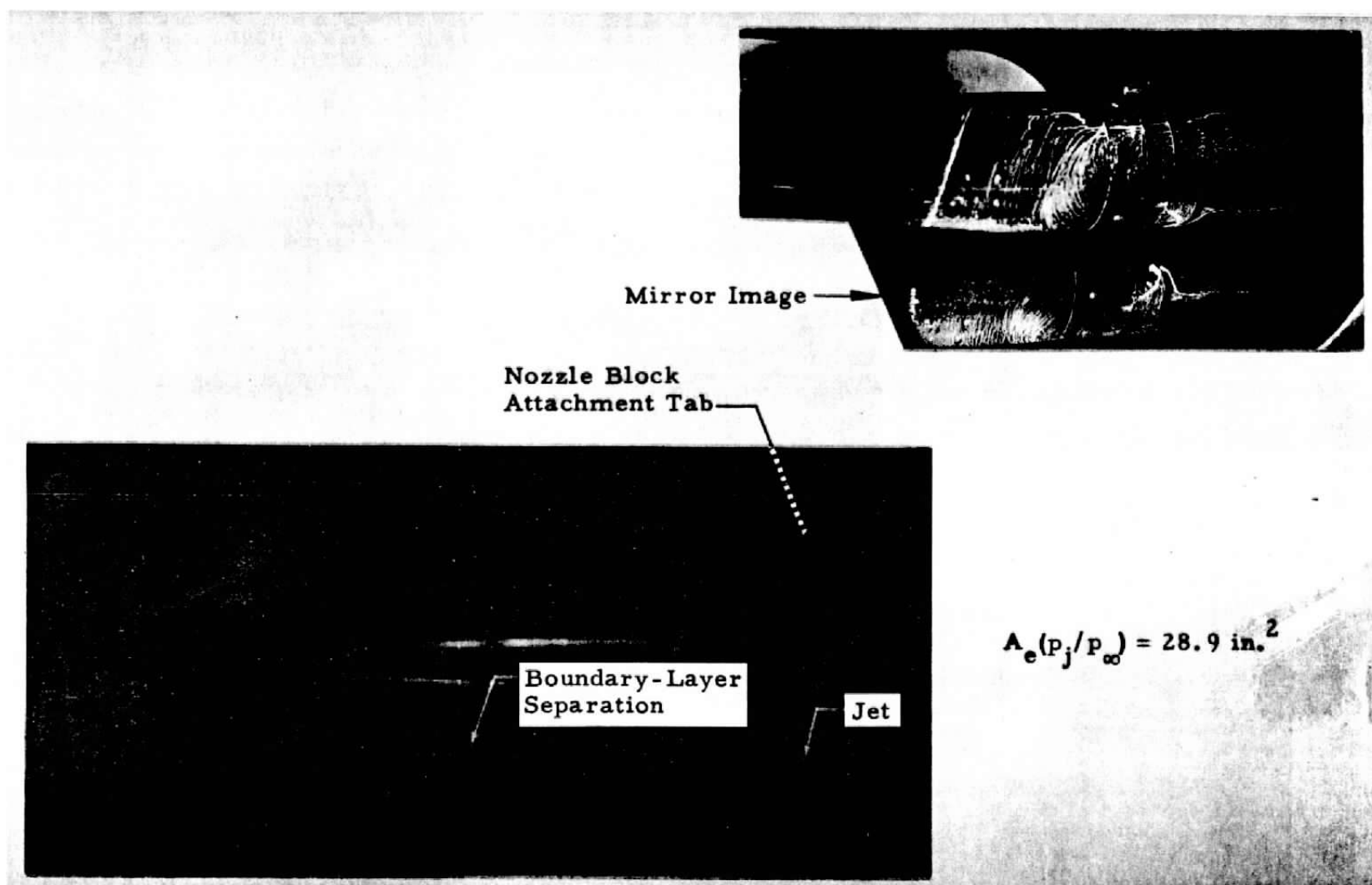


$$p_j/p_\infty = 456$$

$$A_e(p_j/p_\infty) = 18.8 \text{ in.}^2$$

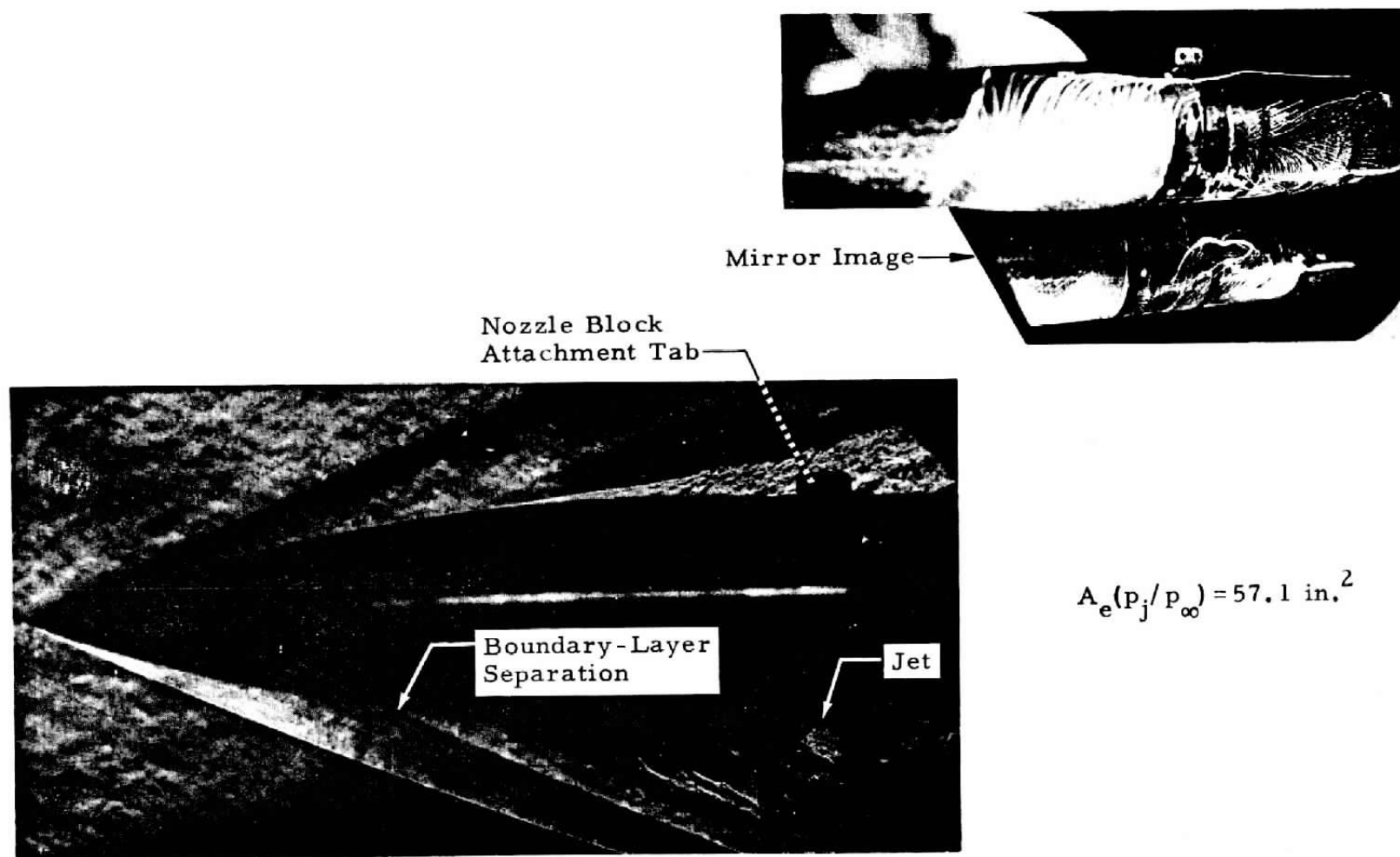
c. $Re_x = 3.2 \times 10^6$

Fig. 43 Concluded



$$a. \text{Re}_x = 3.2 \times 10^6, p_i/p_\infty = 193$$

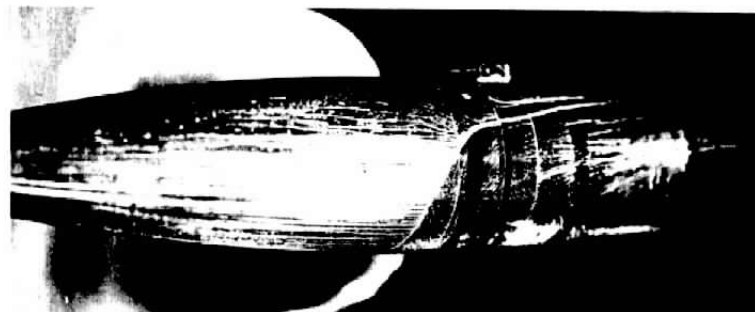
Fig. 44 Typical Flow Patterns about a Nine-Caliber Ogive Generated by a Lateral Jet from a 0.05- by 3-in. (Circumferential Distance) Rectangular Slot, $M_\infty = 3.98$



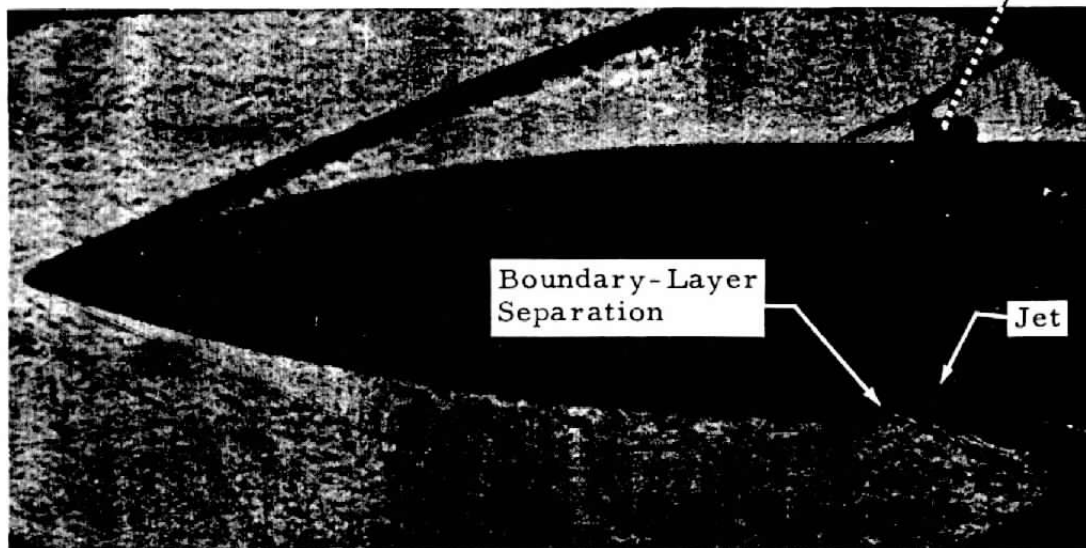
$$A_e(p_j/p_\infty) = 57.1 \text{ in.}^2$$

b. $Re_x = 3.2 \times 10^6$, $p_j/p_\infty = 380$

Fig. 44 Continued



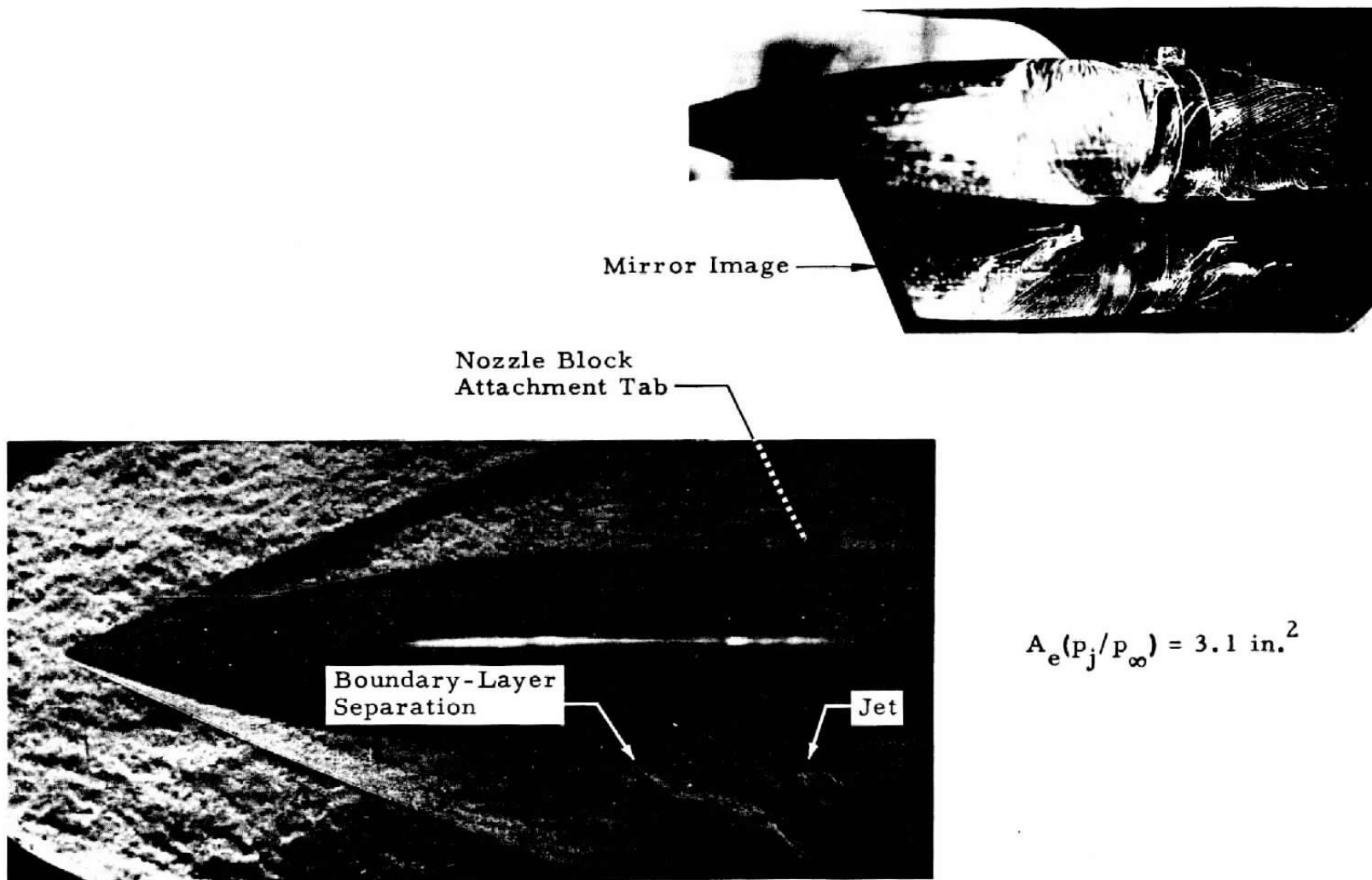
Nozzle Block
Attachment Tab



$$A_e(p_j/p_\infty) = 4.8 \text{ in.}^2$$

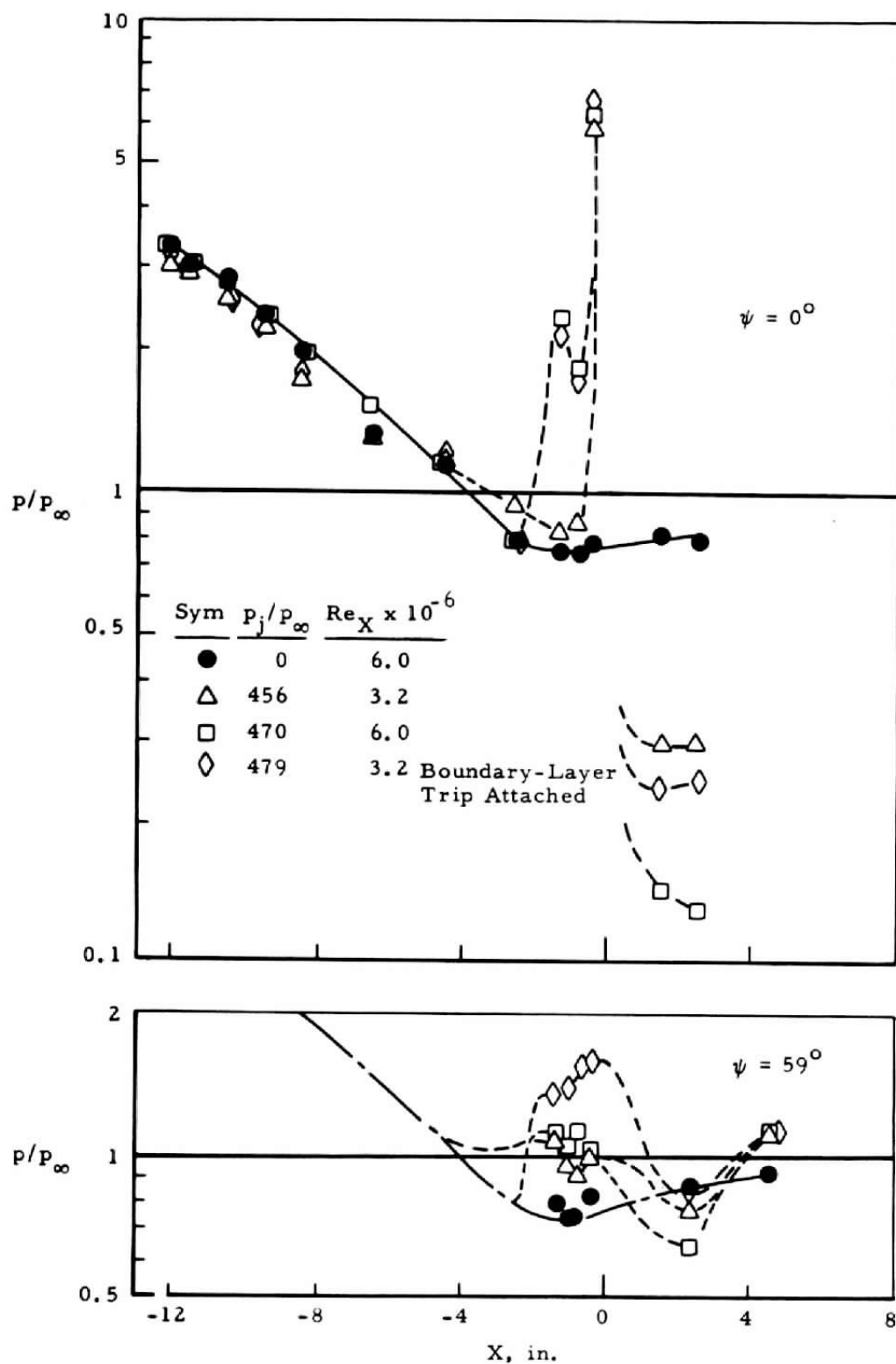
c. $Re_x = 6.0 \times 10^6$, $p_i/p_\infty = 32$

Fig. 44 Continued



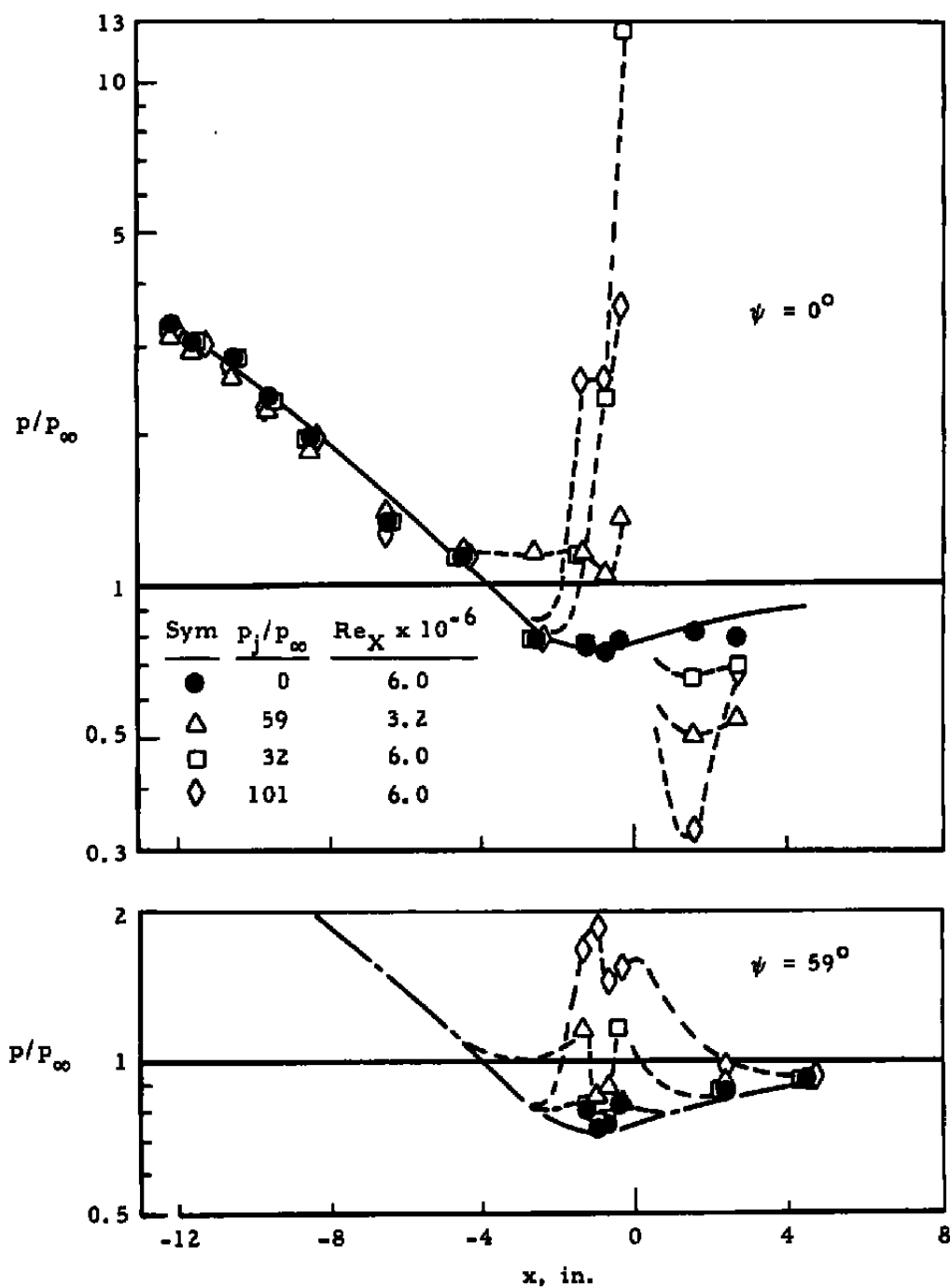
d. $Re_x = 5.8 \times 10^6$, $p_i/p_\infty = 237$

Fig. 44 Concluded



a. 0.25-in.-diam Circular Nozzle

Fig. 45 Influence of the Boundary-Layer Jet Interaction on the Pressure Distribution at $M_\infty = 3.98$ on a Nine-Caliber Ogive



b. 0.05- by 3-in. Rectangular Nozzle

Fig. 45 Concluded

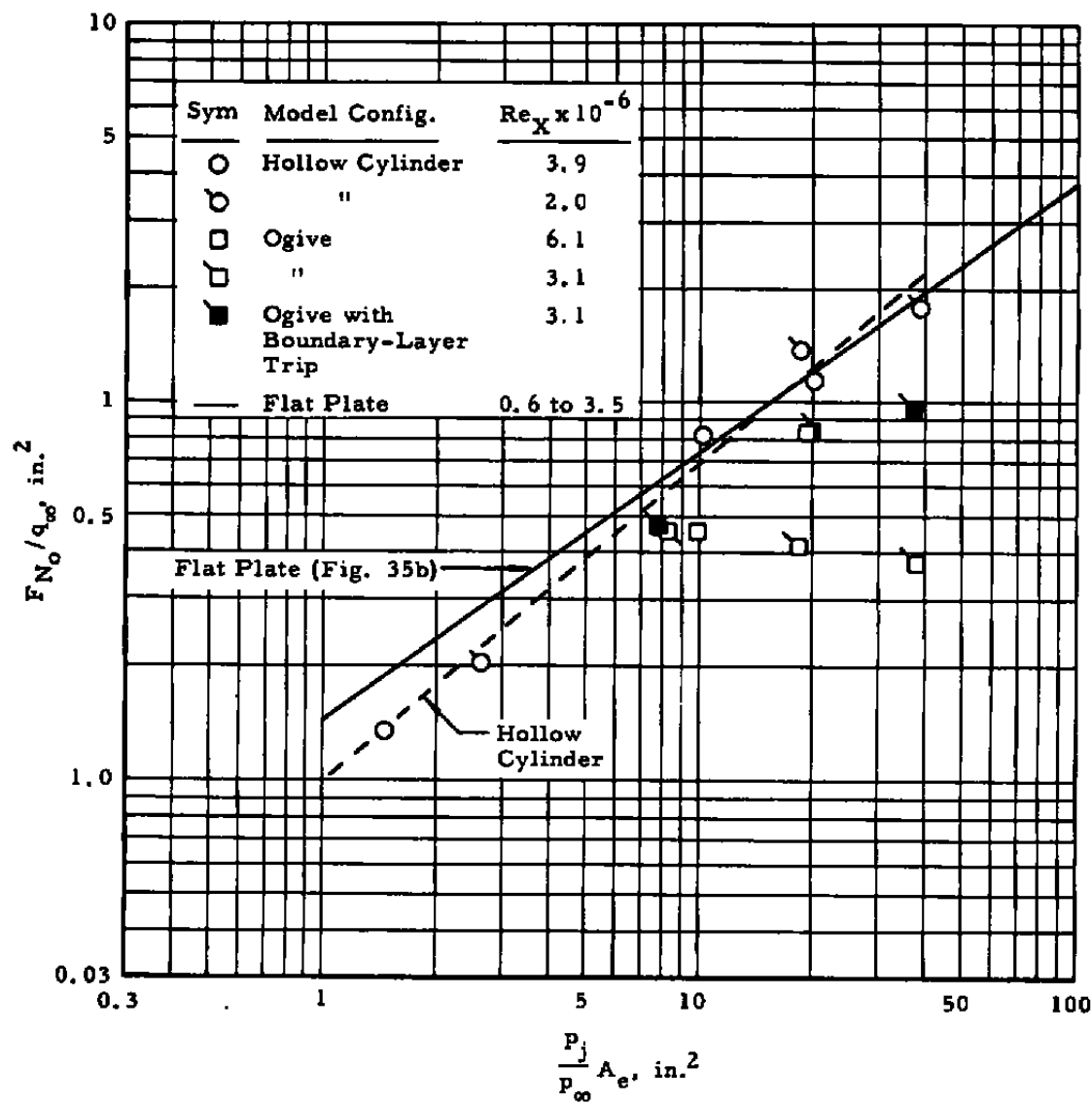


Fig. 46 Comparisons of the Interaction Loads Generated by a Jet from a 0.25-in.-diam Circular Nozzle on the Hollow Cylinder, Ogive, and Flat Plate at $M_{\infty} = 3.98$

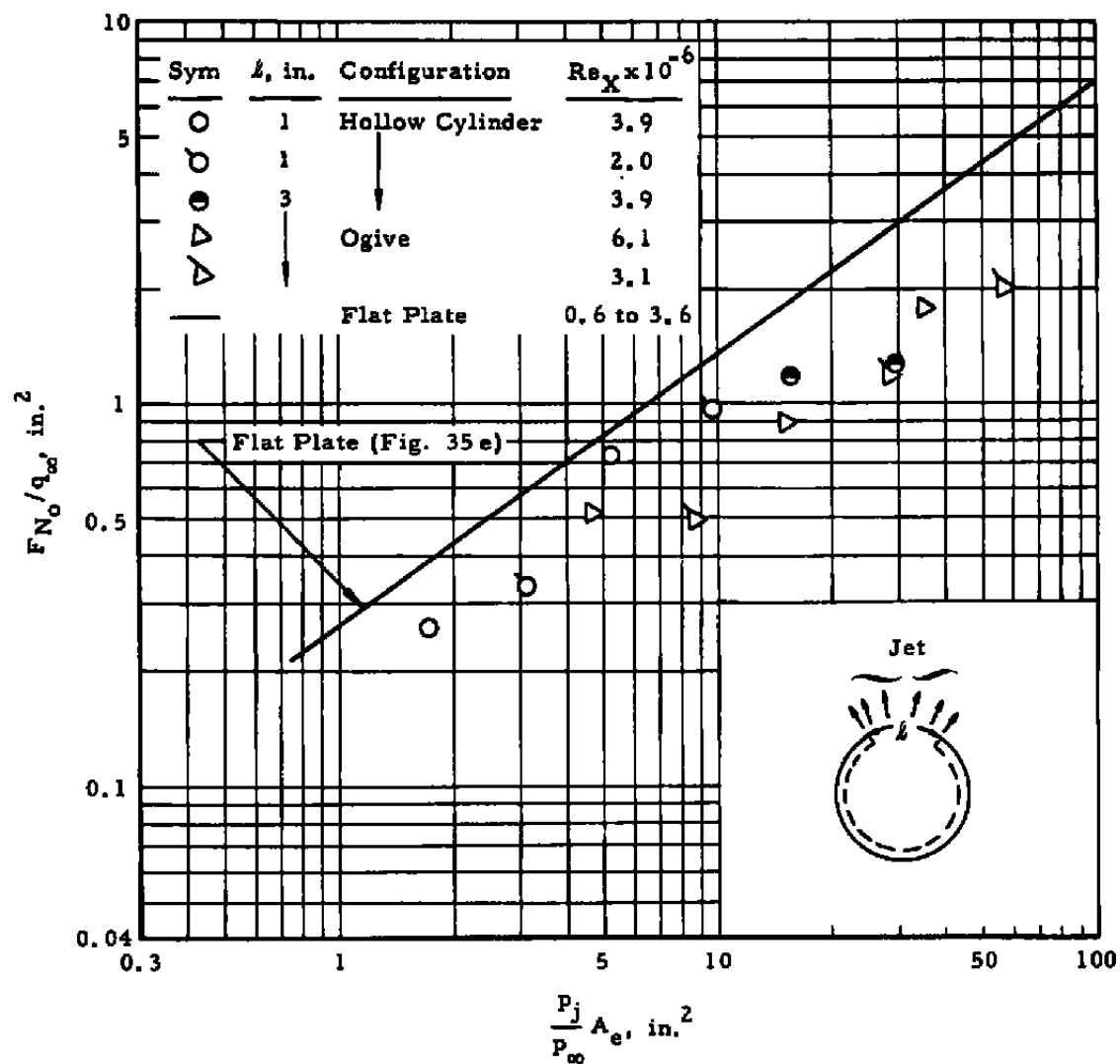


Fig. 47 Comparisons of the Interaction Loads Generated by a Jet from a 0.05-in. Rectangular Nozzle on the Hollow Cylinder, Ogive, and Flat Plate at $M_\infty = 3.98$

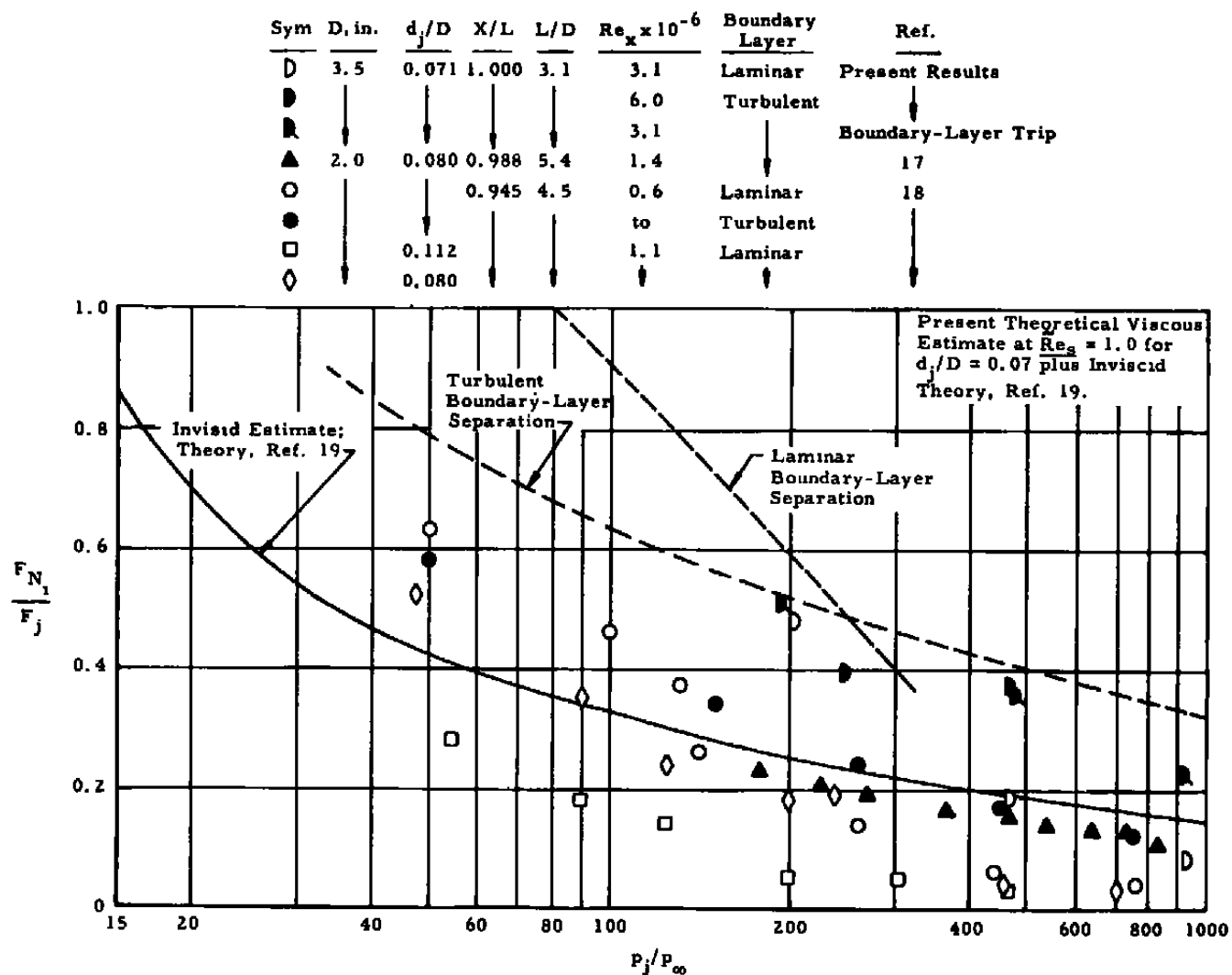


Fig. 48 Comparison of Theoretical and Experimental Interaction Forces Generated on a Nine-Caliber Ogive of Nominal Mach Number 4 by a Lateral Jet

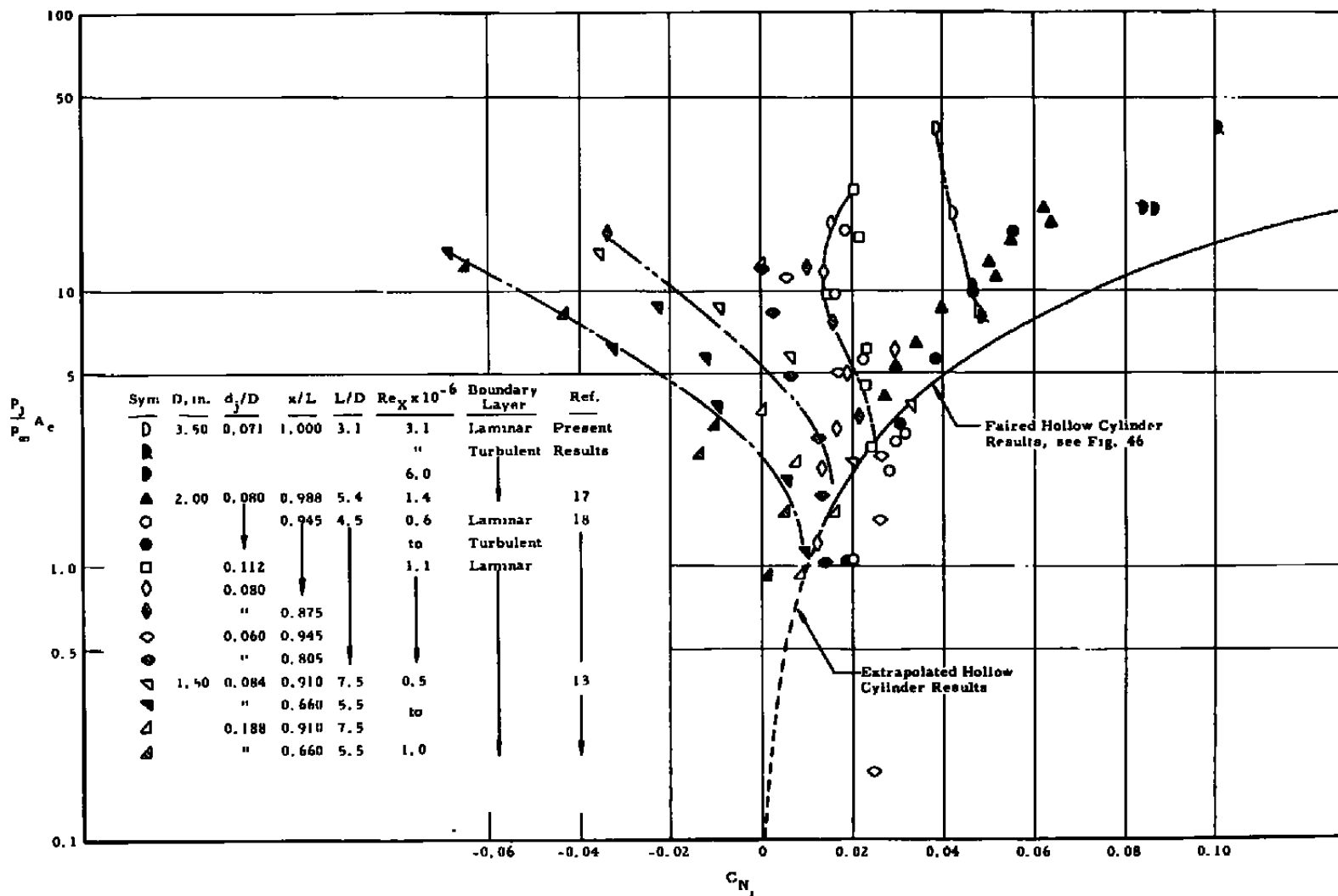


Fig. 49 Influence of the Relative Location of the Jet Nozzle on the Interaction Coefficient, Nine-Caliber Ogive, Nominal Mach Number of 4

Arnold Engineering Development Center
Arnold Air Force Station, Tennessee

Rpt. No. AEDC-TDR-63-22. INTERACTIONS PRODUCED
BY SONIC LATERAL JETS LOCATED ON SURFACES IN
A SUPERSONIC STREAM. April 1963. 125 p.
incl 34 refs., illus.

Unclassified Report

A flat plate, a hollow cylinder, and a nine-caliber ogive containing lateral sonic jets were tested at Mach numbers 2.99, 3.98, and 5.01 in the 12-Inch Supersonic Tunnel (E-1) of the von Karman Gas Dynamics Facility. The interaction forces generated on these bodies were investigated for various sonic nozzle configurations including single circular nozzles, multiple circular nozzles, and slots of various width and span sizes. The nozzles were operated at jet stagnation to free-stream static pressure ratios from 10 to 2000. The force produced on a surface by the interaction of the lateral jet with the supersonic free stream was evaluated from model pressure distributions



1. Jet mixing flow
2. Supersonic flow
3. Control jets
4. Spacecraft
5. Atmosphere entry
6. Aerodynamic configurations
7. Loading (mechanics)
8. Boundary layer
9. Supersonic nozzles
10. Pressure
11. Tests
12. Theory
- I. AFSC Program Area 750A, Project 8953, Task 895305
- II. Contract AF 40(600)-1000
- III. ARO, Inc., Arnold AF Sta, Tenn.
- IV. W. T. Strike, C. J. Schueler, and J. S. Deitering
- V. In ASTIA Collection

and compared with various theoretical estimates. Good agreement was obtained between the present experimental data and the theoretical estimates based on a linear combination of the viscous and inviscid estimates of the jet interaction force. Also, good agreement was obtained between the integrated pressure data and some force measurements. These theoretical and experimental results indicated that significant jet interaction forces are produced. In general, circular sonic jets produced the maximum interaction force when located about 30 jet nozzle diameters forward of the trailing edge of a planar surface or at the base edge of a body of revolution. Rectangular nozzles (slots) generated the largest force when located at the model trailing edge.



Arnold Engineering Development Center
Arnold Air Force Station, Tennessee

Rpt. No. AEDC-TDR-63-22. INTERACTIONS PRODUCED
BY SONIC LATERAL JETS LOCATED ON SURFACES IN
A SUPERSONIC STREAM. April 1963. 125 p.
incl 34 refs., illus.

Unclassified Report

A flat plate, a hollow cylinder, and a nine-caliber ogive containing lateral sonic jets were tested at Mach numbers 2.99, 3.98, and 5.01 in the 12-Inch Supersonic Tunnel (E-1) of the von Karman Gas Dynamics Facility. The interaction forces generated on these bodies were investigated for various sonic nozzle configurations including single circular nozzles, multiple circular nozzles, and slots of various width and span sizes. The nozzles were operated at jet stagnation to free-stream static pressure ratios from 10 to 2000. The force produced on a surface by the interaction of the lateral jet with the supersonic free stream was evaluated from model pressure distributions



1. Jet mixing flow
2. Supersonic flow
3. Control jets
4. Spacecraft
5. Atmosphere entry
6. Aerodynamic configurations
7. Loading (mechanics)
8. Boundary layer
9. Supersonic nozzles
10. Pressure
11. Tests
12. Theory
- I. AFSC Program Area 750A, Project 8953, Task 895305
- II. Contract AF 40(600)-1000
- III. ARO, Inc., Arnold AF Sta, Tenn.
- IV. W. T. Strike, C. J. Schueler, and J. S. Deitering
- V. In ASTIA Collection

and compared with various theoretical estimates. Good agreement was obtained between the present experimental data and the theoretical estimates based on a linear combination of the viscous and inviscid estimates of the jet interaction force. Also, good agreement was obtained between the integrated pressure data and some force measurements. These theoretical and experimental results indicated that significant jet interaction forces are produced. In general, circular sonic jets produced the maximum interaction force when located about 30 jet nozzle diameters forward of the trailing edge of a planar surface or at the base edge of a body of revolution. Rectangular nozzles (slots) generated the largest force when located at the model trailing edge.



Arnold Engineering Development Center
Arnold Air Force Station, Tennessee

Rpt. No. AEDC-TDR-63-22. INTERACTIONS PRODUCED
BY SONIC LATERAL JETS LOCATED ON SURFACES IN
A SUPERSONIC STREAM. April 1963. 125 p.
incl 34 refs., illus.

Unclassified Report

A flat plate, a hollow cylinder, and a nine-caliber ogive containing lateral sonic jets were tested at Mach numbers 2.98, 3.98, and 5.01 in the 12-Inch Supersonic Tunnel (E-1) of the von Karman Gas Dynamics Facility. The interaction forces generated on these bodies were investigated for various sonic nozzle configurations including single circular nozzles, multiple circular nozzles, and slots of various width and span sizes. The nozzles were operated at jet stagnation to free-stream static pressure ratios from 10 to 2000. The force produced on a surface by the interaction of the lateral jet with the supersonic free stream was evaluated from model pressure distributions

1. Jet mixing flow
2. Supersonic flow
3. Control jets
4. Spacecraft
5. Atmosphere entry
6. Aerodynamic configurations
7. Loading (mechanics)
8. Boundary layer
9. Supersonic nozzles
10. Pressure
11. Tests
12. Theory
- I. AFSC Program Area 750A, Project 8953, Task 895305
- II. Contract AF 40(600)-1000
- III. ARO, Inc., Arnold AF Sta, Tenn.
- IV. W. T. Strike, C. J. Schueler, and J. S. Deitering
- V. In ASTIA Collection

and compared with various theoretical estimates. Good agreement was obtained between the present experimental data and the theoretical estimates based on a linear combination of the viscous and inviscid estimates of the jet interaction force. Also, good agreement was obtained between the integrated pressure data and some force measurements. These theoretical and experimental results indicated that significant jet interaction forces are produced. In general, circular sonic jets produced the maximum interaction force when located about 30 jet nozzle diameters forward of the trailing edge of a planar surface or at the base edge of a body of revolution. Rectangular nozzles (slots) generated the largest force when located at the model trailing edge.

Arnold Engineering Development Center
Arnold Air Force Station, Tennessee

Rpt. No. AEDC-TDR-63-22. INTERACTIONS PRODUCED
BY SONIC LATERAL JETS LOCATED ON SURFACES IN
A SUPERSONIC STREAM. April 1963. 125 p.
incl 34 refs., illus.

Unclassified Report

A flat plate, a hollow cylinder, and a nine-caliber ogive containing lateral sonic jets were tested at Mach numbers 2.98, 3.98, and 5.01 in the 12-Inch Supersonic Tunnel (E-1) of the von Karman Gas Dynamics Facility. The interaction forces generated on these bodies were investigated for various sonic nozzle configurations including single circular nozzles, multiple circular nozzles, and slots of various width and span sizes. The nozzles were operated at jet stagnation to free-stream static pressure ratios from 10 to 2000. The force produced on a surface by the interaction of the lateral jet with the supersonic free stream was evaluated from model pressure distributions

1. Jet mixing flow
2. Supersonic flow
3. Control jets
4. Spacecraft
5. Atmosphere entry
6. Aerodynamic configurations
7. Loading (mechanics)
8. Boundary layer
9. Supersonic nozzles
10. Pressure
11. Tests
12. Theory
- I. AFSC Program Area 750A, Project 8953, Task 895305
- II. Contract AF 40(600)-1000
- III. ARO, Inc., Arnold AF Sta, Tenn.
- IV. W. T. Strike, C. J. Schueler, and J. S. Deitering
- V. In ASTIA Collection

and compared with various theoretical estimates. Good agreement was obtained between the present experimental data and the theoretical estimates based on a linear combination of the viscous and inviscid estimates of the jet interaction force. Also, good agreement was obtained between the integrated pressure data and some force measurements. These theoretical and experimental results indicated that significant jet interaction forces are produced. In general, circular sonic jets produced the maximum interaction force when located about 30 jet nozzle diameters forward of the trailing edge of a planar surface or at the base edge of a body of revolution. Rectangular nozzles (slots) generated the largest force when located at the model trailing edge.

Arnold Engineering Development Center
Arnold Air Force Station, Tennessee

Rpt. No. AEDC-TDR-63-22. INTERACTIONS PRODUCED
BY SONIC LATERAL JETS LOCATED ON SURFACES IN
A SUPERSONIC STREAM. April 1963. 125 p.
incl 34 refs., illus.

Unclassified Report

A flat plate, a hollow cylinder, and a nine-caliber ogive containing lateral sonic jets were tested at Mach numbers 2.99, 3.98, and 5.01 in the 12-Inch Supersonic Tunnel (E-1) of the von Kármán Gas Dynamics Facility. The interaction forces generated on these bodies were investigated for various sonic nozzle configurations including single circular nozzles, multiple circular nozzles, and slots of various width and span sizes. The nozzles were operated at jet stagnation to free-stream static pressure ratios from 10 to 2000. The force produced on a surface by the interaction of the lateral jet with the supersonic free stream was evaluated from model pressure distributions



1. Jet mixing flow
2. Supersonic flow
3. Control jets
4. Spacecraft
5. Atmosphere entry
6. Aerodynamic configurations
7. Loading (mechanics)
8. Boundary layer
9. Supersonic nozzles
10. Pressure
11. Tests
12. Theory
- I. AFSC Program Area 750A, Project 8953, Task 895305
- II. Contract AF 40(600)-1000
- III. ARO, Inc., Arnold AF Sta, Tenn.
- IV. W. T. Strike, C. J. Schueler, and J. S. Deitering
- V. In ASTIA Collection

and compared with various theoretical estimates. Good agreement was obtained between the present experimental data and the theoretical estimates based on a linear combination of the viscous and inviscid estimates of the jet interaction force. Also, good agreement was obtained between the integrated pressure data and some force measurements. These theoretical and experimental results indicated that significant jet interaction forces are produced. In general, circular sonic jets produced the maximum interaction force when located about 30 jet nozzle diameters forward of the trailing edge of a planar surface or at the base edge of a body of revolution. Rectangular nozzles (slots) generated the largest force when located at the model trailing edge.



Arnold Engineering Development Center
Arnold Air Force Station, Tennessee

Rpt. No. AEDC-TDR-63-22. INTERACTIONS PRODUCED
BY SONIC LATERAL JETS LOCATED ON SURFACES IN
A SUPERSONIC STREAM. April 1963. 125 p.
incl 34 refs., illus.

Unclassified Report

A flat plate, a hollow cylinder, and a nine-caliber ogive containing lateral sonic jets were tested at Mach numbers 2.99, 3.98, and 5.01 in the 12-Inch Supersonic Tunnel (E-1) of the von Kármán Gas Dynamics Facility. The interaction forces generated on these bodies were investigated for various sonic nozzle configurations including single circular nozzles, multiple circular nozzles, and slots of various width and span sizes. The nozzles were operated at jet stagnation to free-stream static pressure ratios from 10 to 2000. The force produced on a surface by the interaction of the lateral jet with the supersonic free stream was evaluated from model pressure distributions



1. Jet mixing flow
2. Supersonic flow
3. Control jets
4. Spacecraft
5. Atmosphere entry
6. Aerodynamic configurations
7. Loading (mechanics)
8. Boundary layer
9. Supersonic nozzles
10. Pressure
11. Tests
12. Theory
- I. AFSC Program Area 750A, Project 8953, Task 895305
- II. Contract AF 40(600)-1000
- III. ARO, Inc., Arnold AF Sta, Tenn.
- IV. W. T. Strike, C. J. Schueler, and J. S. Deitering
- V. In ASTIA Collection

and compared with various theoretical estimates. Good agreement was obtained between the present experimental data and the theoretical estimates based on a linear combination of the viscous and inviscid estimates of the jet interaction force. Also, good agreement was obtained between the integrated pressure data and some force measurements. These theoretical and experimental results indicated that significant jet interaction forces are produced. In general, circular sonic jets produced the maximum interaction force when located about 30 jet nozzle diameters forward of the trailing edge of a planar surface or at the base edge of a body of revolution. Rectangular nozzles (slots) generated the largest force when located at the model trailing edge.



Arnold Engineering Development Center
Arnold Air Force Station, Tennessee

Rpt. No. AEDC-TDR-63-22. INTERACTIONS PRODUCED
BY SONIC LATERAL JETS LOCATED ON SURFACES IN
A SUPERSONIC STREAM. April 1963. 125 p.
incl 34 refs., illus.

Unclassified Report

A flat plate, a hollow cylinder, and a nine-caliber ogive containing lateral sonic jets were tested at Mach numbers 2.99, 3.98, and 5.01 in the 12-Inch Supersonic Tunnel (E-1) of the von Karman Gas Dynamics Facility. The interaction forces generated on these bodies were investigated for various sonic nozzle configurations including single circular nozzles, multiple circular nozzles, and slots of various width and span sizes. The nozzles were operated at jet stagnation to free-stream static pressure ratios from 10 to 2000. The force produced on a surface by the interaction of the lateral jet with the supersonic free stream was evaluated from model pressure distributions



1. Jet mixing flow
2. Supersonic flow
3. Control jets
4. Spacecraft
5. Atmosphere entry
6. Aerodynamic configurations
7. Loading (mechanics)
8. Boundary layer
9. Supersonic nozzles
10. Pressure
11. Tests
12. Theory
 - I. AFSC Program Area 750A, Project 8953, Task 895305
 - II. Contract AF 40(600)-1000
 - III. ARO, Inc., Arnold AF Sta, Tenn.
 - IV. W. T. Strike, C. J. Schueler, and J. S. Deitering
 - V. In ASTIA Collection

and compared with various theoretical estimates. Good agreement was obtained between the present experimental data and the theoretical estimates based on a linear combination of the viscous and inviscid estimates of the jet interaction force. Also, good agreement was obtained between the integrated pressure data and some force measurements. These theoretical and experimental results indicated that significant jet interaction forces are produced. In general, circular sonic jets produced the maximum interaction force when located about 30 jet nozzle diameters forward of the trailing edge of a planar surface or at the base edge of a body of revolution. Rectangular nozzles (slots) generated the largest force when located at the model trailing edge.



Arnold Engineering Development Center
Arnold Air Force Station, Tennessee

Rpt. No. AEDC-TDR-63-22. INTERACTIONS PRODUCED
BY SONIC LATERAL JETS LOCATED ON SURFACES IN
A SUPERSONIC STREAM. April 1963. 125 p.
incl 34 refs., illus.

Unclassified Report

A flat plate, a hollow cylinder, and a nine-caliber ogive containing lateral sonic jets were tested at Mach numbers 2.99, 3.98, and 5.01 in the 12-Inch Supersonic Tunnel (E-1) of the von Karman Gas Dynamics Facility. The interaction forces generated on these bodies were investigated for various sonic nozzle configurations including single circular nozzles, multiple circular nozzles, and slots of various width and span sizes. The nozzles were operated at jet stagnation to free-stream static pressure ratios from 10 to 2000. The force produced on a surface by the interaction of the lateral jet with the supersonic free stream was evaluated from model pressure distributions



1. Jet mixing flow
2. Supersonic flow
3. Control jets
4. Spacecraft
5. Atmosphere entry
6. Aerodynamic configurations
7. Loading (mechanics)
8. Boundary layer
9. Supersonic nozzles
10. Pressure
11. Tests
12. Theory
 - I. AFSC Program Area 750A, Project 8953, Task 895305
 - II. Contract AF 40(600)-1000
 - III. ARO, Inc., Arnold AF Sta, Tenn.
 - IV. W. T. Strike, C. J. Schueler, and J. S. Deitering
 - V. In ASTIA Collection

and compared with various theoretical estimates. Good agreement was obtained between the present experimental data and the theoretical estimates based on a linear combination of the viscous and inviscid estimates of the jet interaction force. Also, good agreement was obtained between the integrated pressure data and some force measurements. These theoretical and experimental results indicated that significant jet interaction forces are produced. In general, circular sonic jets produced the maximum interaction force when located about 30 jet nozzle diameters forward of the trailing edge of a planar surface or at the base edge of a body of revolution. Rectangular nozzles (slots) generated the largest force when located at the model trailing edge.



Arnold Engineering Development Center
Arnold Air Force Station, Tennessee

Rpt. No. AEDC-TDR-63-22. INTERACTIONS PRODUCED
BY SONIC LATERAL JETS LOCATED ON SURFACES IN
A SUPERSONIC STREAM. April 1963. 125 p.
incl 34 refs., illus.

Unclassified Report

A flat plate, a hollow cylinder, and a nine-caliber ogive containing lateral sonic jets were tested at Mach numbers 2.99, 3.98, and 5.01 in the 12-inch Supersonic Tunnel (E-1) of the von Kármán Gas Dynamics Facility. The interaction forces generated on these bodies were investigated for various sonic nozzle configurations including single circular nozzles, multiple circular nozzles, and slots of various width and span sizes. The nozzles were operated at jet stagnation to free-stream static pressure ratios from 10 to 2000. The force produced on a surface by the interaction of the lateral jet with the supersonic free stream was evaluated from model pressure distributions



1. Jet mixing flow
2. Supersonic flow
3. Control jets
4. Spacecraft
5. Atmosphere entry
6. Aerodynamic configurations
7. Loading (mechanics)
8. Boundary layer
9. Supersonic nozzles
10. Pressure
11. Tests
12. Theory
 - I. AFSC Program Area 750A, Project 8953, Task 895305
 - II. Contract AF 40(600)-1000
 - III. ARO, Inc., Arnold AF Sta, Tenn.
 - IV. W. T. Strike, C. J. Schueler, and J. S. Deitering
 - V. In ASTIA Collection

and compared with various theoretical estimates. Good agreement was obtained between the present experimental data and the theoretical estimates based on a linear combination of the viscous and inviscid estimates of the jet interaction force. Also, good agreement was obtained between the integrated pressure data and some force measurements. These theoretical and experimental results indicated that significant jet interaction forces are produced. In general, circular sonic jets produced the maximum interaction force when located about 30 jet nozzle diameters forward of the trailing edge of a planar surface or at the base edge of a body of revolution. Rectangular nozzles (slots) generated the largest force when located at the model trailing edge.



Arnold Engineering Development Center
Arnold Air Force Station, Tennessee

Rpt. No. AEDC-TDR-63-22. INTERACTIONS PRODUCED
BY SONIC LATERAL JETS LOCATED ON SURFACES IN
A SUPERSONIC STREAM. April 1963. 125 p.
incl 34 refs., illus.

Unclassified Report

A flat plate, a hollow cylinder, and a nine-caliber ogive containing lateral sonic jets were tested at Mach numbers 2.99, 3.98, and 5.01 in the 12-inch Supersonic Tunnel (E-1) of the von Kármán Gas Dynamics Facility. The interaction forces generated on these bodies were investigated for various sonic nozzle configurations including single circular nozzles, multiple circular nozzles, and slots of various width and span sizes. The nozzles were operated at jet stagnation to free-stream static pressure ratios from 10 to 2000. The force produced on a surface by the interaction of the lateral jet with the supersonic free stream was evaluated from model pressure distributions



1. Jet mixing flow
2. Supersonic flow
3. Control jets
4. Spacecraft
5. Atmosphere entry
6. Aerodynamic configurations
7. Loading (mechanics)
8. Boundary layer
9. Supersonic nozzles
10. Pressure
11. Tests
12. Theory
 - I. AFSC Program Area 750A, Project 8953, Task 895305
 - II. Contract AF 40(600)-1000
 - III. ARO, Inc., Arnold AF Sta, Tenn.
 - IV. W. T. Strike, C. J. Schueler, and J. S. Deitering
 - V. In ASTIA Collection

and compared with various theoretical estimates. Good agreement was obtained between the present experimental data and the theoretical estimates based on a linear combination of the viscous and inviscid estimates of the jet interaction force. Also, good agreement was obtained between the integrated pressure data and some force measurements. These theoretical and experimental results indicated that significant jet interaction forces are produced. In general, circular sonic jets produced the maximum interaction force when located about 30 jet nozzle diameters forward of the trailing edge of a planar surface or at the base edge of a body of revolution. Rectangular nozzles (slots) generated the largest force when located at the model trailing edge.



Arnold Engineering Development Center
Arnold Air Force Station, Tennessee

Rpt. No. AEDC-TDR-63-22. INTERACTIONS PRODUCED
BY SONIC LATERAL JETS LOCATED ON SURFACES IN
A SUPERSONIC STREAM, April 1963. 125 p.
incl 34 refs., illus.

Unclassified Report

A flat plate, a hollow cylinder, and a nine-caliber ogive containing lateral sonic jets were tested at Mach numbers 2.99, 3.98, and 5.01 in the 12-Inch Supersonic Tunnel (E-1) of the von Karman Gas Dynamics Facility. The interaction forces generated on these bodies were investigated for various sonic nozzle configurations including single circular nozzles, multiple circular nozzles, and slots of various width and span sizes. The nozzles were operated at jet stagnation to free-stream static pressure ratios from 10 to 2000. The force produced on a surface by the interaction of the lateral jet with the supersonic free stream was evaluated from model pressure distributions



1. Jet mixing flow
2. Supersonic flow
3. Control jets
4. Spacecraft
5. Atmosphere entry
6. Aerodynamic configurations
7. Loading (mechanics)
8. Boundary layer
9. Supersonic nozzles
10. Pressure
11. Tests
12. Theory
- I. AFSC Program Area 750A, Project 8953, Task 895305
- II. Contract AF 40(600)-1000
- III. ARO, Inc., Arnold AF Sta, Tenn.
- IV. W. T. Strike, C. J. Schueler, and J. S. Deitering
- V. In ASTIA Collection

and compared with various theoretical estimates. Good agreement was obtained between the present experimental data and the theoretical estimates based on a linear combination of the viscous and inviscid estimates of the jet interaction force. Also, good agreement was obtained between the integrated pressure data and some force measurements. These theoretical and experimental results indicated that significant jet interaction forces are produced. In general, circular sonic jets produced the maximum interaction force when located about 30 jet nozzle diameters forward of the trailing edge of a planar surface or at the base edge of a body of revolution. Rectangular nozzles (slots) generated the largest force when located at the model trailing edge.



Arnold Engineering Development Center
Arnold Air Force Station, Tennessee

Rpt. No. AEDC-TDR-63-22. INTERACTIONS PRODUCED
BY SONIC LATERAL JETS LOCATED ON SURFACES IN
A SUPERSONIC STREAM, April 1963. 125 p.
incl 34 refs., illus.

Unclassified Report

A flat plate, a hollow cylinder, and a nine-caliber ogive containing lateral sonic jets were tested at Mach numbers 2.99, 3.98, and 5.01 in the 12-Inch Supersonic Tunnel (E-1) of the von Karman Gas Dynamics Facility. The interaction forces generated on these bodies were investigated for various sonic nozzle configurations including single circular nozzles, multiple circular nozzles, and slots of various width and span sizes. The nozzles were operated at jet stagnation to free-stream static pressure ratios from 10 to 2000. The force produced on a surface by the interaction of the lateral jet with the supersonic free stream was evaluated from model pressure distributions



1. Jet mixing flow
2. Supersonic flow
3. Control jets
4. Spacecraft
5. Atmosphere entry
6. Aerodynamic configurations
7. Loading (mechanics)
8. Boundary layer
9. Supersonic nozzles
10. Pressure
11. Tests
12. Theory
- I. AFSC Program Area 750A, Project 8953, Task 895305
- II. Contract AF 40(600)-1000
- III. ARO, Inc., Arnold AF Sta, Tenn.
- IV. W. T. Strike, C. J. Schueler, and J. S. Deitering
- V. In ASTIA Collection

and compared with various theoretical estimates. Good agreement was obtained between the present experimental data and the theoretical estimates based on a linear combination of the viscous and inviscid estimates of the jet interaction force. Also, good agreement was obtained between the integrated pressure data and some force measurements. These theoretical and experimental results indicated that significant jet interaction forces are produced. In general, circular sonic jets produced the maximum interaction force when located about 30 jet nozzle diameters forward of the trailing edge of a planar surface or at the base edge of a body of revolution. Rectangular nozzles (slots) generated the largest force when located at the model trailing edge.

